POLITECNICO DI TORINO

I Facoltà di Ingegneria
Corso di Laurea Magistrale in Ingegneria dei Materiali

Tesi di Laurea Magistrale

Thin samples preparation for the TEM characterization of materials for microelectronics

Artifacts of Gallium Focused Ion Beam on lamella for TEM Microscopy

Supervisor: Jean Gabriel Mattei
Tutor: Milena Salvo

Candidate: Audrey Mayrat

December 2020

Acknowledgment

I would like to thank Mr. Jean-Gabriel MATTEI, my internship supervisor who overseed me throughout my internship and even after, both for the TEM handling and at the editorial level.

I would also like to thank him for all the EDX analysis that he made, allowing me to complete my internship.

I would also like to thank Mr. Frederic LORUT and Mr. Christophe CHARLES who took care of all the preparation for the lamella observed during my internship.

I would also like to thank Ms. Alexia VALERY and Ms. Karen DABERTRAND for their help and their measures regarding the ASTAR / Acom-TEM results, without which this would have been impossible.

I thank all of them, as well as Mr. Laurent CLEMENT and Ms. Nadine BICAIS, for their guidance and advice during my internship.

I would also like to thank the entire CarPhy especially the physical characterization team for their warm welcome.

I thank the company STMicroelectronics for giving me this opportunity.

I also want to thank my professors Pr. Milena SALVO, Pr. Benoit NAIT-ALI, and the Pr. Elsa THUNE, for their attention and their help throughout my internship and master thesis.

Tables of contents

I. Introduction

In 1965, observing the evolution in the 5 previous years, Gordon Moore predicted the evolution of integrated circuit. He defined then what is known nowadays as the Moore's Law: "the number of transistors that can be placed on an integrated circuit doubles every two years" [1]. Since, the actual progress followed that estimation, as we can see in the Figure 1, where the Moore's estimation and the real development of processors are similar [2].

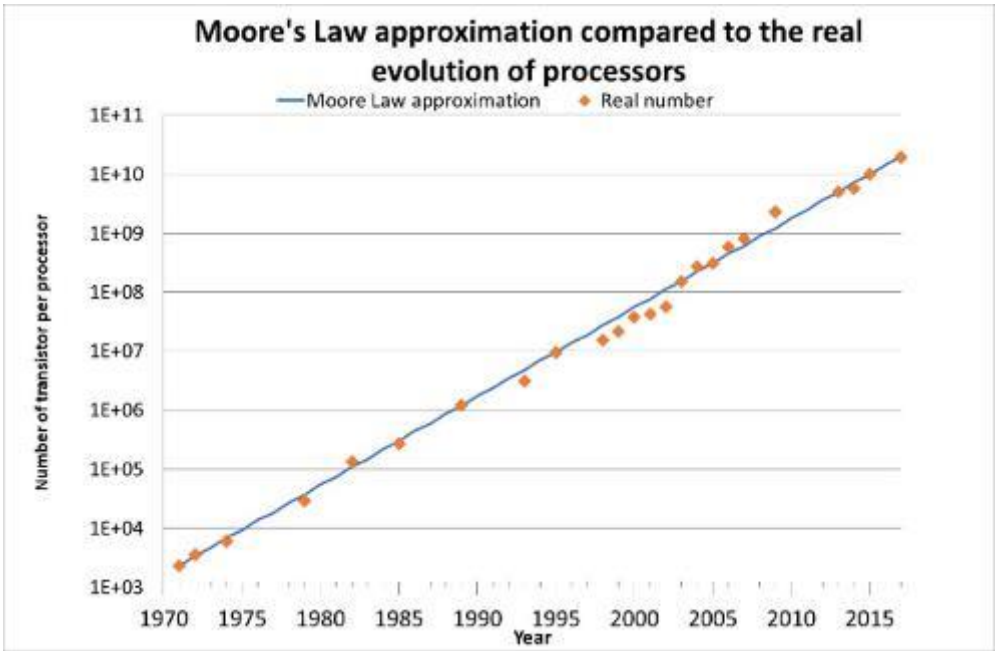

Figure 1: Moore's Law - The number of transistors on integrated circuit chips (1971-2018)

This evolution can also be viewed as if every 2 years, the size of the transistors was divided by 2. This was the path of miniaturization. By allowing the possibility to put more and more transistors on a chip with identical dimensions, the computing capacity increased exponentially. Therefore, it allowed the rise of nowadays new technologies thanks to the improvement of the processors, as used in laptop or smartphone. This would have been impossible with the former circuits. Diverse parameters were improved for years to reach it. However, an important aspect is the progress of material science [1].

The miniaturization also brought new process and analytical needs. From the lithography to the specimen observation, all aspects needed to be adapted to the size of the devices, especially when it came to observe microelectronic chips. Indeed, the resolution of optical microscopes only allowing a resolution of 0.2µm, their ability was quickly overwhelmed by the transistor miniaturization. Transistor nowadays can go down to a size of 7 nm. To observe them or their defects, an extremely high resolution is thus needed. That is why the Transmission Electronic Microscopy (TEM), with its resolution of 0.1 nm, is widely used in the semiconductor industry. As in, for example, STMicroelectronics where I completed my master's internship [3].

A. Problematics

As seen, the analysis by TEM technique is nowadays a necessity. However, this technique does not come without any inconvenience. The most important parameter is the sample preparation. To allow the electronic transmission, it needs to be transparent to electron: the lamella needs to be extremely thin. The thickness also can vary in function of the analysis wanted. It usually varies from 100nm to 40 nm. To get that thinness, several sample preparation techniques exist. Among them, an approach consists of mechanical and argon polishing of cross-section or planar specimens: a hole is thus performed thanks

to the Argon ion beam. The measures are done on the edges of the gap, them being thin enough to allow the electron transmission. However, that method does not allow a precise area selection. To observe a microelectronic device that parameter needs to be taken in account. That is why the usual process is performed using a dual beam, composed by a Focused Ion Beam (FIB) and a Scanning Electron Microscopy (SEM). The dual beam, contrarily to other methods, allows the selection a cross-section on a specific area and to extract it precisely [3] [4].

The characterization laboratories of STMicroelectronics use an extensive range of dual beam to produce the TEM samples. The preparation is performed with a Gallium ion beam (Ga+) which cut the sample in a selected part to extract a lamella. However, the Ga + ion beam induces a multitude of ballistic shocks, thermodynamic effects in the material, thus causing amorphization at the level of the sample surface [5][6][7][8]. It also leads to a modification of the composition due to Ga+ entering the sample.

Knowledge of the effects of the preparation and their minimization is an important quality criterion for the TEM lamella analysis. Therefore, it has an important impact on the quality of the observations and results.

Indeed, some experiments performed on a TEM instrument such as high-resolution imaging or Electron Energy Losses spectroscopy requires samples thinner than usual. The challenge is to prepare, using FIB technique, TEM lamella thinner than 50 nm while preserving its structural order and consequently avoiding any amorphization from the ion beam.

High energy ion beam has the advantage of a fast milling and better cutting precision. However, the ions having higher kinetics energy, they go deeper into the sample. They also transmit more energy to the lattice's atoms. The effect of the ion beam depends on many parameters like the composition or the atomic structure [5][6]. Other more indirect phenomena can happen like the sample's warming, especially visible while studying polymers. In our study, it may be necessary to detect any possible phase change (melting, phase switch, …).

To define the real impact of the ion-beam energy on the materials, different protocols will be used for the thinning by changing the polishing steps. The settings of the dual beams allow us to use a gallium beam accelerated with a tension of 30keV, 16keV, 8keV, 5keV and 2keV. The lamellae are made parting from high energy beam (30keV) and reducing it to the inferior tension step. Removing the previous impacted layer thanks to the lower energy beam, the goal is to only leave the last beam impact.

On these lamellas the priority is to determine the amorphous/crystalline rate, the thickness of both the lamella and the amorphous layer, thanks to conventional and hight resolution TEM analysis. In parallel X Ray Energy Dispersive Spectroscopy (X EDS/EDX) is used to determine the gallium penetration in the lamella.

In the first part, this project will focus on silicon material, a major component in the field of microelectronics whose results are already known to check the validity of the method. Then we will study the impact on the $Ge_2Sb_2Te_5$ compound, a material providing interesting applications in the microelectronic field especially for phase change memory cells (PCM cells).

B. Materials of this study:

To optimize the lamella preparation, the knowledge of the impact of the ion beam on all materials may be necessary. This study will focus on 2 materials known to be impacted by the FIB: the monocrystalline silicon and the GeSbTe. Both materials are used in electronic devices for different application. First, their properties and their application need to be seen to understand what is expected from them (use, measures, expected variation). Then, it will be possible to go deeper on the impact of the dual beam and thus to study the impact of the dual-beam preparation.

1. Monocrystalline Silicon

The monocrystalline silicon used in microelectronics is usually with 99.99999999% purity. It is an almost defect free single crystal a with a structure based on a face cubic centred unit cell with a cell parameter of 0,543nm. However, it is a more complex structure as it can be considered the result of two interpenetrating face-centred cubic crystals. Thus, the silicon crystal unit cell contains four additional atoms in its tetrahedral sites (half full). Its structure is represented in Figure 2 [9]. In brief, a silicon unit cell is composed of 9 atoms: 8 at the edges, 6 at the face centers, and 4 atoms in tetrahedral sites.

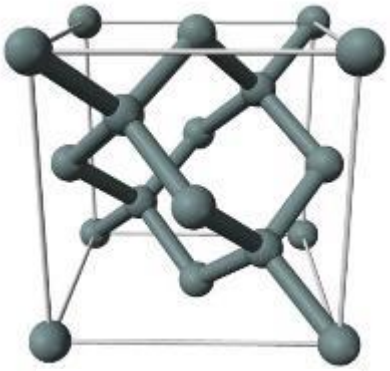

Figure 2: Silicon unit cell

Because of the asymmetrical and non-uniform lattice distance between atoms, single-crystal silicon exhibits anisotropic physical and mechanical characteristics.

It is an intrinsic semiconductor: the electronic conduction is done thanks to electron holes pairs and electrons by heat. Its low conductivity is compensated by doping the silicon with other elements such as Boron or Arsenic to control the number and the charge of activated carrier. It is then an extrinsic semiconductor [10].

Applications

Monocrystalline silicon is the most used semiconductor in the electronic field for several reasons. The raw material used is low cost, a major part of the cost comes from the process to create the monocrystalline wafer. Also, its mechanicals properties added to its electrical properties allow it to serve as a mechanical support for the circuits. As the silicon resists against both high temperature and high electrical current, it has a great resistance to electrical breakdown. Furthermore, the high resistivity of the silicon enables the possibility of parallel batch fabrication, with higher reliability and a significant drop of the fabrication cost [11].

2. $Ge_xSb_yTe_z$

$Ge_xSb_yTe_z$ or GST is a chalcogenide glass made of germanium, antimony, and tellurium under different stoichiometry. It is one of the most promising phase-change material for phase-change memory (PCM) applications. The GST used there is the $Ge_2Sb_2Te_5$ enriched with Germanium.

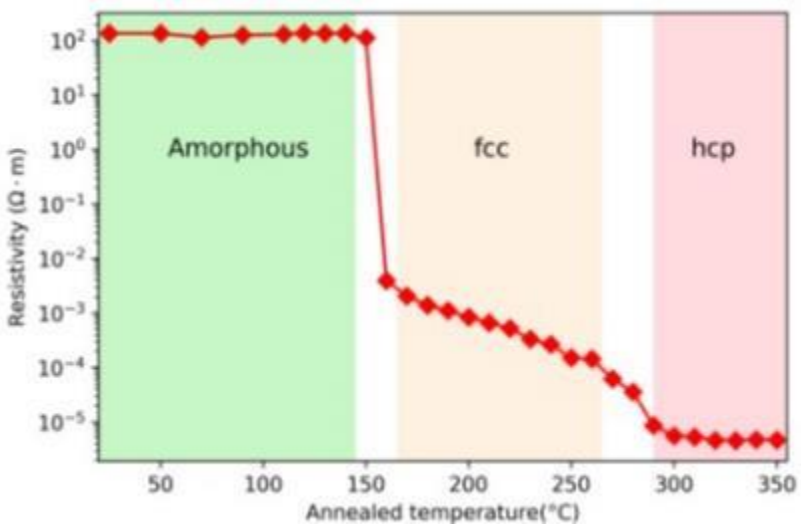

Figure 3: Phase changing phenomenon and the evolution of the resistivity [12].

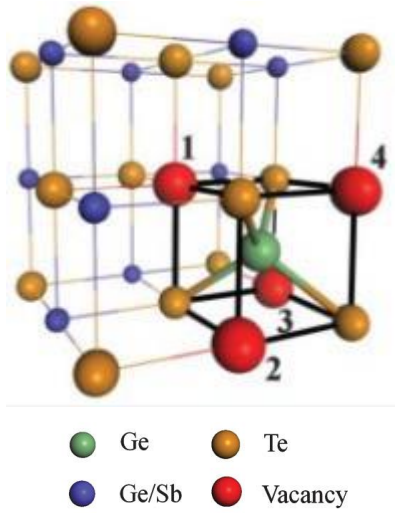

Figure 4: Ge-Sb-Te with an FCC unit cell [13]

Depending on the annealing temperature, the phase present at a lower temperature will vary. It goes from an amorphous structure to a polycrystalline CFC structure with a cell parameter of 0,60117 nm and a germanium in one tetrahedral site, see Figure 4 [13][14] . This first transition appears near 150°C. At higher temperature there is a second transition near 230°C; the FCC lattice becomes hexagonal close-packed (HCP). However, those temperatures vary according to the GST stoichiometry. Indeed, a doping in germanium, can bring the FCC phase transition to a temperature above 350 degrees Celsius. At a higher temperature, there is a second transition from FCC to compact hexagonal (HC). Since the GST used in STMicroelectronics is for high temperature application, it is a $Ge_2Sb_2Te_5$ enriched with germanium.

Those different phases present different resistivity. In the same phase interval, the annealing temperature has a negligible impact on the resistivity. However, the resistivity difference between states is important as seen in Figure 3. While the amorphous phase has a high resistivity 10^2 Ωm, similarly to a semiconductor, the crystalline states are far better conductors. Its resistivity is at least divided by 100 000 for the FCC states, and by more than 10 million for the HCP states [13].

The resistivity difference between the amorphous and the FCC states is high enough to be easily detected by sensors. That is why the GST allows the storage of logical bit by switching between the 2 states [15][16].

Applications

The storage of the logical bit makes thus the Ge-Sb-Te a remarkable material for phase change memory application thanks to its high speeds write and erase processes while maintaining a high endurance and high-power efficiency [13].

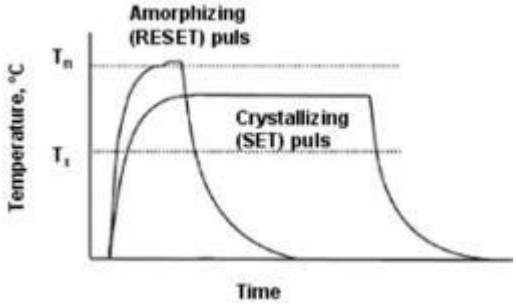

Figure 5: Set and Reset temperature evolution

Thanks to a filament (heater) the GST is heated up by Joule effect, it is then possible to differentiate 2 cases as seen in Figure 5:

- The RESET current: If the material reaches its melting point and rapidly cooled (around 50-100ns) the material goes from a previous crystalline to an amorphous phase.
- The SET current: With a longer but lower temperature rise, only the crystallization point is reached. It allows the phase change from amorphous to polycrystalline (FCC)

The resistivity change between amorphous and crystalline allows the storage of the logical bit. If there is a high resistivity (amorphous) no current pass through, the bit 0 is written. However, if we have a low

resistivity (crystalline) then the current can pass through the material and the bit 1 is written. Therefore, the SET current allows the bit to pass from 0 to 1 while the reset from 1 to 0 [17] [18].

In PCM cells, the key characteristic is the state of the GST: if there is an amorphous dome or not. An amorphization due to the preparation would consequently bias the observation and thus the conclusion on the device.

A simple example of it would be to know if a memory cell is effective or not. If a part of the crystalline GST is amorphized by the ion-beam, then an amorphized state would be observed where a crystalline is expected. The cell would be said non effective because of it, giving us a false negative.

That is why the knowledge of the impact of ion-beam energy on the GST is necessary if we want to have a better analysis of PCM cells by TEM.

II. Instrumentation

The observation of those devices needs thus a high resolution. A few options exist with a sufficient resolution. However, transmission electron microscopes are one of the only instrumentations allowing both morphological and structural analysis at the same time. Also, some specific TEMs allow the compositional analysis too. Yet, the transmission of the electron beam through the lamella require thin samples. This thickness requires specific lamella preparation. STMicroelectronics use the milling by dual beam; it allows both the selectivity and the possibility of extracting several lamellas from the same sample.

A. The sample preparation: the dual beam

The usual sample preparation done in STMicroelectronics is by Helios Dual beams. They are composed of a Gallium Focused Ion Beam (FIB) and a Scanning electron Microscope (SEM). It allows the micromachining required to the preparation of a TEM lamella.

1. The Focused Ion Beam

Several different ions beam can be used as Gallium, Xenon or Argon, in function of the preparation. The ion beam composition is directly dependant of the equipment, mainly dependant on the liquid metal ion source. STMicroelectronics use only gallium ion.

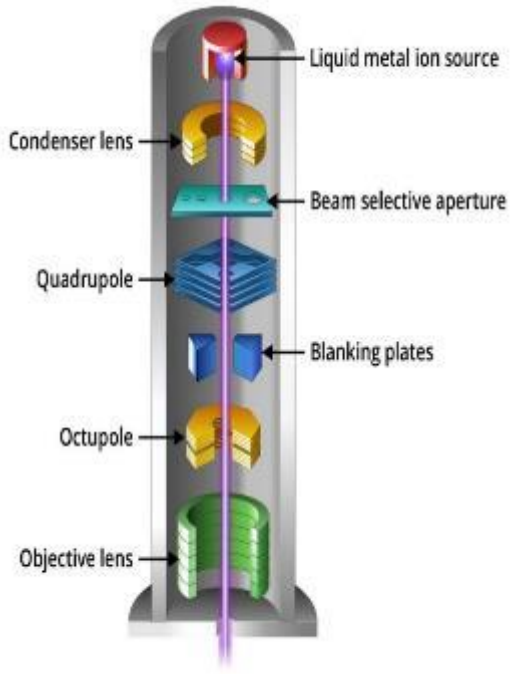

Figure 6: FIB column (source: MyScope Training, Microscopy Australia) CC BY-SA 4.0

The simplified schema of a fib column is presented in Figure 6. The liquid metal ion source produces the ion beam that is condensed and deflected by electromagnetic fields.

The tension of acceleration is also defined by the equipment, dependant on the constructor. The ones used there have the settings: 30, 16, 8, 5 and 2 keV. A High acceleration tension will have a better

milling power, faster and more precise. At lower tension however it will be longer to obtain a sample, and the ion beam will be less precise, with an extremely irregular form (potatoid).

The impact between the ion beam and the sample causes different interactions.

- Emission of secondary particle: secondary ions or secondary electrons are emitted. Those are usually used to record images.
- Sputtering: the removal of atoms on the surface of the solid. That process is usually used to cut and mill the material. The secondary ions can be used in SIMS analysis (compositional analysis).
- Vacancies, dislocations, and interstitials: they are formed when the removal happens in the depth of the sample, the atoms will be misplaced in the vicinity leaving a vacancy where it was before the collision.
- Projected Range: the interaction takes place until the ion is implanted at a specific depth R_{proj}.

In addition to those interactions directly linked to the incoming ions, another phenomenon must be considered: the collision cascade.

If the kinetic energy of the misplaced atoms is high enough, they can also act as a projectile and collide with other atoms. With lower energy, they can also create new cascades. That is well represented in Figure 7 thanks to the Monte Carlo simulation. While a single ion enters the sample following the ion trajectory (graph 1), the atomic collision path (graph2) does not follow it faithfully. That deviation is due to the collision cascade in the sample. The collisions are not only due to the incoming atom but also to the misplaced ones.

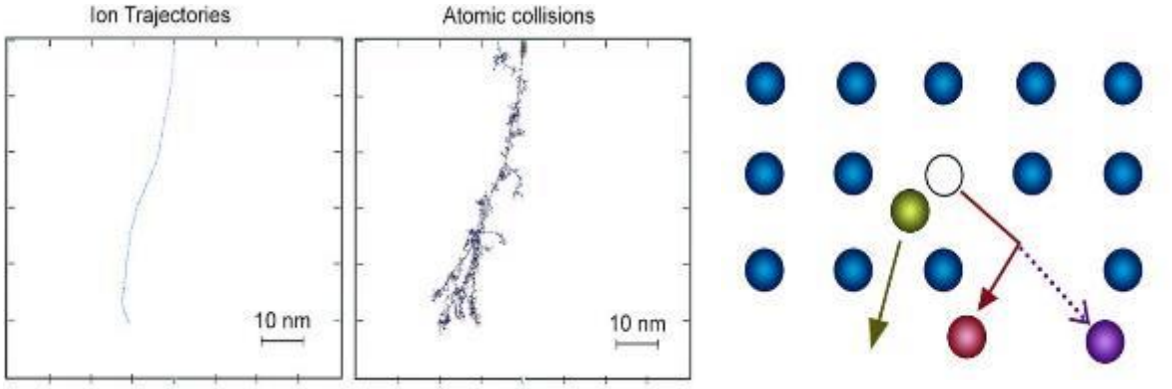

Figure 7: Collision cascade simulated with the Monte Carlo simulation (source: MyScope Training, Microscopy Australia) CC BY-SA 4.0

2. Dual-Beam

The Dual beam is a FIB column fitted with a Scanning Electron Microscope (SEM) column (Figure 8). While the e-beam is at the vertical, its angle with the ion beam is around 52° (usually but instrument dependant). Gas injection systems are also present. They allow material deposition (Si, Cr, Pt, ...) during the preparation. As an example, they are used for the deposition of a protective layer as Carbon or Platinum or even for preferential etching.

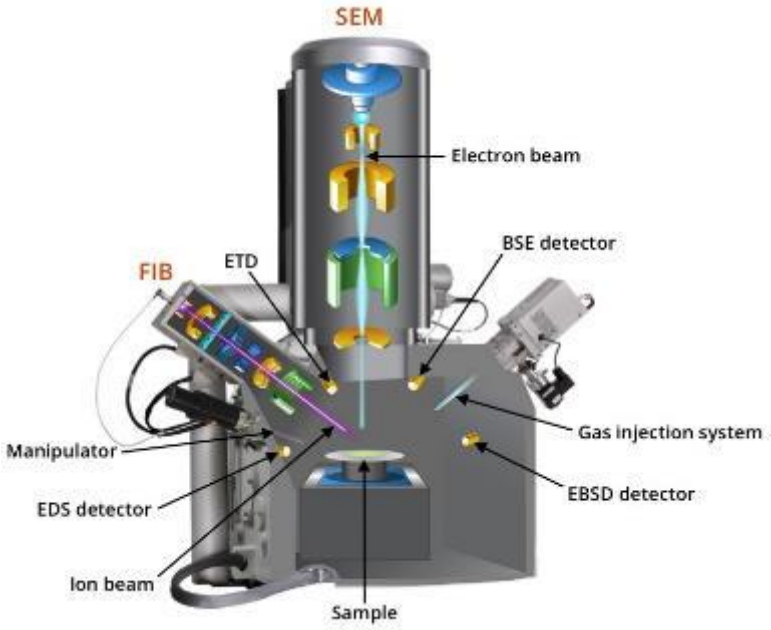

Figure 8: Dual-beam FIB schematics (source: My Scope Training, Microscopy Australia) CC BY-SA 4.0

The SEM column allows the observation of the sample under another angle than the FIB, with a minimal impact on the sample compared to an ion-beam. The sample is thus observable under 2 different angles during the whole process.

Only the sample is tilted. It is done under a different angle with a five-axis (x-y-z-rotate-tilt) stage to allow a precise and reproducible positioning of samples in the chamber.

The manipulator or omniprobe (Figure 9) is a sharp needle that allows a thin sample section to be lifted out and relocated in the chamber (on the sample itself or on grids).

The observation of the needle is by both SEM and FIB imaging, allows the sub micrometres precision during the manipulation.

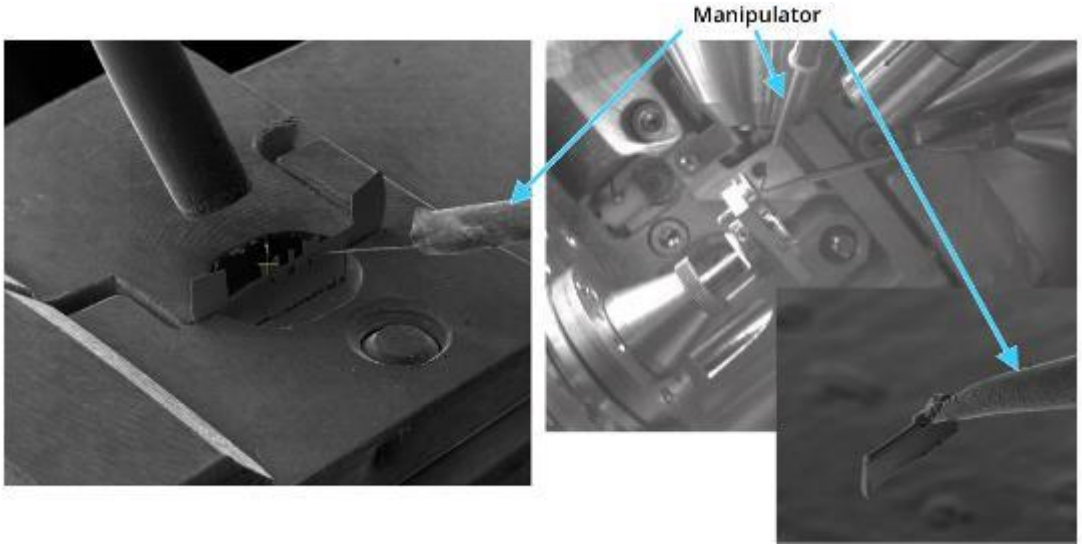

Figure 9: Manipulator used in the TEM lamella preparation while posing the lamella on the grid (source: MyScope Training, Microscopy Australia) CC BY-SA 4.0

3. Sample preparation: lift-out technique

The dual beam can use several methods to prepare TEM sample. Compared to others, the lift-out technic allows obtaining site-specific cross-section, extremely useful to observe integrated circuit. It also permits the serial cross-sectioning of materials, and thus the observation of several critical points on a unique bulk. This is extremely useful for integrated circuit or inhomogeneous materials.

a. Sample preparation steps

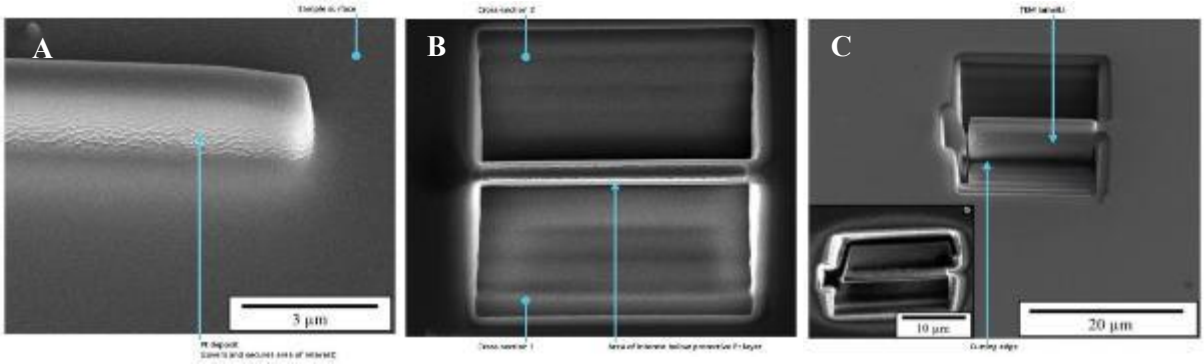

Figure 10: Protection of the sample, Cross-sectioning and J-cut (from right to left) to prepare a TEM lamella by Lift-out technics, source: My Scope Training, Microscopy Australia) CC BY-SA 4.0

After the sample introduction in the dual-FIB, pre-treatment can be necessary especially for insulating materials: a thin coat of high adsorbing materials is deposited.

Then a protection layer is added on the top surface along the desired area. In Figure 10A, platinum is deposited thanks to the gas injection system. This way, the platinum layer will protect the lamella from gallium irradiation: by absorbing gallium atoms, it allows the protection of the superior part of the lamella. During the whole process, monitoring the thickness of the deposition is mandatory to prevent degradation of the upper part of the lamella.

On each side of the lamella, two rectangular shafts (cross-sections) are dug, as seen in Figure 10B. Those cross-sections allow the access of the lower section to ion-beam milling.

A complete side of the lamella and the lower part are thus visible thanks to the cross-section dug (Figure 6C). The last side remaining is partially cut from the whole to conserve the stability of the lamella during the lift-out manipulation.

b. Lift-out steps

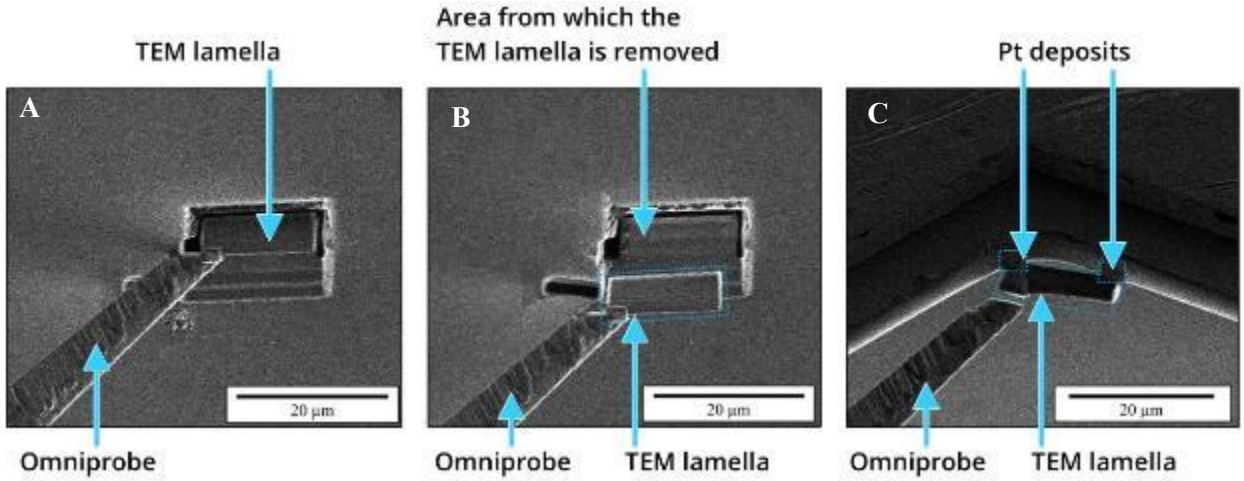

Figure 11: Lift-out of the sample, source: MyScope Training, Microscopy Australia) CC BY-SA 4.0

After the J-cut is done, it is possible to proceed with the omniprobe. Brought closed the platinum without contact, a new platinum deposition is done, as seen in Figure 11A. Both the needle and the lamella are linked with minimal damages.

The remaining part linking lamella and sample is milled away by the FIB. The omniprobe can then remove the lamella (Figure 11B).

The TEM lamella is then glued to a TEM grid thanks to platinum deposit. The link between the lamella and the omniprobe is then cut away, as in Figure 11C.

c. Thinning

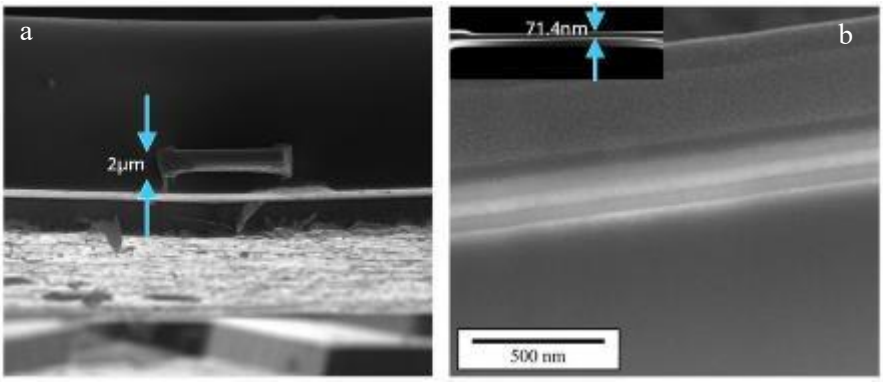

Figure 12: Thinning of the extracted sample to obtain an electron transparent surface (thickness<100nm)

At this step, the lamella is not thin enough to be transparent to electrons. This requires several thinning steps to reach a thickness inferior to 100 nm. The thinning steps can be seen in Figure 12, passing from 2µm to 71.4 nm. During that step, the ion beam is used as a grazing beam, parallel to the surface of the future lamella.

4. Artefacts and Thinning: the impact of the ion beam

The Gallium beam needed for the thinning has a destructive impact on the lamella. The gallium ions enter the sample, disorganising the crystalline network and therefore cause a surface amorphization. This amorphization is directly dependant of the acceleration tension of the beam. As we can see in Figure 13, the 30 keV energy beam has an impact twice as large as an energy beam of 8 keV and 5 times larger than a 2 keV.

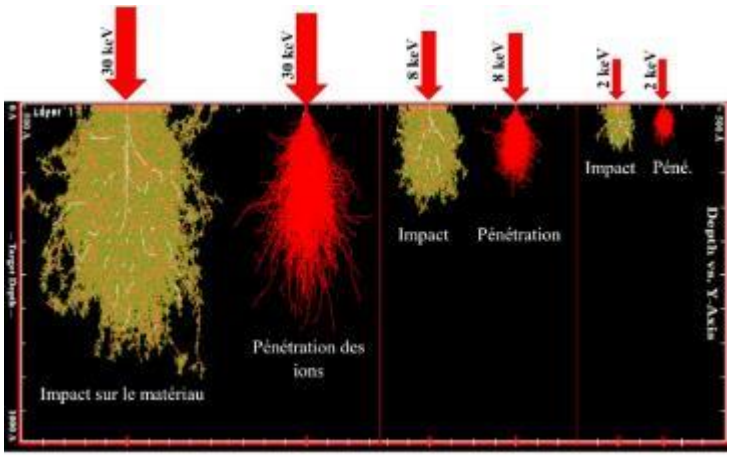

Figure 13 : Impact of a gallium ion beam on monocrystalline silicon

The purpose of thinning is then to erode the amorphous layer induced by high-energy beams. The Figure 14 shows this process. By decreasing the energy of the gallium beam as the preparation progress, it reduces the thickness of the amorphous layer. For example, a fine lamella preparation made with high-energy beams will lead to a totally amorphous lamella.

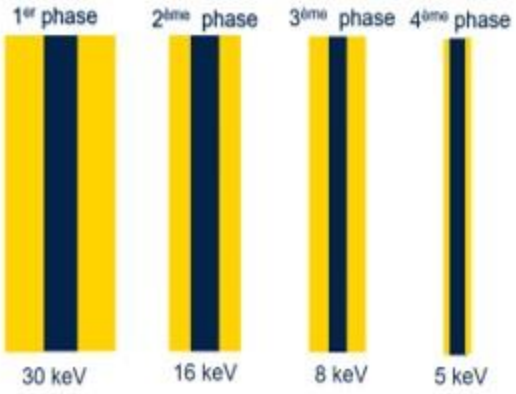

Figure 14 : Thinning steps of a TEM lamella, in yellow is represented the amorphous layers (in blue the crystalline remaining part)

To obtain a better-quality lamella in the best time, it is, therefore, necessary to determine how thick a lamella is possible and necessary to refine with a given energy beam to obtain as little amorphous as possible.

B. Transmission Electronic Microscopy (TEM)

The TEM analysis with the advancement of electronics technology such as nanotechnology became a key point of nowadays characterization. Indeed, the optical microscope with a resolution of 0.2µm became quickly insufficient for the resolution required. Optical technologies were at its maximum resolution and blocked by physical theory: the photons, uncharged particles are harder to collimate than charged one and their wavelength are not small enough to probe the nanoscale. However, an electron microscope can display a lower wavelength, that can go down to the pico-scale for high energy ones, which enable nanoscale probing. That is why the use of electronic microscopy is preferred especially the TEM which allows a resolution down to 0.1nm (for non-Cs corrected microscope). The use of electromagnetics lenses instead of optical lenses is necessary: they produce an electromagnetic field that will condense or project the electron beam.

1. Instrumentation

The basic functioning of all TEMs follows the same logic: an electron beam, in a high vacuum, goes through a thin sample and thanks to a set of electromagnetic lenses the projected image is magnified at the wanted size.

It is always composed of several parts; an example of the full alignment is represented in Figure 15. Other techniques can be fitted to the TEM to measures other phenomena such as X-ray, as will be addressed in the next part.

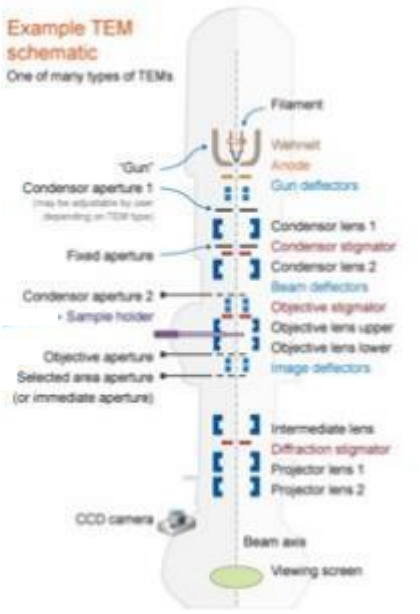

Figure 15: TEM schematics (source: MyScope Training) CC BY-SA 4.0

The electron gun generates the electron beam. Under a high intensity, the filament will emit electrons by Joule effect. Those electrons will be focused and accelerated by the Wehnelt and the anode as seen in Figure 16. An extremely high vacuum is necessary in that part to prevent the destruction of the filament leading to the gun's breakdown.

The electron beam goes then through the column passing through diverse component. One of the first components is the condenser C2 which condenses the electron beam to regulate the intensity. Furthermore, the condensor aperture can induce an astigmatism of the electron beam that can be easily corrected thanks to the stigmators condensor.

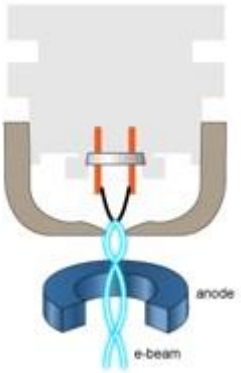

Figure 16: Electron Gun

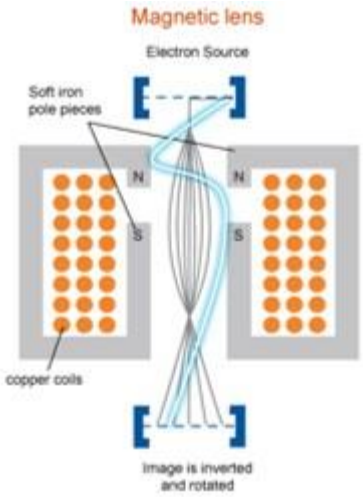

Figure 17:Electromagnetic lens

Magnetic electron lens (Figure 17) are composed of 2 parts:

- a pole-piece: a cylindrically symmetrical core of soft iron with a hole drilled through it (bore)
- a coil of copper wire which surrounds each pole-piece.

When an electrical current flow through the coil, a magnetic field is created in the bore. The strength of the field controls the ray paths since electrons are charged particles, focusing all rays on the same path. Due to the Joule effect, the coil temperature increase, therefore the lenses need to be cooled down.

The field needs to be radially symmetrical since any deviation causes aberrations such as astigmatism.

The astigmatism is handled thanks to the stigmators, composed by several poles (example in Figure 18), they produce weaker fields than. electromagnetic lenses. However, each pole being held separately it is possible to modify the field in precise position. By adjusting it, it is possible to compensate the astigmatism.

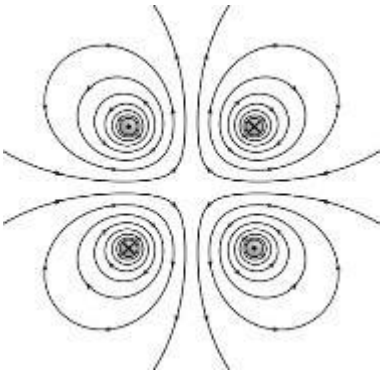

Figure 18: Stigmator quadrupole

The e-beam cross the sample, thin enough to be transparent to electrons. The e-beam will be thus diffracted or and scattered depending on the structural order of the sample. However other phenomena can occur as described in the next part. The focus is performed via the objective lens by adjusting the objective current. Then a set of lenses such as intermediate and projectors lenses permit to switch from the focal plane to the image plane and finally to magnify the image.

The projection of the magnified image can be done on the viewing screen: the collisions of the electrons on the screen induce the excitation of the atoms. The deexcitation of the atoms is due to phonon emission in the visible pattern. Since the number of phonons emitted is directly proportional to the number of electrons colliding on a certain area, the light contrast forms the image. To take a shot a special camera is used to substitute the screen.

The entire column is maintained under un high vacuum. The vacuum is mandatory in the column to prevent interaction between the electrons and the atmosphere atoms that would ruin the e-beam (loss of energy, random deviation of the electrons).

2. Interaction solid electrons

In electronic microscopy, the electrons interact with the sample, producing both back scattering electron and secondary electrons. I give information on both the phase contrast (BSE) and on the topography (SE).

In TEM microscopy, the sample is thin enough so that an important part of the incident e-beam can be transmitted. Thus, many phenomena can occur when the e-beam passes through the sample.

The Electronic diffraction is an important aspect: the e-beam is partially deviated by the sample. In this case, the electrons are diffracted by defined plans of a crystalline lattice that act as diffraction grating producing interference patterns (Bragg spots). The e-beam can even be scattered, that phenomenon is predominant for the amorphous area. It tends to form a halo around the transmitted beam (in diffraction mode).

However, passing through the sample the e-beam can sustain energy loss because of the inelastic interactions. Studying that loss, it is possible to determine the composition of chemical elements thanks to EELS technique (Electron Energy Loss spectroscopy).

In parallel, the inelastic interaction can induce an electronic excitation of the sample. The e-beam collides with core electrons from the sample atoms. If those electrons became excited there deexcitation can occur, leading to X-ray emission. The emitted photon is directly related to a specific element and the analysis of the spectrum (EDX), allowing composition determination. A Scanning Transmission Electron Microscope (STEM) allows determining point by point an EDX spectrum, producing a composition map.

3. Imaging mode Analysis

Thanks to the TEM several measures can be done on the same sample, each analysis giving different information. It is to the handler to determine what are his needs to choose wisely what is required from the sample.

i. Selected Area Diffraction

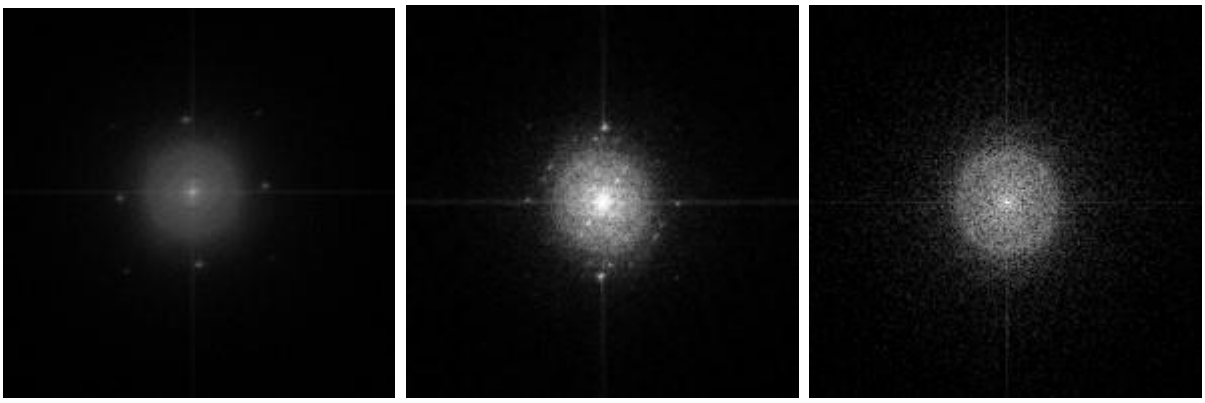

Figure 19: Diffraction pattern of diverse phases (1) Monocrystalline (silicon), (2) Polycrystalline (GST) (3) Amorphous (Silicon)

In the microscope, a diffraction pattern is formed on the focal plane. With a set of lenses, the pattern is projected on the screen or on the camera, allowing the access to the reciprocal lattice. From that pattern,

it is thus possible to deduce the crystallinity and the structure of the surface analysed. Three different basic patterns exist, from them it can be deducted the phase of the area as example in Figure 19:

- monocrystalline (1)
- polycrystalline (2)
- Amorphous (3)

From a monocrystalline and polycrystalline pattern, it is possible to deduce the type of lattice.

New technics, like ASTAR or Acom-tem, are based on this principle. They use the diffraction pattern to create a phase map or crystal orientation map.

ii. Imaging mode: Conventional and High-resolution TEM

The imaging mode allows producing an image that appears thanks to the contrast: a difference of intensity between the points. It is the most important feature of TEM imaging. The contrast can be due to several factors, however, the most used there are:

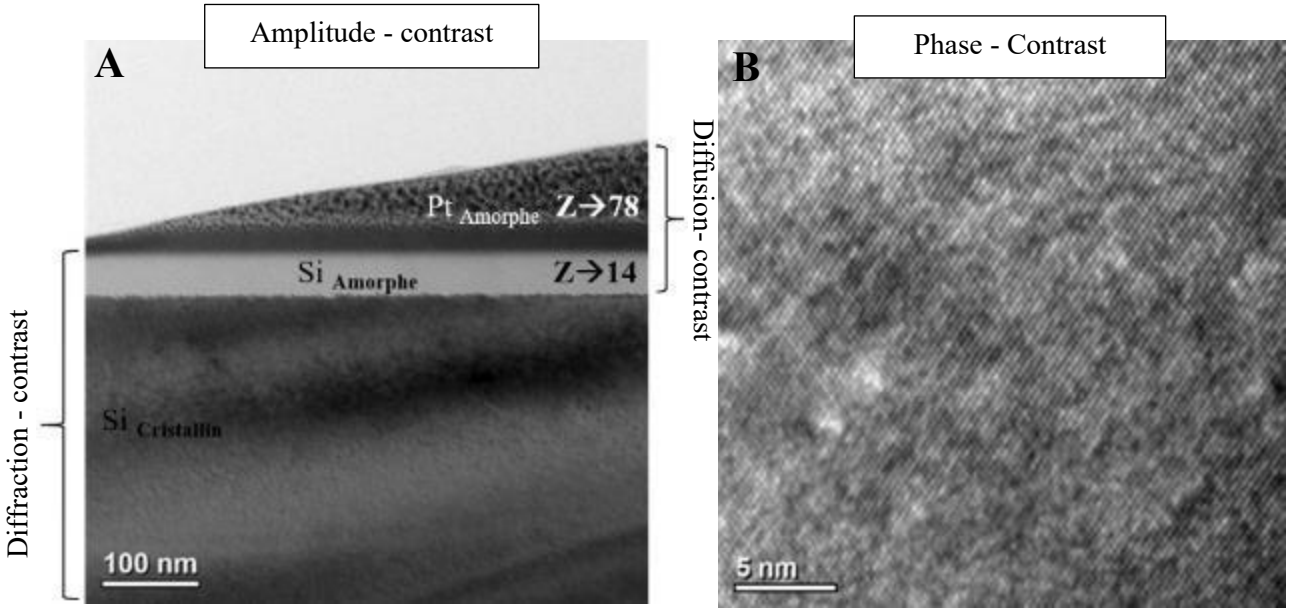

Figure 20: (A) TEM image of a bevel plate of monocrystalline silicon protected by platinum deposit: amplitude contrast (mass + diffraction) (B) TEM image of monocrystalline silicon in HRTEM: phase-contrast

The Amplitude–contrast is present in Figure 20A: the electron loss is due to the absorption or due to the scattering outside of the observable field (high angle). It can be due to the specimen and microscope construction; however, the objective aperture can enhance that contrast. That case can be divided into 2 types

- Mass-thickness (or diffusion) contrast: When the beam illuminates two neighbouring areas with low mass (or thickness) and high mass (or thickness), the heavier region scatters electrons at bigger angles. The low mass region appears then with higher intensity (normal and BF mode)
- Diffraction contrast: occurs due to a specific crystallographic orientation of a grain. The crystal is in Bragg condition, the atomic planes being oriented with a high probability of scattering giving important information on the orientation of the crystals in the sample.

The Phase contrast: It is observed by high-resolution transmission electron microscopy (HRTEM). The images are formed due to differences in phase of electron waves caused by specimen interaction, the

atomic plans acting as split to the electron beam. It is then possible to distinguish the atomic plans (see Figure 20B) or the atoms themselves.

To intensify the amplitude contrast, it is possible to select a specific beam on the focal plan with the objective aperture see Figure 21. If the non-scattered beam is selected (case a) then we obtain a Bright Field imaging. It permits to highlight the non-diffracting zones, the amorphous zones are the lighter and the diffracting ones, due to crystalline zones appear darker. However, if the scattered beams are selected, only diffracted beam under a certain angle to pass, then a Dark Field imaging is obtained. The selection permit to highlight the diffraction plan that produced the spot selected. The crystal lattice is highlighted, generating variation of the lattice as example dislocation, or stacking faults. Those defects are visible by high contrast difference.

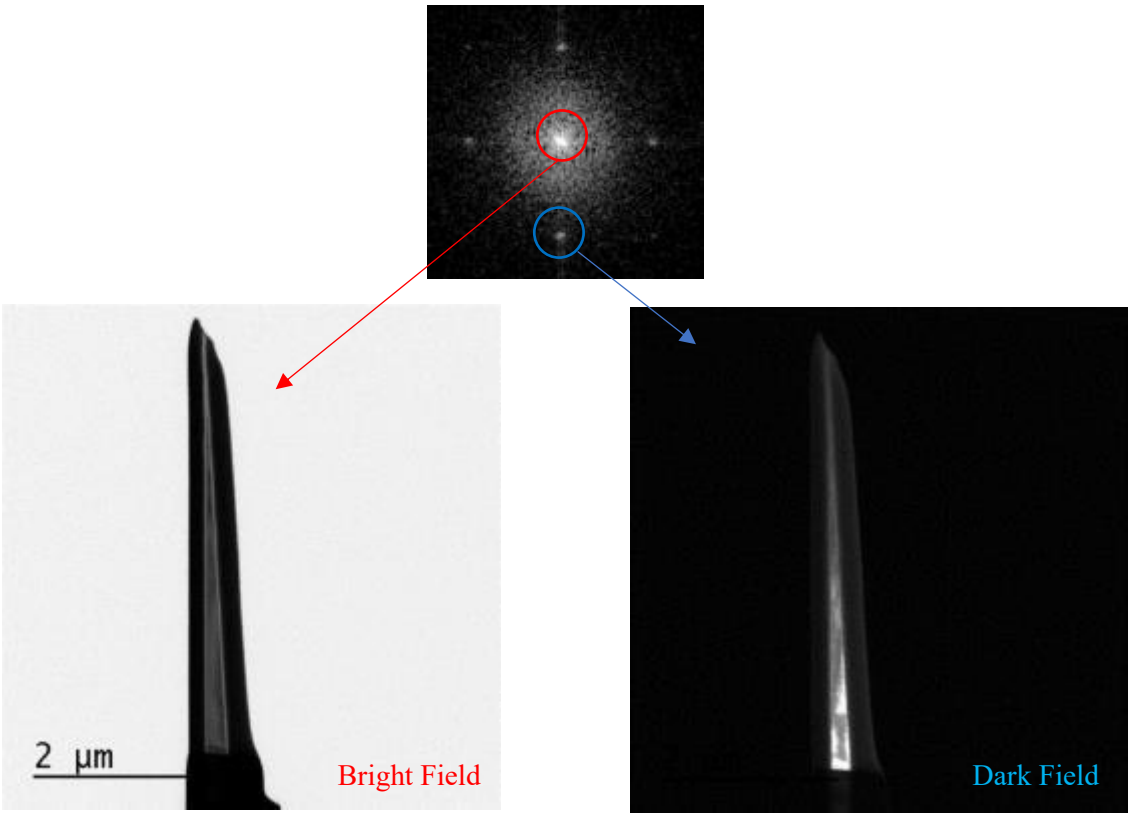

Figure 21: Bright Field mode (with higher contrast) and Dark Field mode

4. Instrumentation procedure

TEM analyses are performed on a Philipps TECNAI (recently ThermoFisher). To obtain the results, we proceed as follows: First the introduction of the lamella in the microscope then the alignments to obtain optimal focus for the acquisition. Finally, both acquisition and the post-processing are done with digital micrograph software (Gatan Microscopy Suit).

1) Assembly operation

For the experiment, a double tilt is used so the sample can be tilted in 2 directions (alpha & beta) allowing to find the zone axis (crystallographic plane normal to the optical axis).

2) TEM manipulation

Selecting the lamella on the grid, it is possible to magnify it keeping a centered e-beam. To improve the imaging, it is important to find both the zone axis and the eucentric position: the sample position where its image projection is exactly on the first image plan. Once found it is still necessary to focus the image and to check the presence of an astigmatism. It is then possible to add apertures to obtain the wanted imaging mode (BF, DF, or just increase the contrast).

3) Post-Processing

After the acquisition, it is necessary to analyse the picture to extract the wanted information. Those manipulations are done with the same software than the shooting one: digital micrograph.

i. Morphological analysis: Amorphization thickness

After differentiating the different part of the picture, the amorphization thickness is measured thanks to the software, as seen in Figure 22. Several measures are done to increase the statistic and to obtain more accurate results.

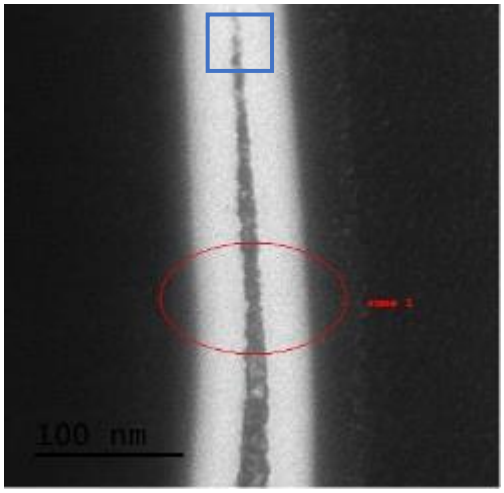

Figure 22: Silicon lamella with amorphization thickness measure with thinning at 16kV

ii. Structural analysis: HRTEM & Fourier Transformation

The Fourier transformation permit to deduce a digital diffraction pattern from a selected area as seen in Figure 23. In the HRTEM imaging, phase difference is visible and can be confirmed by the FT patterns. It allows in case of doubt to settle between monocrystalline (a, c) polycrystalline (b, f) or amorphous (d, e) like in Figure 23.

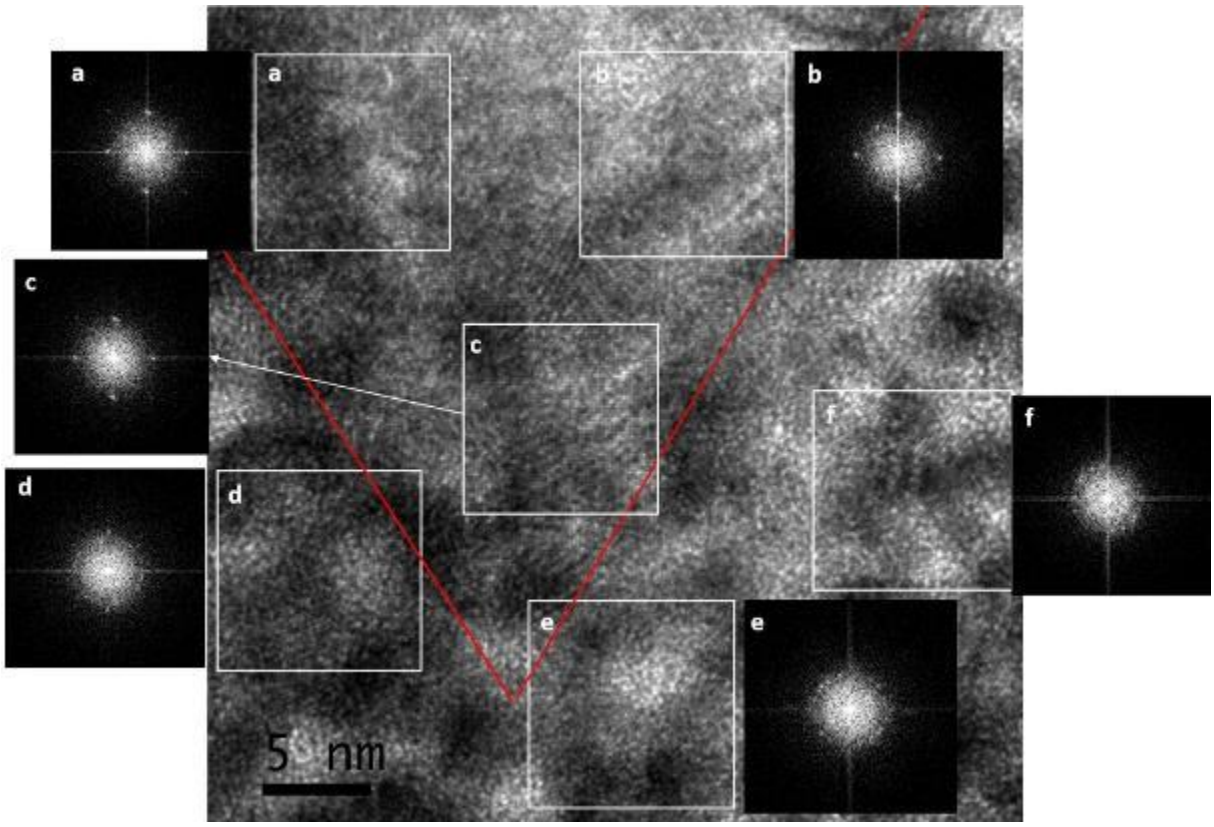

Figure 23:HRTEM of silicon planar lamella (thinning 5kV) with Fourier transformation post-processing simulated patterns on different area

iii. Sample Thickness analysis

Using 2 pictures of the same area, one unfiltered and the other filtered (only selecting the electrons coming from elastic interactions), the software will compute a thickness map (Figure 24A) on which we can extract some profile (Figure 24B). The t-map use a temperature gradient on the t-map to indicate the thickness in a pixel. The profile allows the direct reading of the thickness in an area. The accuracy of the profile is in the software is adapted to the monocrystalline silicon and extrapolate to GST in Annexe 2: Thickness lamella determination and bias.

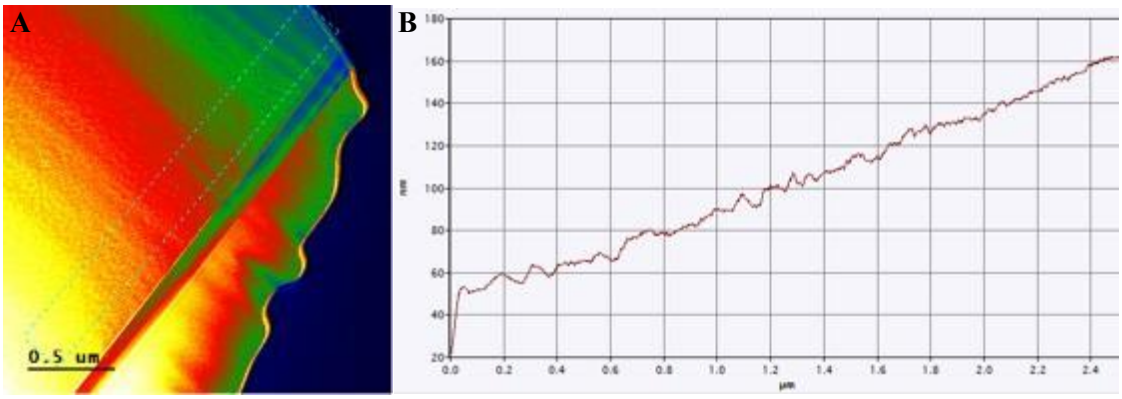

Figure 24: (A) Thickness map 12kx and (B) thickness profile for silicon lamella thinned at 16 keV

C. Simulation

SRIM (TRIM), Stopping and Range of Ions in Matter, is a software that simulates ion-matter interaction. Its calculation system is based on the Binary Collision Approximation method, which is itself based on the Monte Carlo method. The material is simplified as an amorphous. The path of the ions in the material between each impact is considered straight. The ion then loses its energy by colliding with the atomic nuclei composing the material.

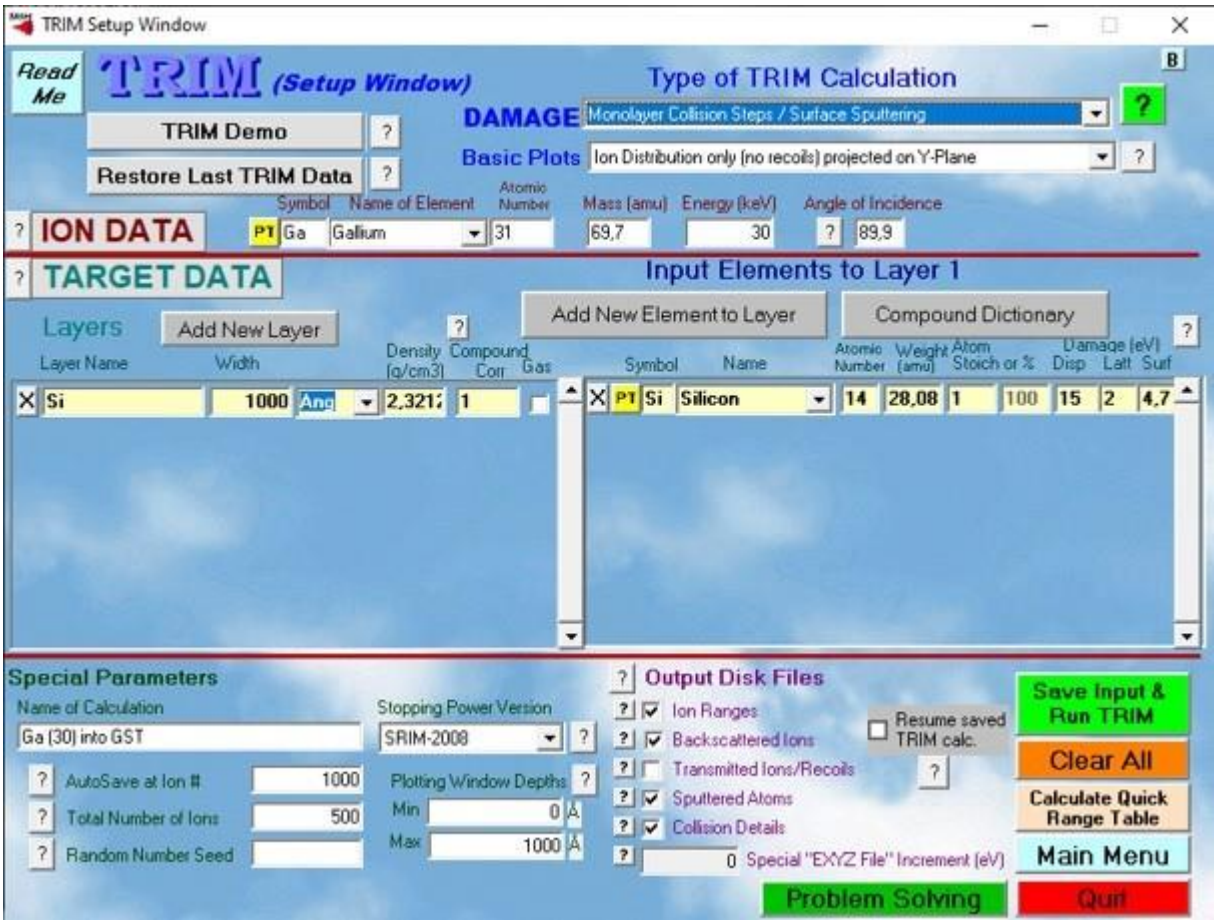

Figure 25: Setup window of the TRIM simulation for a grazing gallium ion beam at 30 keV on silicon (d=2,3212 → monocrystalline density approximation)

As in the setup window Figure 25, The software is used in Sputtering mode to get closer to dual-Beam conditions. The beam used is defined by its acceleration energy, angle of incidence and composition. The target material is then defined by describing its composition/stoichiometry and density. Once the simulation is done, you get different information:

- Ion Range IR {x% Ga} or depth (x) limit crossed by less than (100-x) % of Gallium ions.
- Projected range corresponds to the average path of ions in the material projected on x(deep) and y (surface).

The method projected range is directly given by the software. However, the ion ranges IR {x% Ga} and need a data post-processing explained in Annexe 3: Calculation of IR {x% Ga}.

III. Protocole

To study the experimental impact of the ion beam thinning a specific protocol is applied.

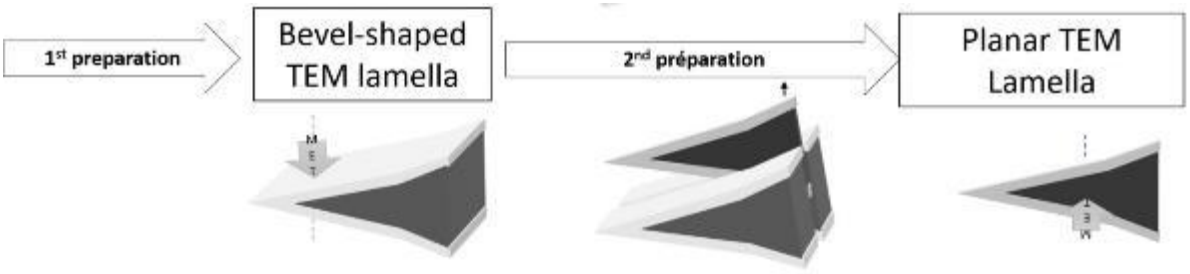

Figure 26: Lamella preparation for the characterization of the ion beam impact.

At first, a bevel-shaped lamella is made (Figure 26A). Its extraction is like the Lift-out technics.

However, during the polishing the lamella is thinned with a bevel-shape and different thinning energy are used, from 30 keV down to the desired acceleration energy (16, 8, 5 keV etc.). The lower energy beams reduce the amorphous layers induced by the previous beams. The preparation of the bevelled lamella allows the preservation of the crystalline lattice in function of the thickness of the lamella.

After a first raw of analysis, the bevel-shaped is covered with a protective layer. It will ease the second preparation, but also protect layer damaged by the first preparation. This way the second preparation will not have an impact on the measures.

Once protected, a planar lamella is extracted from the bevel-shaped lamella. It is done by cutting through the bevel, perpendicular to the bevel as seen in Figure 26B. It makes it possible to obtain a "transverse" section (Figure 26B, Figure 27) of the former lamella and thus to measure directly the amorphous and crystalline phases.

The planar lamella is analysed by EDX (compositional analysis to determine the gallium penetration. Then it is analysed by conventional TEM (morphological analysis) and HRTEM (structural analysis) to study the amorphized layer.

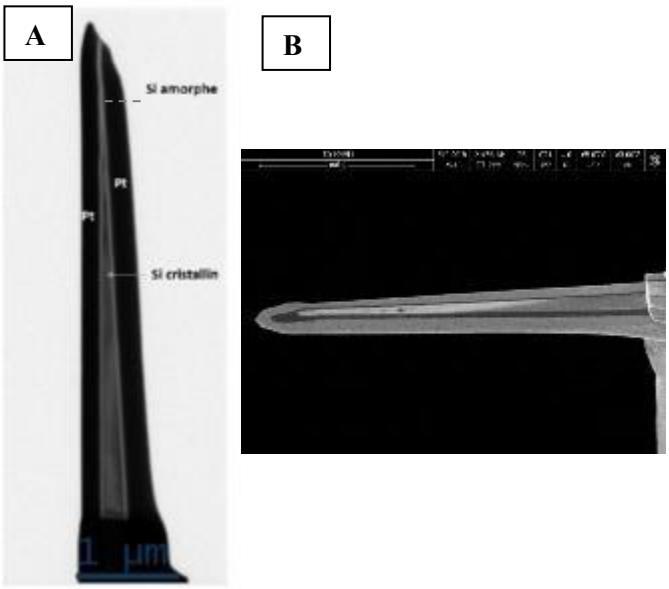

Figure 27: (A)TEM and (B)SEM imaging of a planar lamella

IV. Protocol validation: a study on the monocrystalline silicon

At first, a study on the monocrystalline silicon is carried out to determine the thickness of amorphous generated by the Ga + beam. The method explained before is used on all the lamella to determine its efficiency. In parallel, SRIM simulations are done to know the impact of the beam on the material. Those determine the possible link between the simulated ion penetration and thickness of the amorphous layer created. All those results are compared to the usual values used in the field presented in Table 1. [5-8]

Acceleration tension	*30 keV*	*16 keV*	*5 keV*	*2 keV*
Amorphous Layer Thickness	18-25 nm	14-18 nm	4-6 nm	3-4 nm

Table 1: Experimental amorphization values of silicon extracted from bibliography [5-8]

A. TEM analysis:

The bevel-shaped lamellas are made from the wafer, bulk monocrystalline silicon with a [110] growth orientation. They are thinned in bevel with different acceleration tension like explained previously.

Three different lamellas are done

- 30 keV
- 30keV, 16 keV (named 16 keV)
- 30 keV, 16 keV, 8 keV then 5 keV (named 5 keV)

These lamellae are quickly analysed to determine their quality and then they undergo the second preparation to extract the associated planar lamellas.

During the second the 30 keV is protected by a protective layer of carbon before the platinum (electronic and ionic) deposition. The other lamellas have a direct contact between the silicon and the electronic platinum.

Once all preparations are done, the planar lamellas are analysed by EDX to determine the Gallium penetration thanks to a STEM (Osiris) and by a TEM to measure the amorphous layer.

1. Impact of the 30keV thinning

First, the composition analysis is conducted to determine the experimental gallium penetration in the silicon. The results of the EDX analysis are presented in Figure 28.

The composition map obtained thanks to the EDX marks the presence of oxygen in yellow, gallium in blue and silicon in pink. Other atoms are present, but we choose to concentrate only on those. The silicon lamella in pink the middle is surrounded by an oxide layer indicated by the important presence of oxygen in yellow. It also presents an external layer with an important concentration of gallium ion; this layer is due to the gallium penetration during the first preparation. However, gallium atoms are visible on the whole map. Those are the results of the second preparation: the ion beam was also used (at extremely low acceleration tension) but some equally on the whole sample surface.

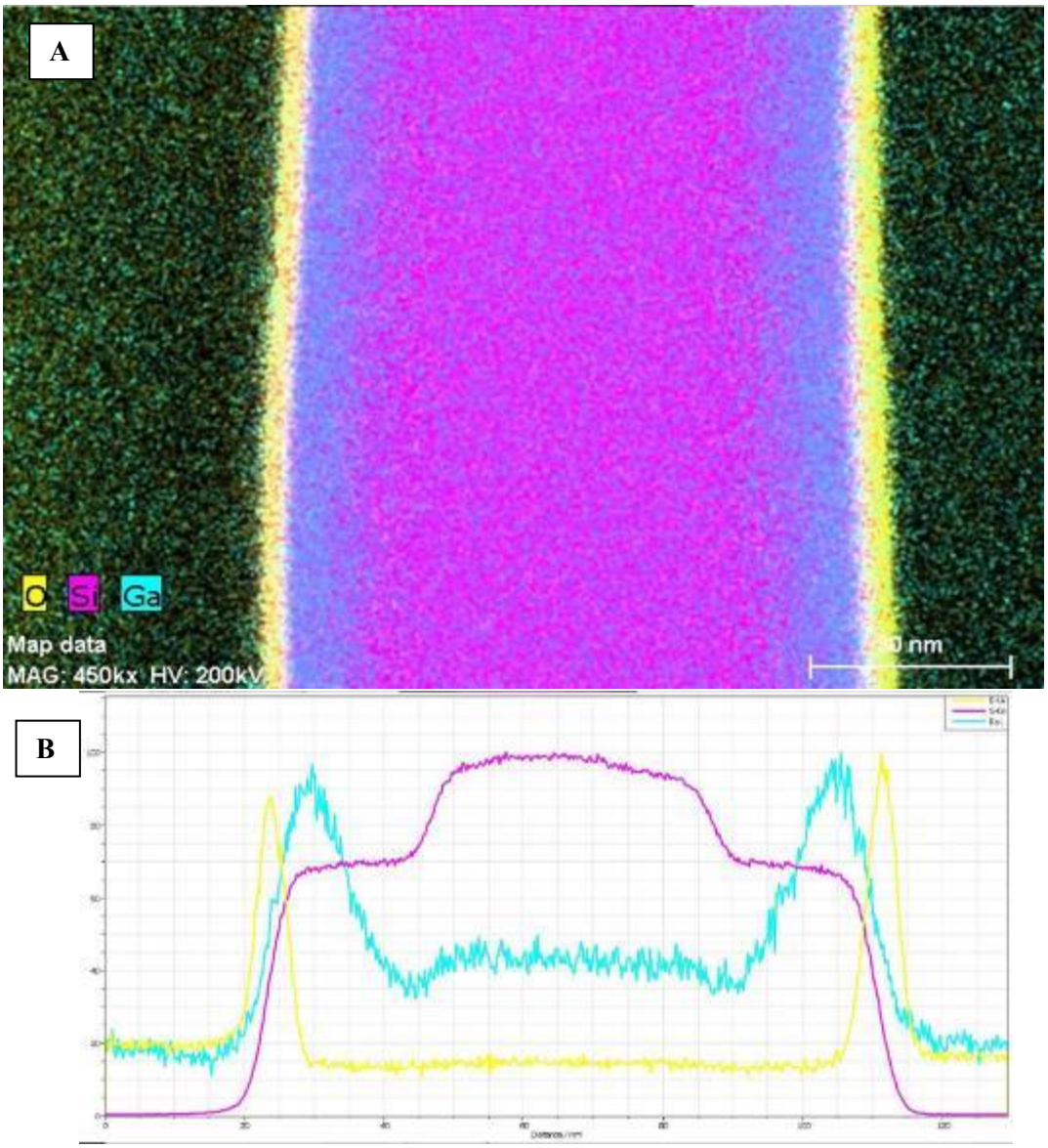

Figure 28: EDX analysis of the Monocrystalline silicon thinned at 30 keV (A) Composition map and (B) Composition profile

To have a better resolution to measure the gallium penetration the composition profile is drawn the same color-codes are used for the oxygen, the silicon, and the gallium than in the composition map. The limits of the silicon lamella are there more defined in between 20 and 115 nm. Thus, the oxidate part seems to be external to the silicon, certainly in the protective layer. The gallium penetration is similar on each side of the lamella (symmetrical aspects of the gallium plot). The gallium penetration is around 21-22 nm. Also, in the silicon plot shows that on the side of the lamella there seems to be a lower quantity of silicon. This is a mark for the same material of an amorphous part on the sides (lower density) but crystalline in the middle (higher density). This variation happens at the same place than the gallium penetration.

Then the lamella was analysed with a conventional TEM to observe and measure the amorphized layer. The photos are shown in Figure 29 for both conventional TEM (A-B) and high resolution (C).

In photo (A), the bevel is covered with protective platinum in black and a layer protective carbon in light grey, surrounding the silicon. A zoom (B), done at the level of the indicated by the square (A), shows different layers: the protective platinum, the carbon deposit in contact with the silicon, and finally a layer of silicon, grey for the amorphous layer, dark grey for the crystalline phase in its centre. This makes it possible to distinguish a first crystal located 2 microns away from the end of the lamella where the thickness is around 50 nm. The lamella has a very stable amorphous thickness measuring on average 22 nm. The high-resolution image (C) makes it possible to confirm the appearance of the first crystal measuring 5 nm in thickness. Thanks to FFT pattern, it is possible to confirm that the phases detected are the crystalline silicon [110] surrounded by the amorphous phase.

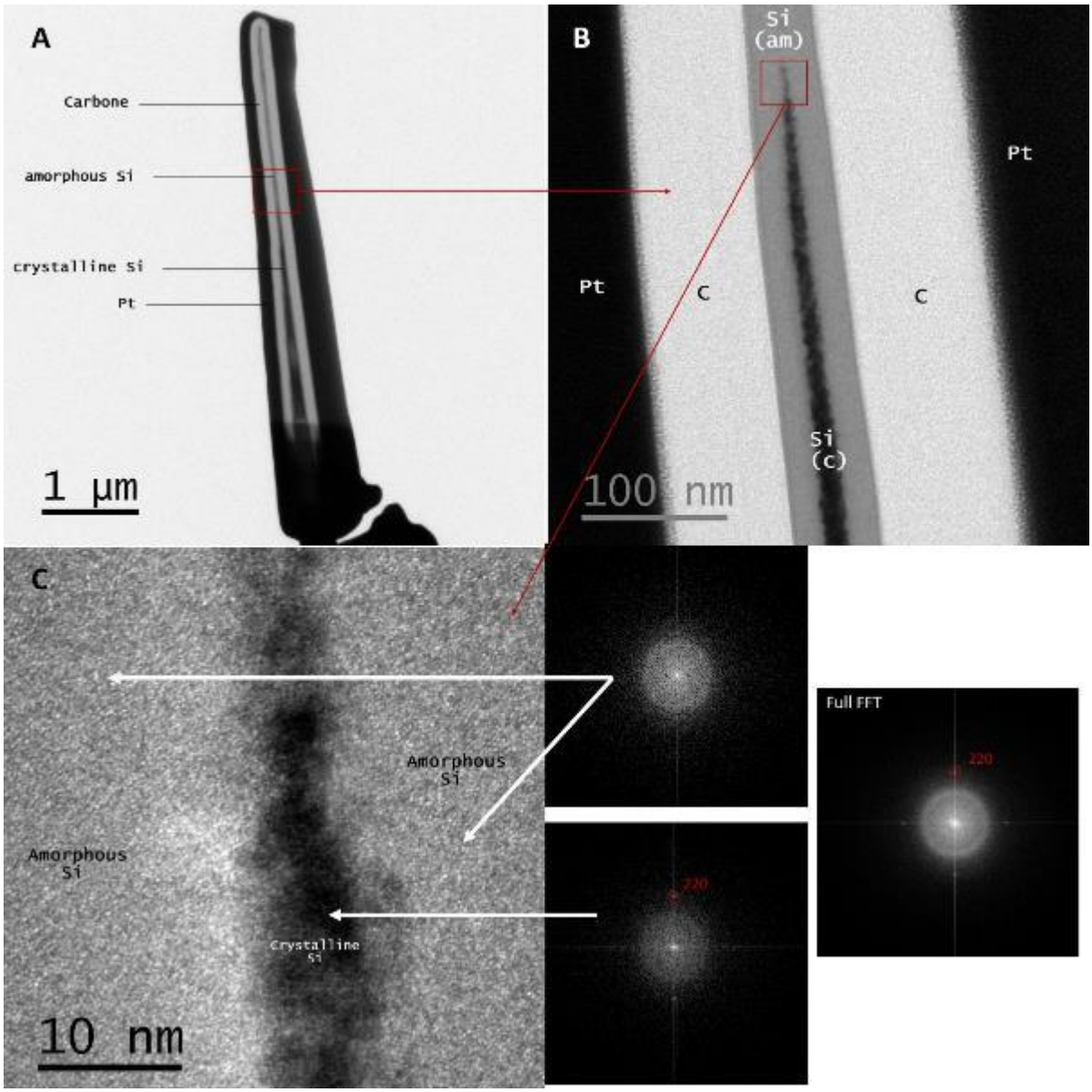

Figure 29: Analysis of the 30keV silicon lamella in (A-B) conventional microscopy and (C)HRTEM with the associated FFT pattern.

The measure of the amorphous layer by TEM and HRTEM (22 nm) is equivalent to the measure of the gallium penetration (21nm-22nm). Therefore, it seems that the gallium penetration is directly linked to the thickness of the amorphous layer.

2. Impact of the 16 keV thinning

The thinning at 30 keV and then 16 keV is analysed first by EDX there also to determine the gallium penetration. The extracted composition profile is presented in Figure 30.

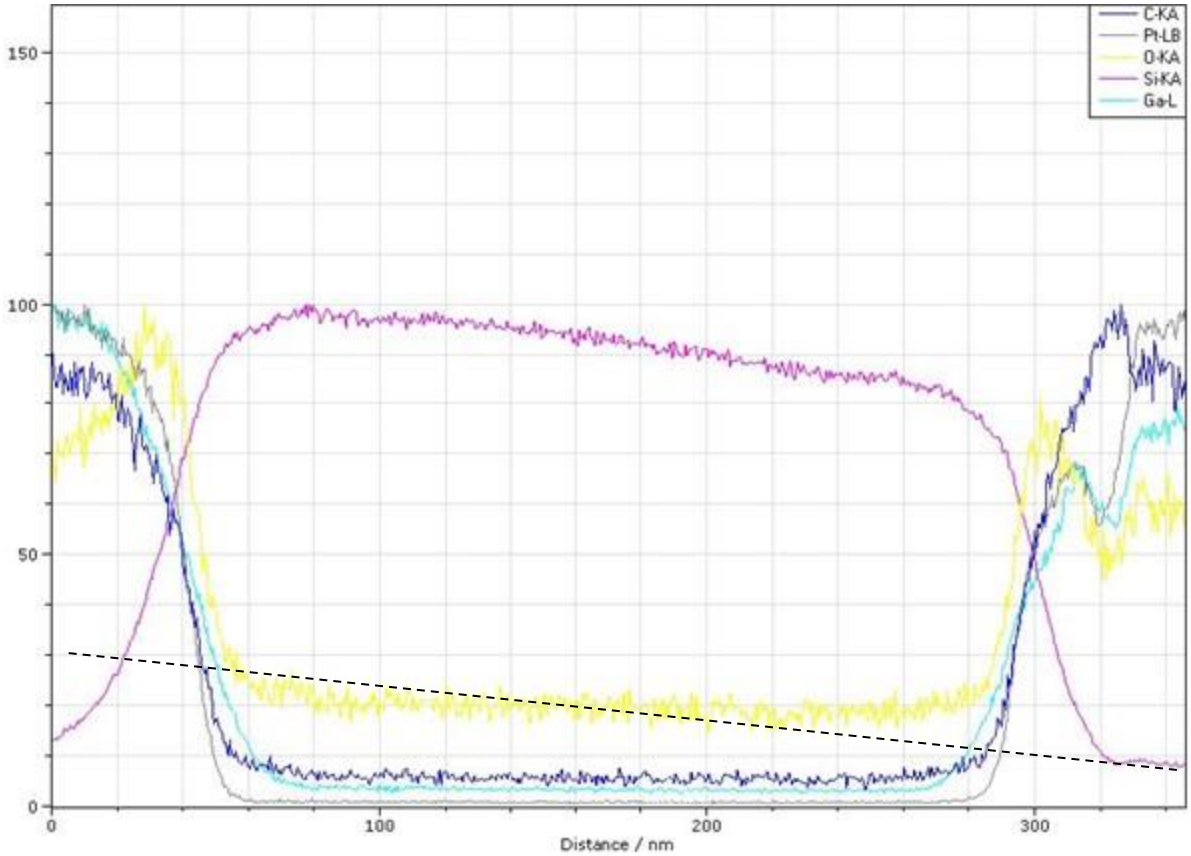

Figure 30: EDX profile on the planar lamella with a thinning down to 16 keV silicon

The profile follows the evolution of Carbon (dark blue) Oxygen (yellow) Platinum (Grey) silicon (Pink) and Gallium (Blue). Contrary to what was observed with the 30keV thinning, the plot is asymmetric. The silicon lamella seems to be contained between 20 and 320 nm. A thin oxidized layer seems to be present on it. The gallium penetration seems thus to be between 30 and 35 nm.

This result is aberrant compared to the previous observation with the 30 keV lamella. Indeed, the gallium penetration for 16 keV seems to be 10 nm superior to the one observed for 30KeV. To get a better idea of the situation, an observation by conventional TEM is done. The results of the analysis TEM (A-B) and HRMET (C) are presented in Figure 31.

In photo (A), the bevel is covered with protective platinum in black surrounding the silicon. A zoom (B), done at the level of the indicated by the square (A), shows different layers: the protective platinum, and a layer of silicon, grey for the amorphous layer, dark grey for the crystalline phase in its middle. The first crystal located 0,8 microns away from the tip of the lamella where the thickness is around 60 nm. The lamella has a very stable amorphous thickness measuring on average 30 nm which corroborate the previous observation. The amorphous layer is too thick especially compared to the consensus (around 16 nm). There could be an explanation of this in the preparation process.

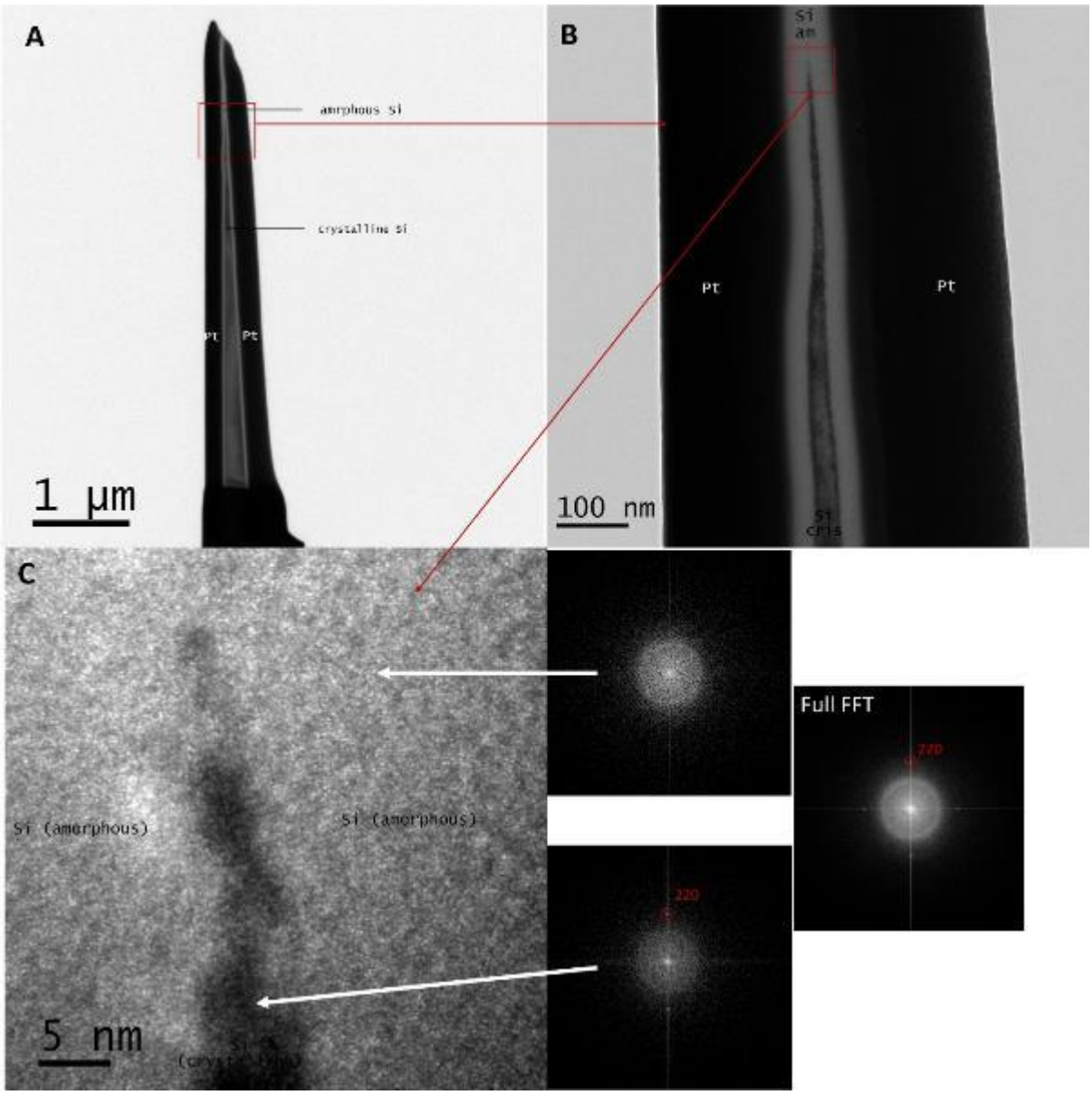

Figure 31 : Analysis of the 16keV silicon lamella in (A-B) conventional microscopy and (C)HRTEM with the associated FFT pattern.

The platinum deposition is done in 2 steps: first the electronic deposition and then the ionic deposition. The platinum comes from an organic molecule. Under an electronic or ionic beam, an organic molecule is polymerized and destroyed leaving only the platinum (and some impurity like gallium, Carbone, or Oxygen). The energy of the ion beam to do the deposition also has an impact on the material, especially since the ion beam has a higher energy than 30 keV. To cushion that effect, the electronic platinum is deposited before the ionic platinum deposition. However, it seems that in this case, electronic deposition was too thin and thus could not absorb the full impact of the ionic deposition. This explains why a thicker amorphous layer is measured.

This second preparation is thus a critical step for the analysis. Besides the electronic platinum, an inner carbon deposition seems to be necessary, like it was done for the 30 keV. It would also help to distinguish better the interface between the amorphous and the protection layer.

Even if the results are aberrant it is noteworthy to know that there also the gallium penetration and the amorphous layer where equal.

3. Impact of the 5 keV thinning

There also the EDX analysis was conducted on the lower part of the lamella. The extracted profile is presented in the Figure 32.

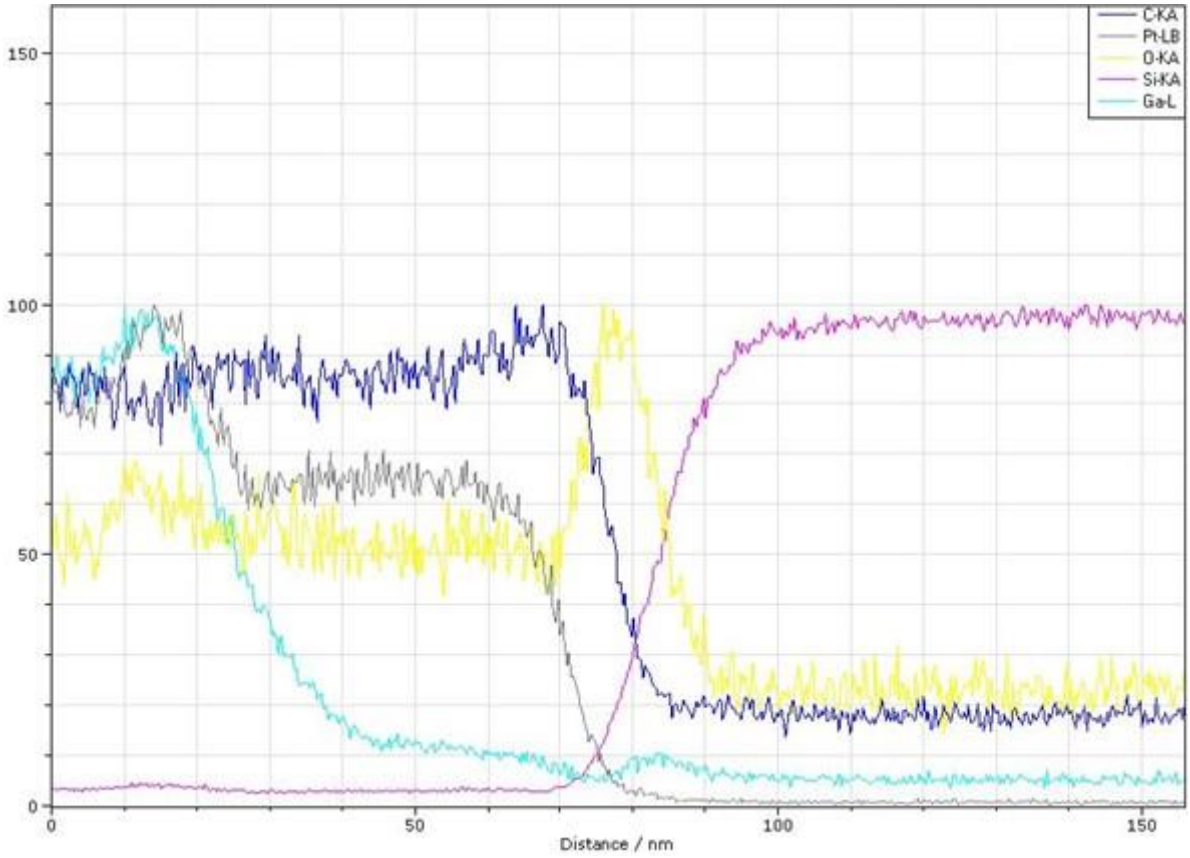

Figure 32: EDX profile of the side of a silicon lamella thinned down to 5 keV

The profile follows the evolution of Carbon (dark blue) Oxygen (yellow) Platinum (Grey) silicon (Pink) and Gallium (Blue). The silicon lamella appears on one side at 80 nm. The gallium plot follows almost no variation however a low augmentation can be seen between 80-90 nm. This variation, compared to the other lamella, is negligible and it seems that no conclusion can be drawn from this analysis.

A coupled analysis between EDX and STEM imaging is presented in Figure 33. It allows us to differentiate the different phases in the lamella. The analysis indicates a significant presence of carbon between the platinum and the silicon (in red in Figure 3A) that could easily pass as amorphous silicon. To study the interface, it was analysed with a higher magnification by EDX (3C). This makes it possible to see, in between the carbon and the silicon layer, a layer of SiO of 3 nm. This layer matches the 4 nm amorphous layer detected in high resolution (3C and 3D). Thus, it seems that the amorphized layer is not composed of silicon but of silicon oxide. The oxidation must have happened during the first TEM checking on the bevel-shaped lamella after the first preparation.

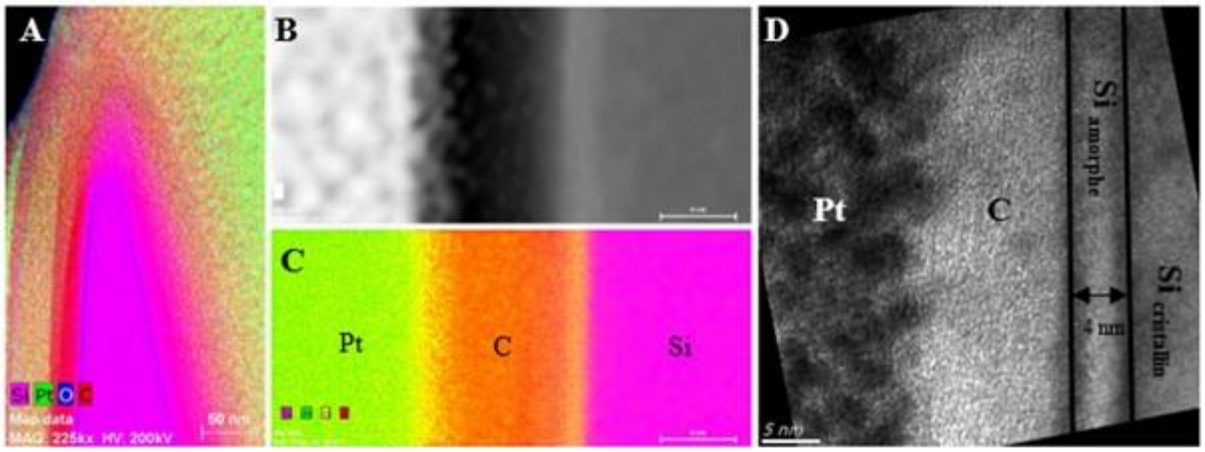

Figure 33: EDX analysis and STEM imaging of the higher part of the lamella 5keV silicon

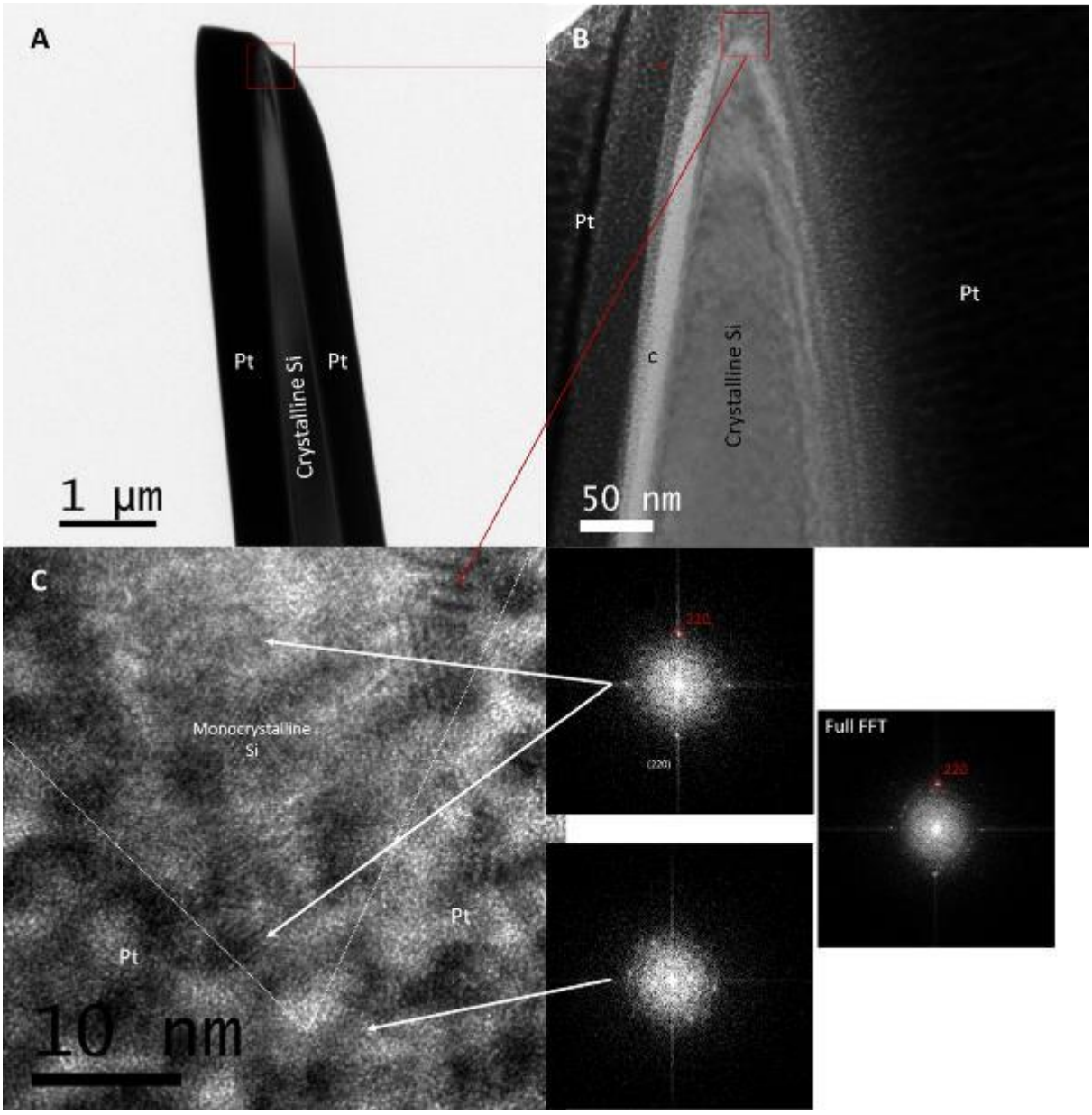

Figure 34 : Analysis of the 16keV silicon lamella in (A-B) conventional microscopy and (C)HRTEM with the associated FFT

The TEM (A-B) and HRMET (C) analysis of the bevel thinned at 30, 16, 8 then 5keV are presented in Figure 2. In photo (A), the monocrystalline silicon bevel appears to be uniformly coated by the protective platinum layer in black without being able to discern any amorphous zone. The bevel point zoom (B) also makes it possible to distinguish the platinum (black) layer from the crystalline silicon layer. An intermediate amorphous layer of carbon is present between the platinum end the silicon. It was already observed by EDX (see Figure 33), confirming its composition. This layer is due to the previous analysis of the bevel-shaped lamella. Indeed, the observation by TEM with a high tension tend to leave a layer of carbon.

In high resolution (Figure C), the extreme tip of the bevel shows a fully crystalline phase (<1nm from the tip) confirmed by FFTs. The phase bordering on the tip corresponds to amorphous / polycrystalline platinum (see FFT). The tip, therefore, appears to be devoid of the amorphous layer. It seems that the amorphous part fused with the platinum deposit during the second preparation, and therefore is not be discernible on its own.

B. Amorphous ratio

1. Form impact

The evolution of the percentage of the amorphous phase in function of the lamella is presented in Figure 35. According to the literature, the thickness of amorphization is independent of the thickness of the lamella. Thus, a second curve is calculated according to this assumption. We are interested to see if the shape of the lamella could have an impact on this assumption.

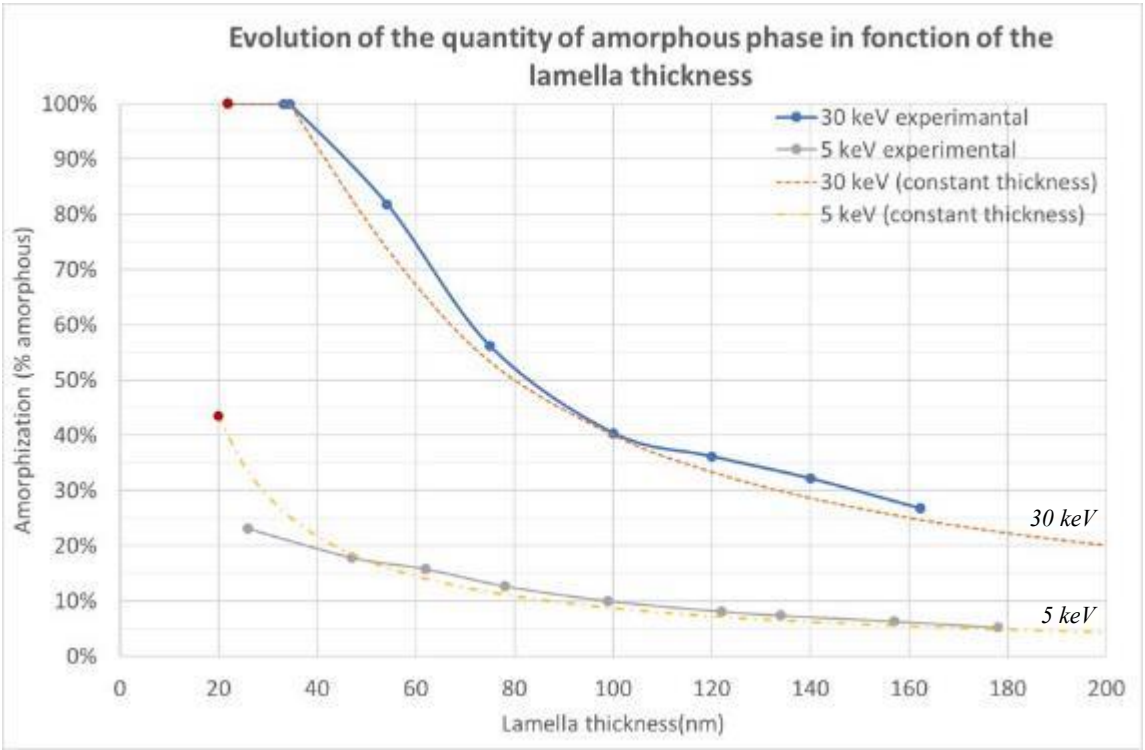

Figure 35: Evolution of the amorphous ratio according to the thickness of the lamella for a 30 keV and 5 keV thinning (solid line) and the curves assuming constancy

The 30 keV lamella does not exceed 160 nm thick. On this interval, the experimental curve and the one supposing thickness consistency are similar. Both have a complete amorphization up to 35-40 nm thick,

and then the amorphous ratio decreases significantly: from 40% amorphous for 100 nm thick to 20% amorphous for 200nm.

The "pseudo theoretical" and experimental curves of the 5 keV lamella also follow a similar trend from 40 nm lamella thickness. The measure of the amorphous layer up to a lamella thickness of 20 nm are not used because it was impossible to discern an amorphous area even on high-resolution images (Figure 34C). Starting from 20 nm, the "pseudo theoretical" curve precedes a significant decrease in the amorphous percentage from 45% amorphous to 15% for 60 nm. Subsequently, the curves slowly decrease from 20% to 10% amorphous between 40 and 100nm before reaching a 5% amorphous plateau from 120 nm lamella thickness.

Therefore, the form of the lamella does not impact the results, by not respecting the constancy, for both high and low acceleration tension.

2. Acceleration tension impact

The energy of the beam, or the acceleration tension, used to thin the sample is the most important aspect to play with for the obtention of a high-quality lamella. The following chart shows the evolution of the amorphous (yellow) and crystalline (blue) ratio depending on the thinning (low and high energy).

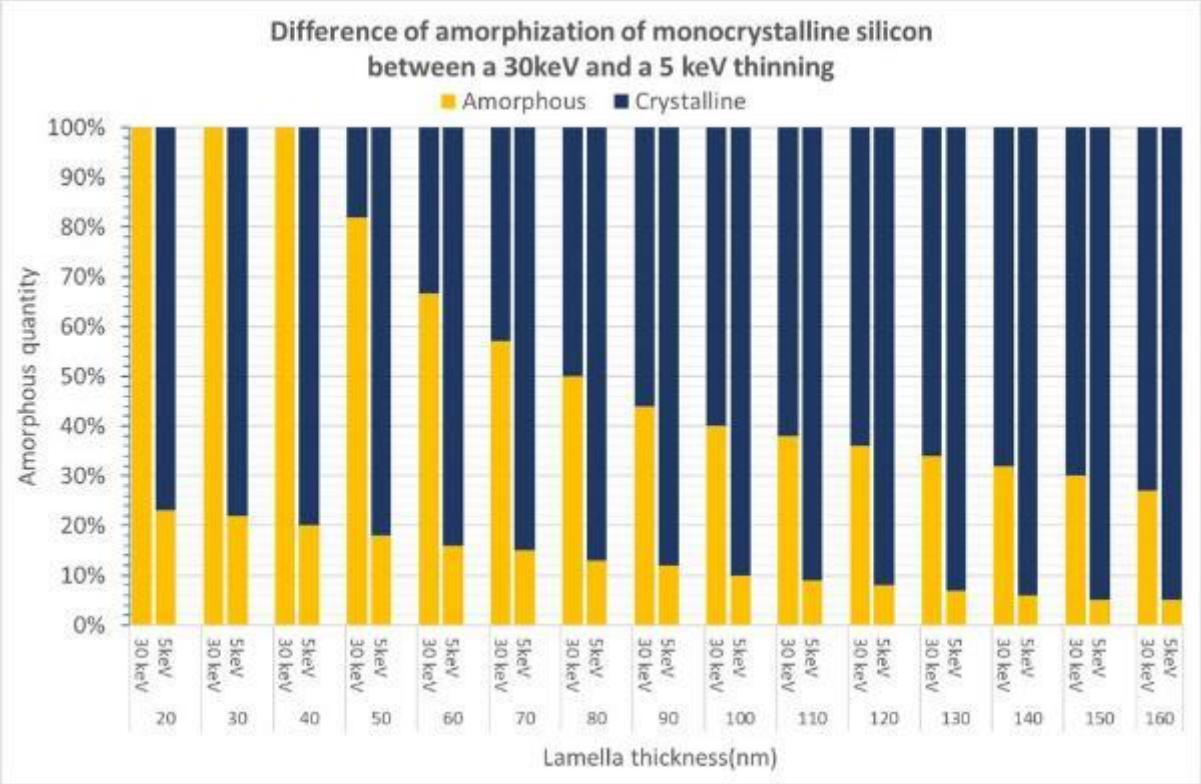

Figure 36: Comparison of the impact of a thinning at 30 keV and of a thinning done to 5 keV

Overall, comparing the 30 keV and 5 keV, it confirms that the 5 keV beam has a far less destructive effect than the 30 keV beam. Indeed, the remaining amorphous percentage following cleaning by the 5 keV beam is overall 4 times lower than the percentage generated by the 30 keV beam.

This confirms that the 5 keV beam amorphizes on a thinner layer than the 30 keV beam, around 4 times less.

3. Thickness impact

The size amorphous layer is independent of the thickness. However, the thickness of the lamella as an impact on the ratio of the lamella. The following bar chart shows the impact of the thickness of the lamella. This ratio is an important criterion for the quality of the analysis.

As an example, in the case of a thin lamella, between 40 and 60 nm, those prepared at 30 keV will keep a crystalline phase of between 10 and 30%. On the contrary, these same samples refined with 30 and the 16, 8 and 5 keV will have between 75% and 80% crystalline. In the case of normal lamella refined between 80 and 110 nm, the lamella with a preparation of 30 keV will have between 50 and 60% crystal, while the lamella refined by beams 16, 8 and then 5 keV present around 90% crystal. The thickness of the lamella has thus a lower impact on the lamella quality for low energy beam polishing.

Also, the analysis of thin lamella requires a preparation with polishing at extremely low acceleration tension. However, if an analysis requires thicker lamella (>120 nm) a preparation with a 30keV ion beam is sufficient.

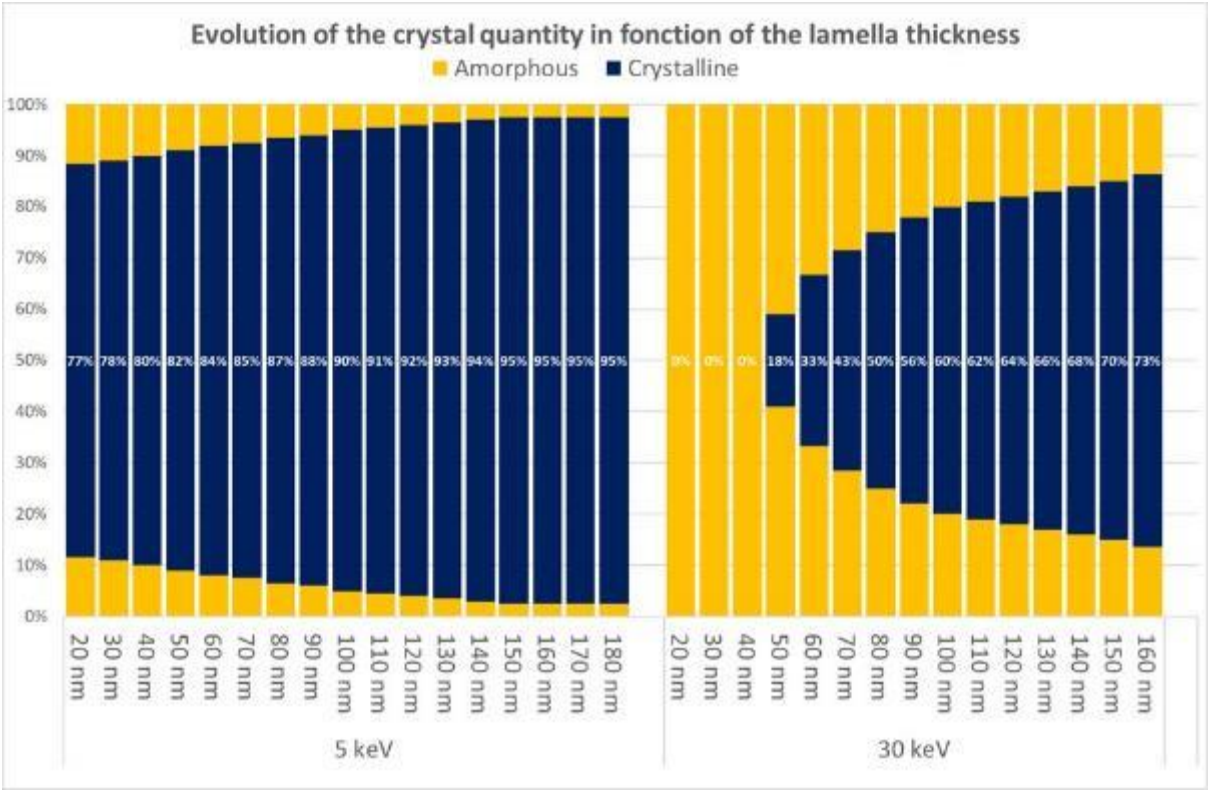

Figure 37 : Impact of the lamella thickness for both a 30 keV and a 5 keV thinning

In conclusion, the impact of the lamella shape on the analysis of the results is negligible. The impact of the 30 keV beam is four times superior to the 5 keV. Thin lamellas will require to a 5 keV polishing to have an acceptable crystalline/amorphous ratio. However, for thick lamella that polishing may not be necessary

C. SRIM Simulation

The interaction between the ion beam and the monocrystalline silicon is simulated by SRIM for single Gallium beams with acceleration energies of 30, 16, 8, 5 and 2 keV with a grazing angle (angle in SRIM 89.9 degree). Figure 38 summarizes all the results obtained and compares the results from the literature as well as the results obtained by the TEM analysis. The values found in the literature are represented by the green bar diagram. The results of the TEM analyses, in red, are also in agreement with these (except in the case of 16 keV). The SRIM software can determine the path of ions in the matter. The impact of these ions on the crystalline network can cause amorphization.

Therefore, we will assume a direct link between the penetration values of the ions and the amorphization created by them (like it was observed experimentally). All values used are averages, which makes it possible to ignore the number of incident gallium ions. So, we can compare the amorphous layer to the values derived from SRIM. However, the acceleration tension is not the only impact, in fact, a polishing time needs to be considered. For a same probability of depth penetration, the longer is the polishing the more there will be ions penetrating ions in the materials and thus the thicker will be the amorphous layer. That is why the ion range x% is used, it allows to say for a specific preparation the equivalent ion penetration (quantity of ion assimilated to the impact on the network).

The data extracted from the simulation are IR {50%}, IR {75%}, IR {90%}, IR {95%}, IR {99%}, IR {100%} and the projected range. The simulation giving a good approximation of what is observed are IR {90%}, IR {95%}, and the projected range.

For strong acceleration currents, the IR {95%} allow for a good approximation of amorphous thickness. However, for lower energy beam, the most adapted simulation is IR {90%} and the projected range. This difference seems quite small (2-3 nm) but represents a 30% error. The projected range there also allows a good approximation, like the IR {99%}.

D. Conclusion

The amorphous layer created by the first preparation on the monocrystalline silicon appeared clearly thanks to the TEM analysis both conventional and high resolution. The layer was fully amorphous and its thickness directly dependant of the acceleration tension used as the last polishing step. This layer is also equivalent to the gallium penetration measured thanks to EDX.

These results agree with the literature and correspond to the IR {90%} and IR {9%} (equal to the Projected Range) resulting from the SRIM simulations. Thus, for the silicon material, it is necessary to carry out various refining steps while reducing the energy of the ion beam to preserve the crystalline system.

However, it is noted that the second preparation is a critical step, both for the bias observed with the 16 keV analysis and for the new gallium implantation. The addition of carbon seems therefore necessary to avoid damages and will allow a better contrast between the lamella and its protection. With these issues in mind, the protocol can be applied to GST with minimal error.

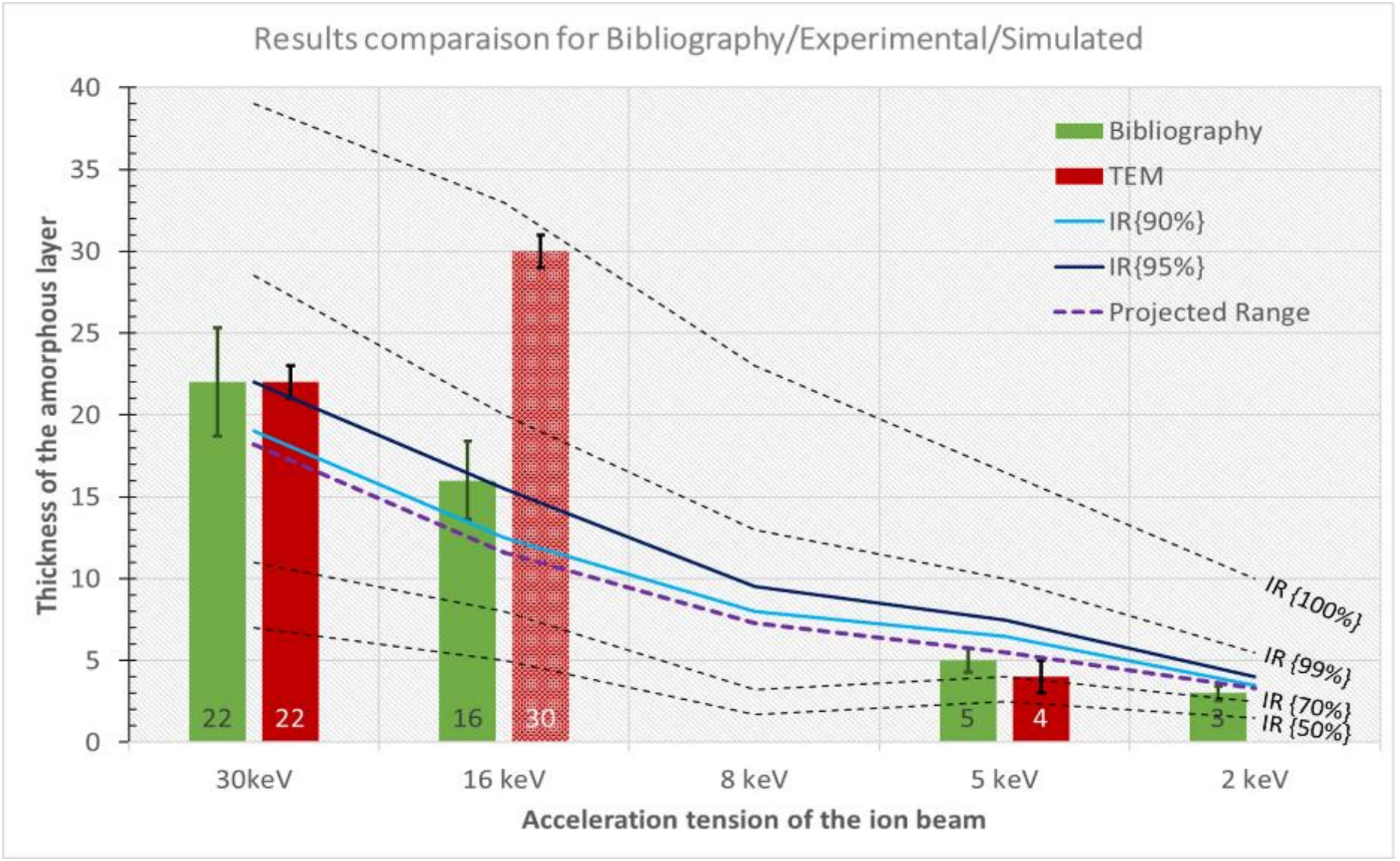

Figure 38 : Comparison of the results obtained by simulation to the experimental results and to the bibliographic values

V. Application on the $Ge_xSb_yTe_z$

The protocol to measure the impact of the FIB on a lamella has been checked thanks to the study on the monocrystalline silicon. It is thus possible to do this study on the $Ge_2Sb_2Te_5$ enriched in germanium and expect significant results.

The GST is constituted by germanium antimonies and tellurium, which if they have different atomic mass are neighbour in the atomic table (see Figure 39). Similar comportment to silicon is thus expected.

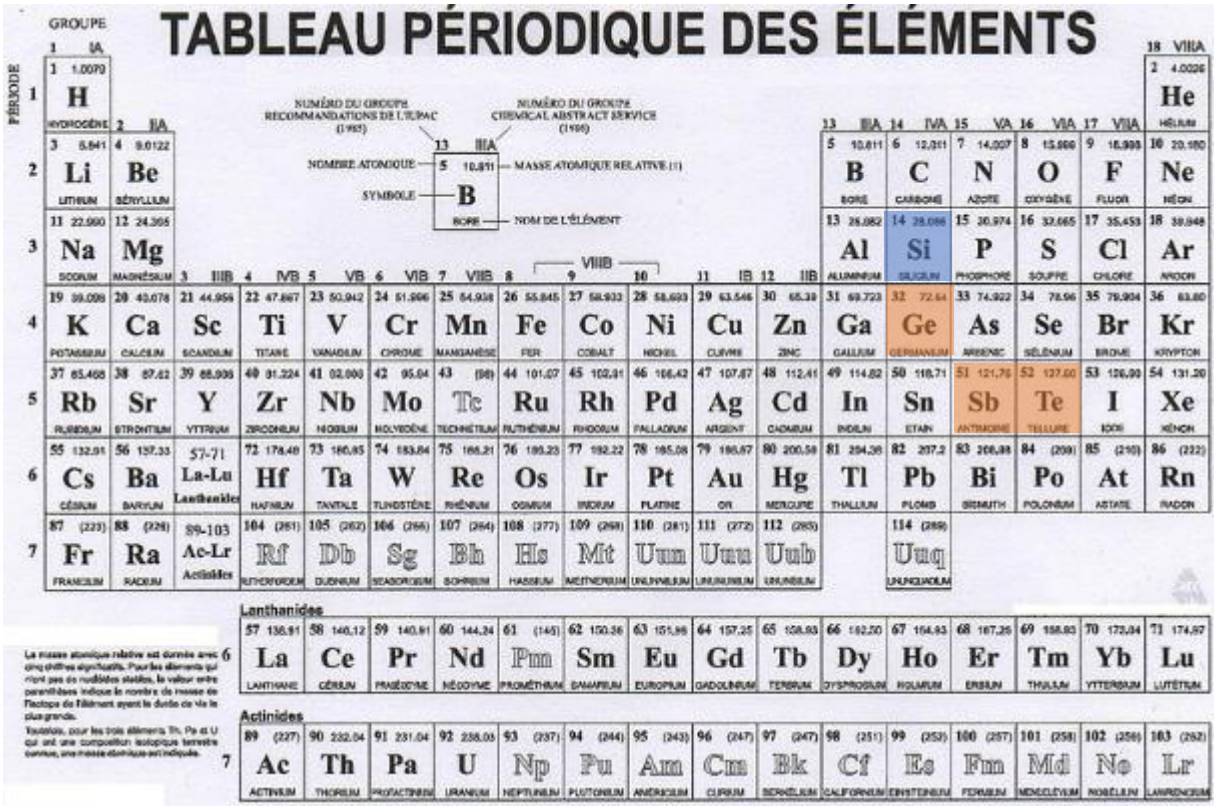

Figure 39: Periodic table of elements (Wikipedia)

Another difference that may have an impact on the results is the polycrystalline aspect of this material. Especially since, as visible in the phase map in Figure 40, the material is inhomogeneous. It is composed by both germanium crystals and GST crystals (both with FCC structure) without any preferential crystal orientation.

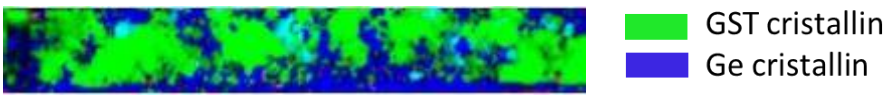

Figure 40: Phase mapping of the GST enriched in germanium used at STMicroelectronics (ASTAR Analysis)

However, similar results to silicon are expected especially with high energy beam: clear and homogeneous amorphous layer, stable measures, ion penetration equivalent to the amorphous layer…

A. TEM analysis

For reasons of times, only the 30 keV preparation was studied. Since it is the highest acceleration tension used for the polishing, it can be considered as a 'critical' preparation and should give a good idea of the impact at lower energy. The bevel-shaped lamella is not like with silicon extracted from bulk but contains a unique line (100 nm thick) of GST. The planar lamella is thus extracted from this precise part and may contains Silicon (the substrate) or TiN (the top electrode) since this two layers are in contact with the GST (see Figure 41). The planar lamella extracted is presented in Figure 42. Its polycrystalline GST is protected by both an outer Platinum layer and an inner Carbone layer.

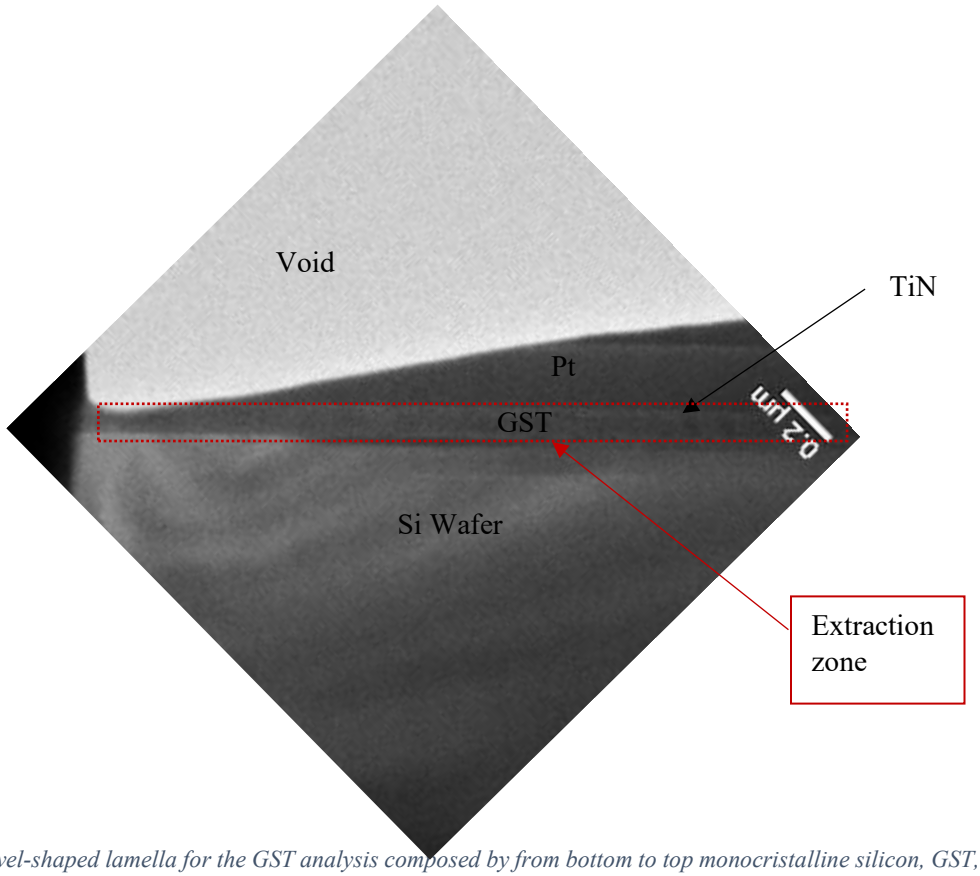

Figure 41: Bevel-shaped lamella for the GST analysis composed by from bottom to top monocristalline silicon, GST, TiN, Platinum

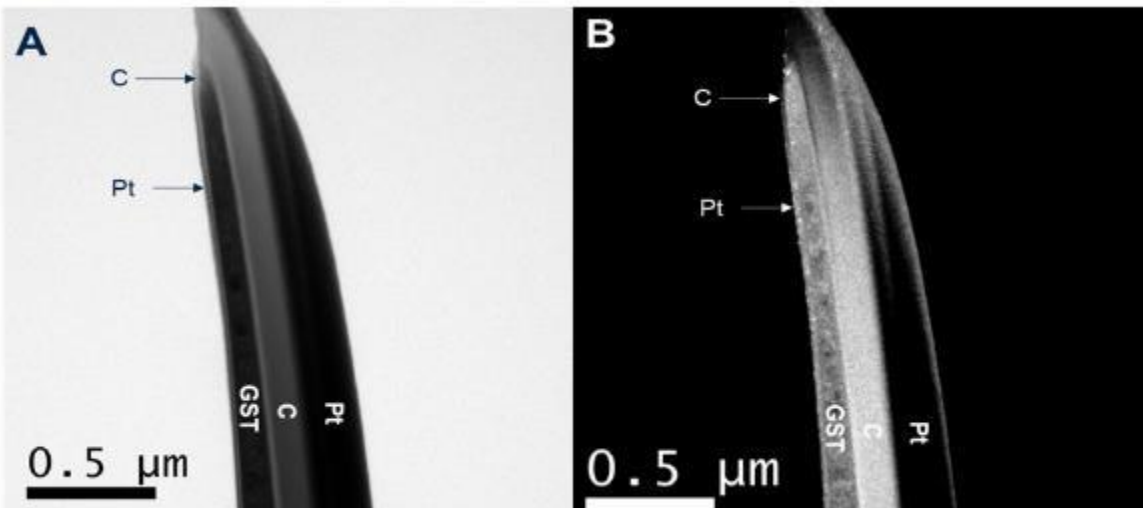

Figure 42: Planar lamella of GST thinned at 30 keV extracted from a bevel-shaped lamella similar to Figure 41 (A) Bright Field and (B) Dark Field

1. Composition analysis: EDX analysis

The EDX analysis is conducted on the lower part of the planar lamella presented in Figure 42. Figure 43 presents the EDX analysis of the planar lamella protected by a layer of carbon and platinum (A).The EDX mapping (B) confirm that the GST used is composed of homogeneously GST crystals (Te-Ge yellow) and Ge crystals (Ge blue).

The Gallium composition map is not shown there, the composition map is not conclusive. However, the

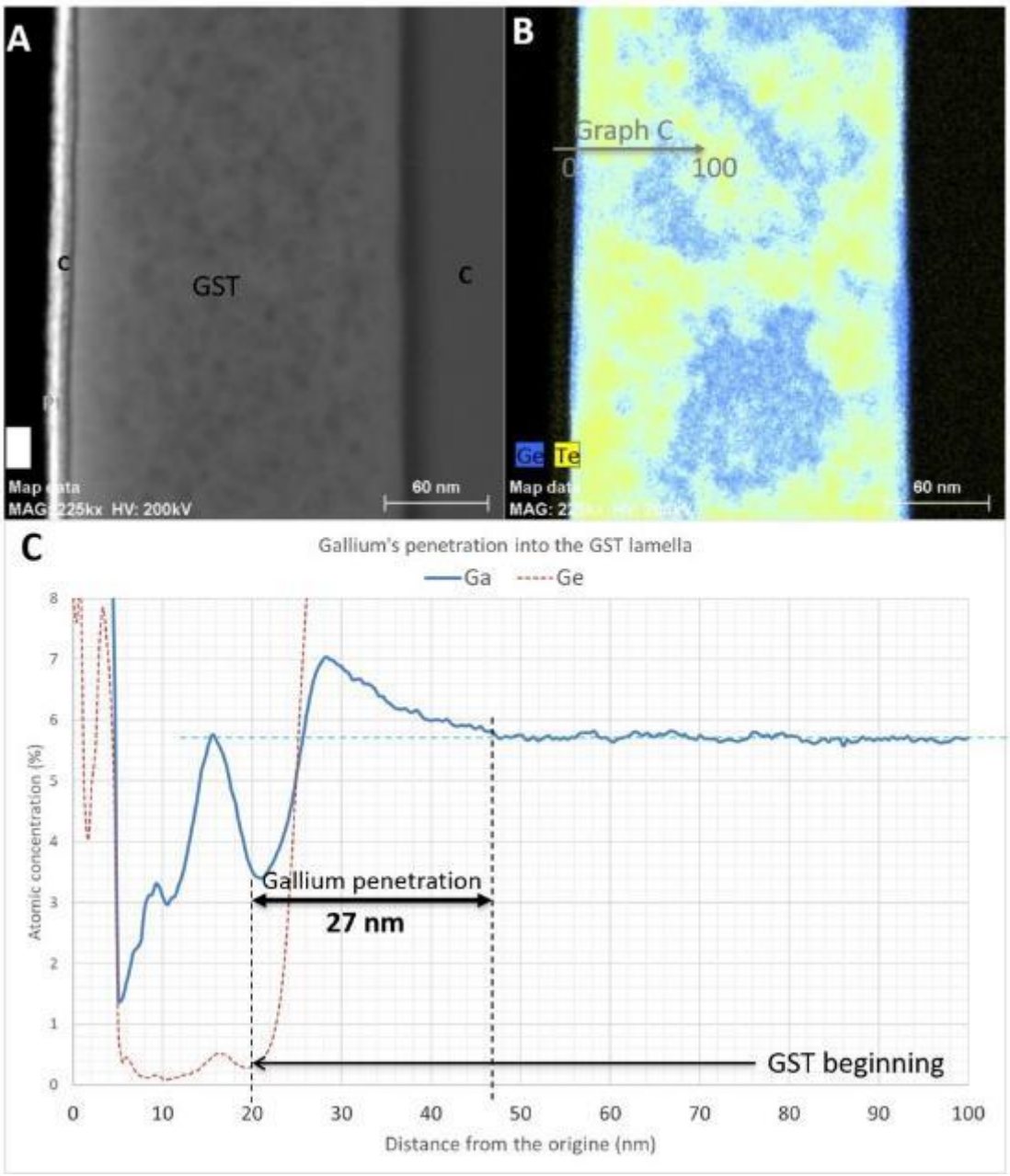

Figure 43: EDX analysis of the GST thinned at 30 keV (A) Corresponding STEM imaging (B) Composition map and (C) Composition profile for Ge and Gallium

composition profile for both Ge and Ga are presented in Figure 43C. The red dotted Ge curve defines the beginning of the GST bevel (from 20nm). The gallium plot, in blue, interests us only in the GST part, thus from 20nm. It undergoes a strong increase to a maximum value around 28 nm, 8 nm depth in the GST, and then decreases more gradually until it reaches a plateau value at 47nm (27 nm in the GST). This plateau is, like for the silicon lamella, the results of the second preparation where the Ga ions also penetrate evenly the surface of the lamella.

The gallium penetration with a 30 keV into the GST during the first preparation is therefore 27 nm. However, there is an important gallium concentration 7nm away from the surfaces.

Therefore, a visible and homogeneous amorphous layer of 27 nm is expected on each side of the lamella, alike the silicon case.

2. Morphological analysis: Conventional TEM

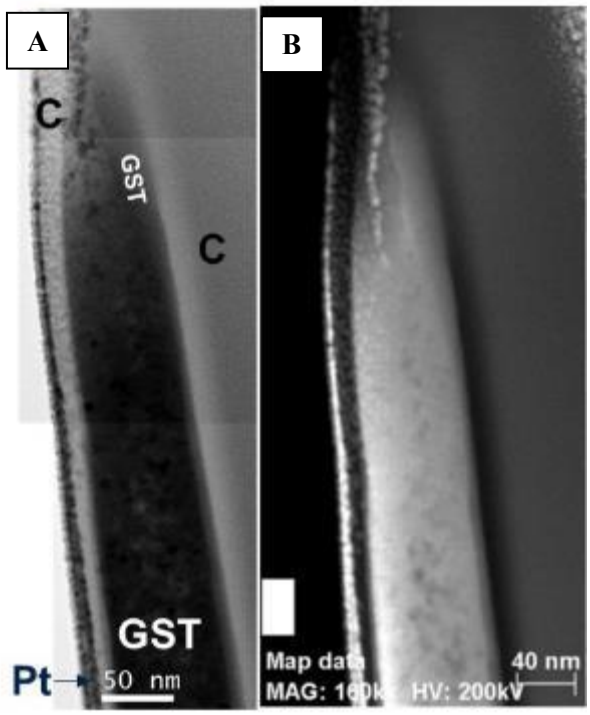

Figure 44: Planar Lamella (A) Bright Field TEM and (B) Dark field (STEM)

A Conventional TEM analysis was conducted like it was done on silicon. The first results are shown in Figure 44. The platinum layer and the carbon protection are both easily visible on the bright field (A) and the dark field(B). However, the amorphous layer expected is not present. It is possible to see on the side a slight contrast difference on both DF and BF.

To study this interface, a zoom was done on the lower part of the lamella (less sensitive). The photo is shown in Figure 45A and thanks to the post-processing software the contrast was increased (B-C). In this way, between the carbon and the GST bulk, a layer around 26±2 nm layer is highlighted. This contrast cannot be due to the presence of gallium since its atomic mass is like the Ge predominant in GST studied. However, this layer is irregular and inhomogeneous (granular aspects). It seems that the layer may still contain some crystals.

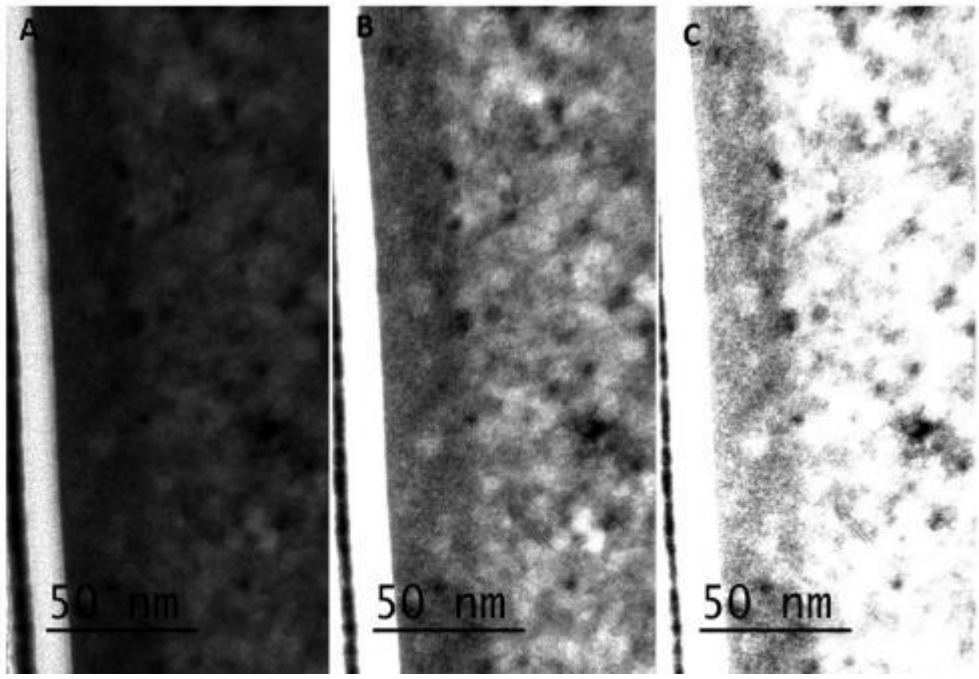

Figure 45: Side of the bevel-shaped lamella with an augmentation of contrast done in post processing

3. Structural analysis: HRTEM

To understand what happened in the layer impacted by the ion beam high-resolution photo are taken at the interface. A quick analysis presented in Figure 46, was done to understand what phase was present in the interface. The high resolution does not allow to firmly dissociate the amorphous phase. However, thanks to the FFT, it seems that there are nanocrystals in an amorphous matrix.

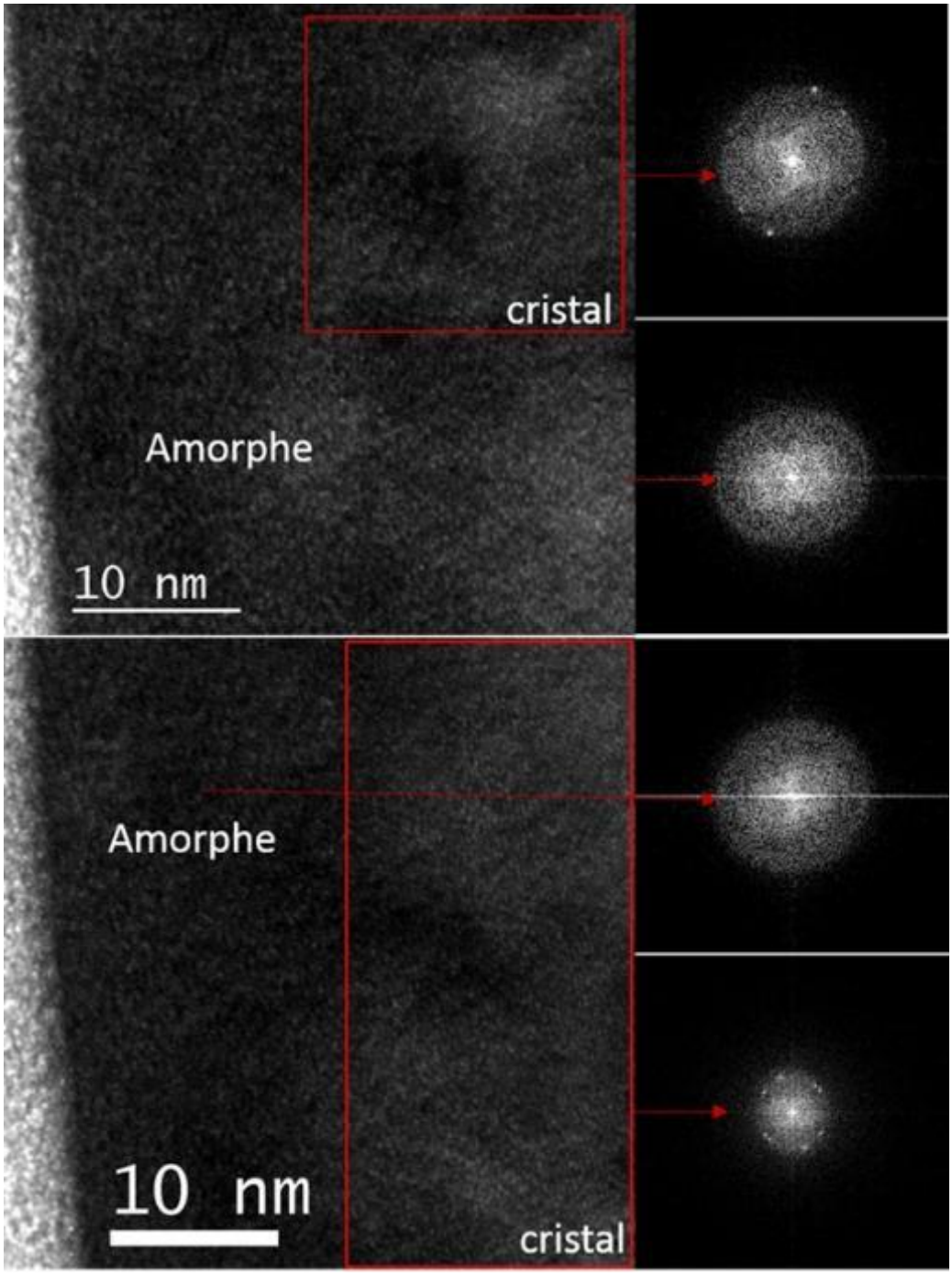

Figure 46: HRTEM photo of the GST impacted by the ion beam with FFT patterns

It is thus possible to separate 2 different layers:

- The fully amorphized layer
- The partially amorphized layer

The measures are done on the HRTEM analysis is presented in Figure 47. Each photo is done in a different place on the lamella. The distinction between amorphous and crystalline was done thanks to

small area FFT patterns. On average, the pure amorphous layer measures 15 nm. The mixed intermediate layer measures 12 nm. The thickness impacted by the 30 keV beam is thus 27 nm.

This last measure corresponds to the gallium penetration measurement measured previously by EDX, like it was the case for the silicon.

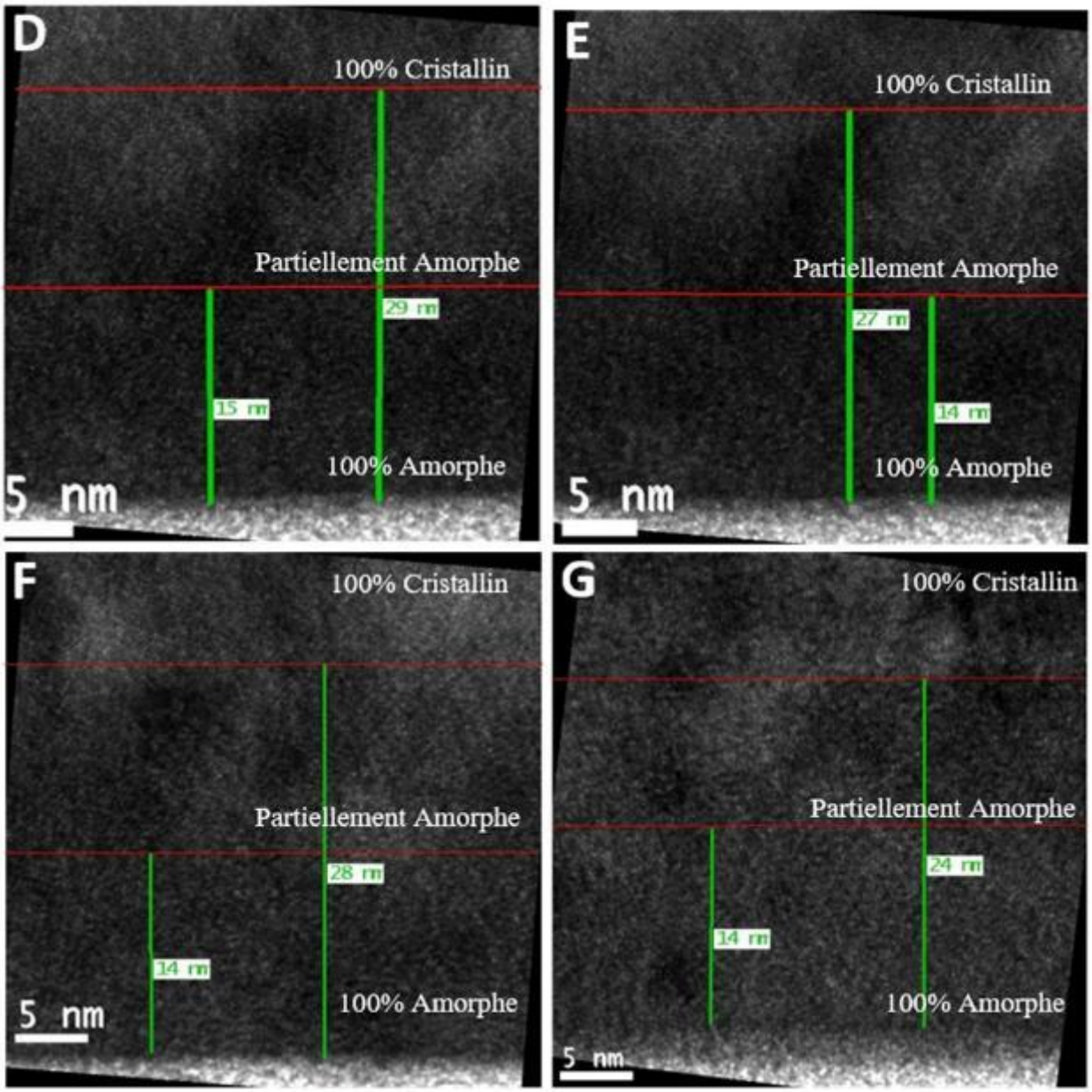

Figure 47 : Measures of the fully amorphized and mixed layer on the HRTEM photos

However, the lack of contrast between the crystalline and the amorphous part make those results extremely imprecise. These results may be used but the bias can be important, and caution needs to be used if employed directly.

The lack of contrast between the phases is a significant issue to analyse the amorphization of the GST, on that was not expected. In this part, the distinction between the crystalline and the amorphous states is complicated and imprecise in HRTEM. Thus, FFT pattern where used on a small area of the HRTEM to discern the crystals. To have better and more precise results it would be useful to directly get a phase map. A newly developed technics allows thanks to the analysis ‘area-per-area’ of the diffraction pattern: ASTAR or Acom-Tem

B. Structural Analysis on the bevel-shaped: ASTAR/Acom-Tem

As seen in the previous part the lack of contrast is an unexpected challenge encountered to discern phases in the GST. The possibility to use the ASTAR technology is thus a good opportunity to check our previous results and to get more information on the lamella.

The ASTAR (commercial name) or ACOM-TEM (Automated crystal orientation mapping) is a new characterization technique using a conventional Transmission electron microscope and an external device allowing the recording of the diffraction pattern. It set up by the CNRS and marketed by Nanomesas. It allows both phase mapping and crystalline orientation map.

Selecting a specific area, that directly represents the resolution, a diffraction pattern is obtained. The pattern is optimized to make it comparable to theorical patterns. Examples of diffraction patterns are presented in Figure 48.

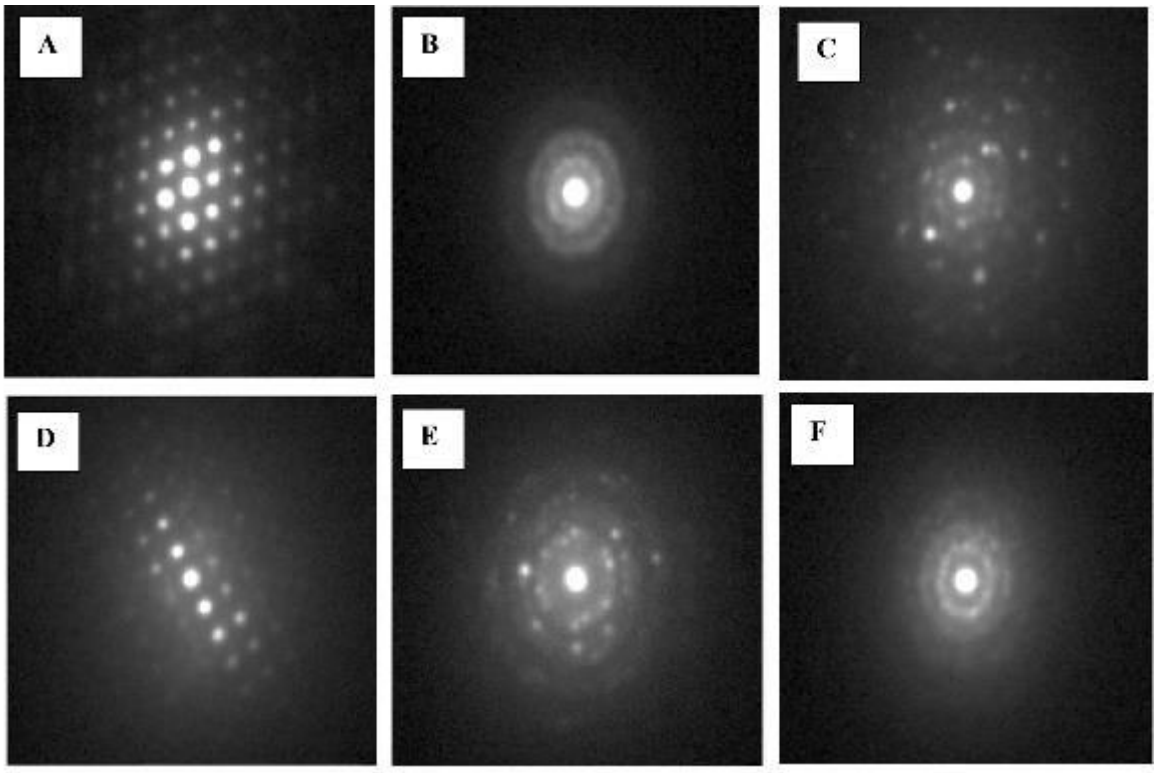

Figure 48 : Example of pattern used by ASTAR during the data acquisition:
(A) Monocrystalline silicon
(B) Amorphous silicon
(C) Polycrystalline Ge (FCC)
(D) Monocrystalline GST
(E) Polycrystalline GST (FCC)
(F) Amorphous GST/Ge

Selecting the expected phases in the material, the software will use their database to compare it to the measured diffraction pattern. It will define statistically which phase is the more likely and the associated orientation.

Combining TEM imagining and the results from the ASTAR analysis it is possible to obtain a phase map and an orientation map ad example. [20]

A similar study was conducted on the Monocrystalline Silicon in Annexe 4: Analysis ASTAR on Monocrystalline Silicon.

1. Phase Mapping

The Astar analysis has been carried out one on the bevel-shaped lamella (Figure 49A) to see the direct impact of the ion beam on the lamella. Pairing it to profile should give a good idea of the state of lamella in function of its thickness.

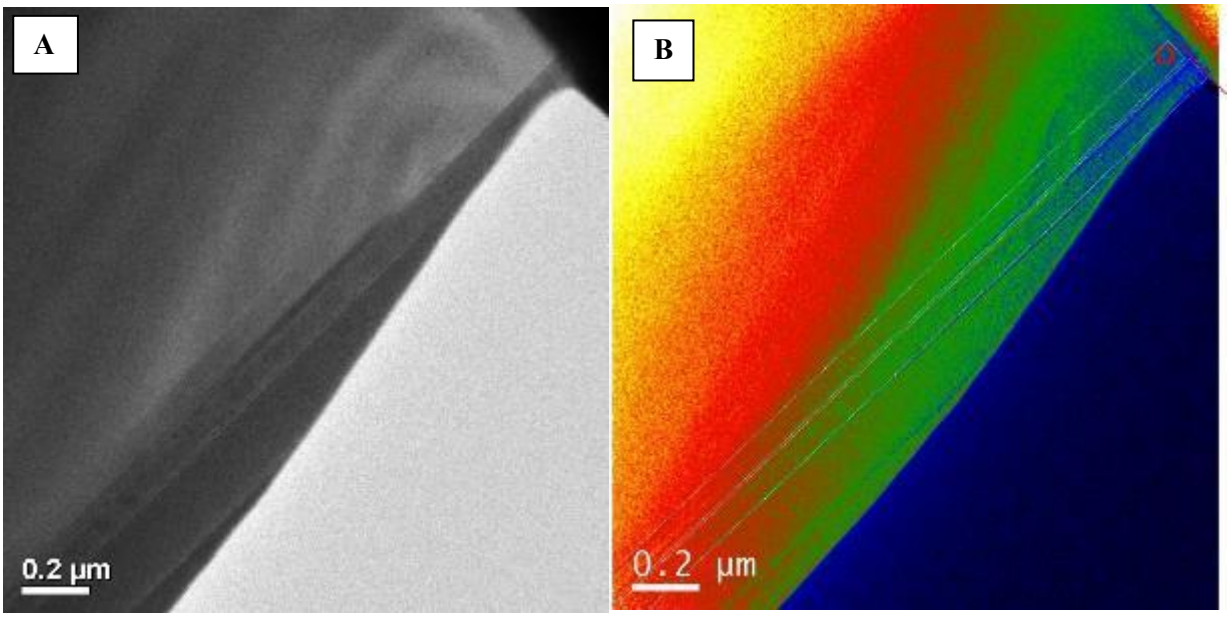

Figure 49: Thickness map of the bevel-shaped GST lamella thinned at 30 keV (TEM image and thickness map associated)

To correlate the results between the ASTAR analysis and the thickness, the t-map in Figure 49B was necessary. The profile (Figure 50C) was done on the GST layer, however like seen in the Annexe 2: Thickness lamella determination and bias, it should have a negligeable impact (±5nm).A

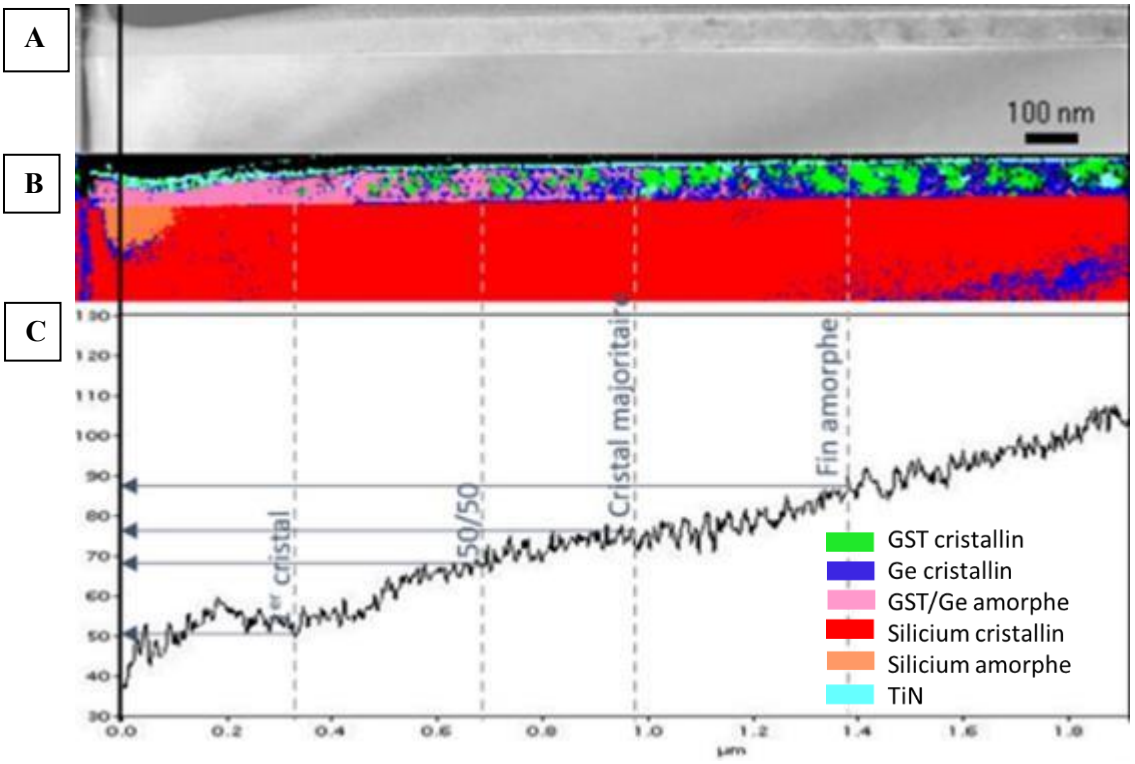

*Figure 50: TEM image, equivalent phase map and associated profile of the 30keV GST bevel-shaped lamella 500 pts * 70 pts, step 4 nm*

The phase map in Figure 50B is done by ASTAR and associated to its TEM imaging (Figure 50A) and its thickness. A 100 nm layer of enriched GST is visible. $Ge_2Sb_2Te_5$ crystals appear in green and Ge crystals appear in dark blue. The amorphous phase of both GST and Ge appears pink. A thin layer of crystalline TiN is present above the GST in azure blue. The substrate is a monocrystalline silicon appearing red under the GST layer. On the thinnest part the amorphous silicon appears orange.

The first crystal appears about 50-55 nm thick of the lamella. A large crystalline portion is present from 65-70 nm thick and the amorphous matrix becomes minority from 75-80 nm. From an 85-90 nm thickness, no more amorphous phases are visible looking through the lamella.

There is thus a transition between the fully amorphized layer and the polycrystalline material (non-impacted. The amorphous portion visible in the transition layer decreases when the lamella thickness increase. To observe this layer another Astar analysis is conducted on its start with a better resolution. The results are presented in Figure 51.

The same color-codes is used. There the first crystals also appear between 50-55nm. It is then possible to observe the presence of nanocrystals, at first around 10 nm for the GST smaller for Ge, in an amorphous matrix. With the increase of the thickness, both crystals grow and the amorphous matrix decrease. Around 70 nm, the GST crystals reach a size around 50 nm and the Ge crystals around 10 nm.

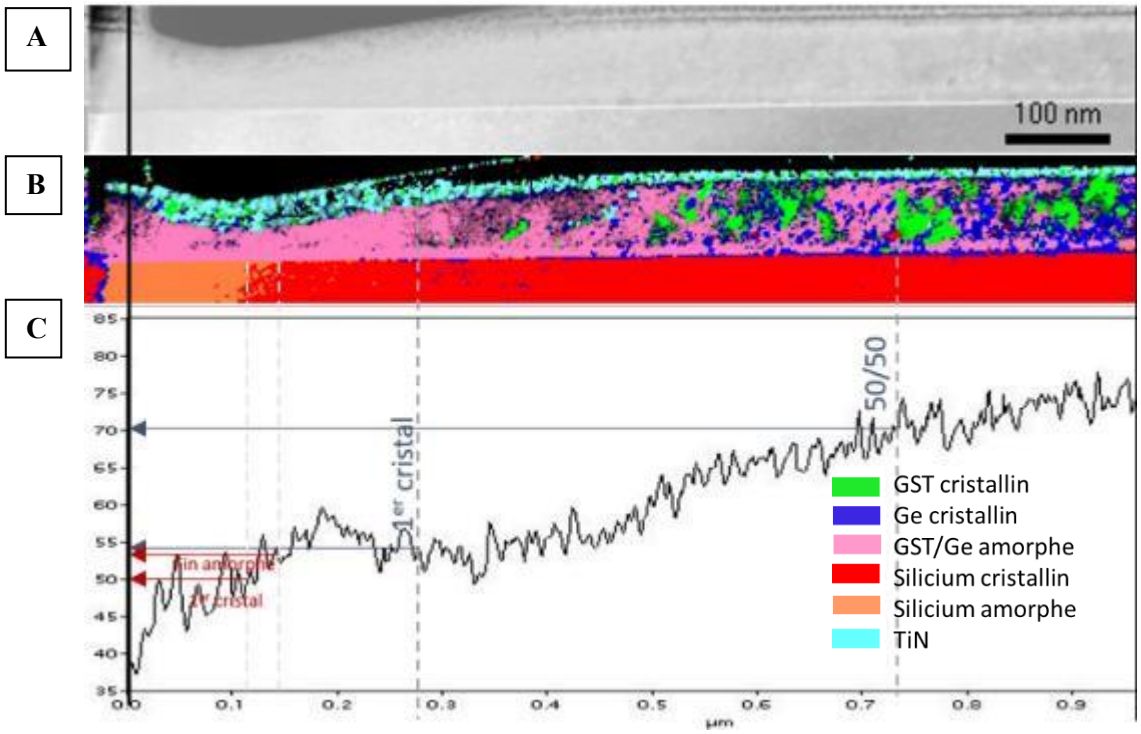

*Figure 51: : TEM image, equivalent phase map and associated profile of the 30keV GST bevel-shaped lamella, resolution 500 pts * 70 pts, step 2 nm*

The size difference and the position between crystals may not be due to the lamella preparation but to the original inhomogeneity and size of the crystals in the GST as shown in Figure 40. However, to check if the composition of the crystals or their orientation as an impact on their destruction on the ion beam a selective Orientation Mapping for both Ge crystal and GST is necessary.

2. Orientation Mapping

Thus on the thanks to the second analysis, presented in Figure 51, another data processing allowed the creation of the orientation mapping presented in Figure 52.

The axis is defined by the microscope: The Y-axis coincides with the TEM column, the X and Z are orthoradial to it. It allows to state the orientation of each crystal with the microscope has a reference, by using a colour-gradient.

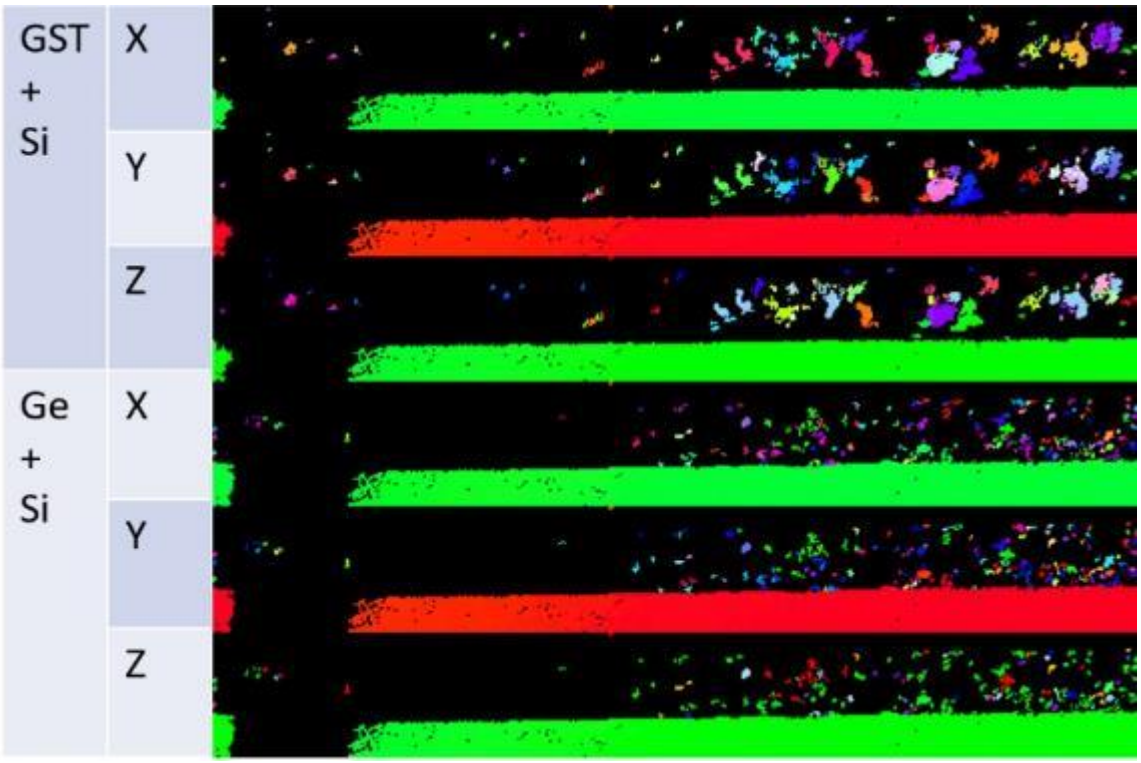

Figure 52: Orientation mapping for both [GST+Si] and [Ge+Si] in function of the 3 axis of the microscope (X,Y,Z)

The monocrystalline silicon appears under the GST, its uniform colour is typical of a monocrystalline material (with a preferential orientation).

The orientation map eased the observation of single crystals of GST and Ge. There seems to be no preferential crystal between GST and Ge. Both crystals appear around the same thickness, their size depending only on their size before the lamella preparation. This confirms the former observation with the Phase mapping.

For the GST crystals, the crystals are multi-coloured with no preferential tint. No colour being predominant, the GST crystals seem to be randomly oriented in X, Y, Z. The observation can be done for the Ge crystals. In both cases, a similar pattern is visible on non-impacted GST Astar analysis.

In conclusion for a 30 keV thinning, there seems to be no composition or orientation selectivity.

3. Comparison to HRTEM analysis

Thanks to the ASTAR analysis, crystals were detected in an amorphous matrix. The former analysis allowed the positioning of those crystals and their apparition gradient.

Some HRTEM analysis has been carried out on specific points on the lamella, see Figure 53. However, if it is possible to discern the difference between purely amorphous (A) and the purely crystalline state (C), the transition (B) is hardly visible and the signal is scrambled, no useful information can be extracted of it.

Therefore, the future analysis to determine the impact of the ion beam on GST preparation will all need ASTAR analysis if useful information needs to be extracted. This is especially for analysis through the bevel-shaped lamella.

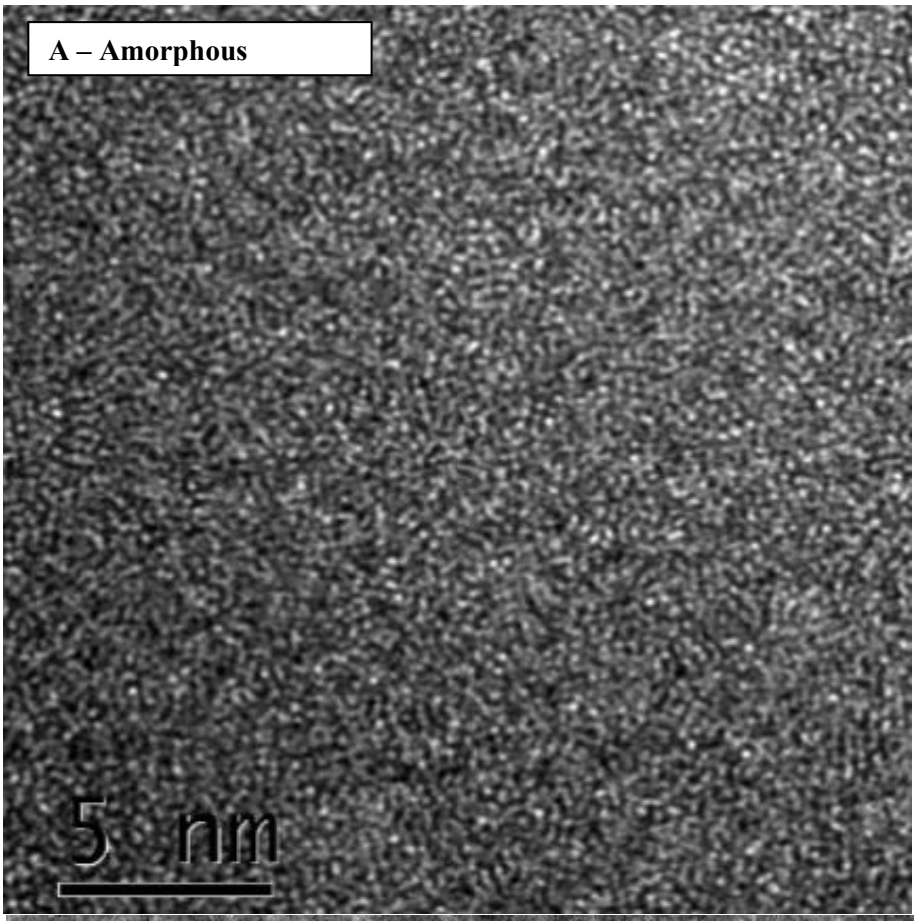
A – Amorphous
5 nm

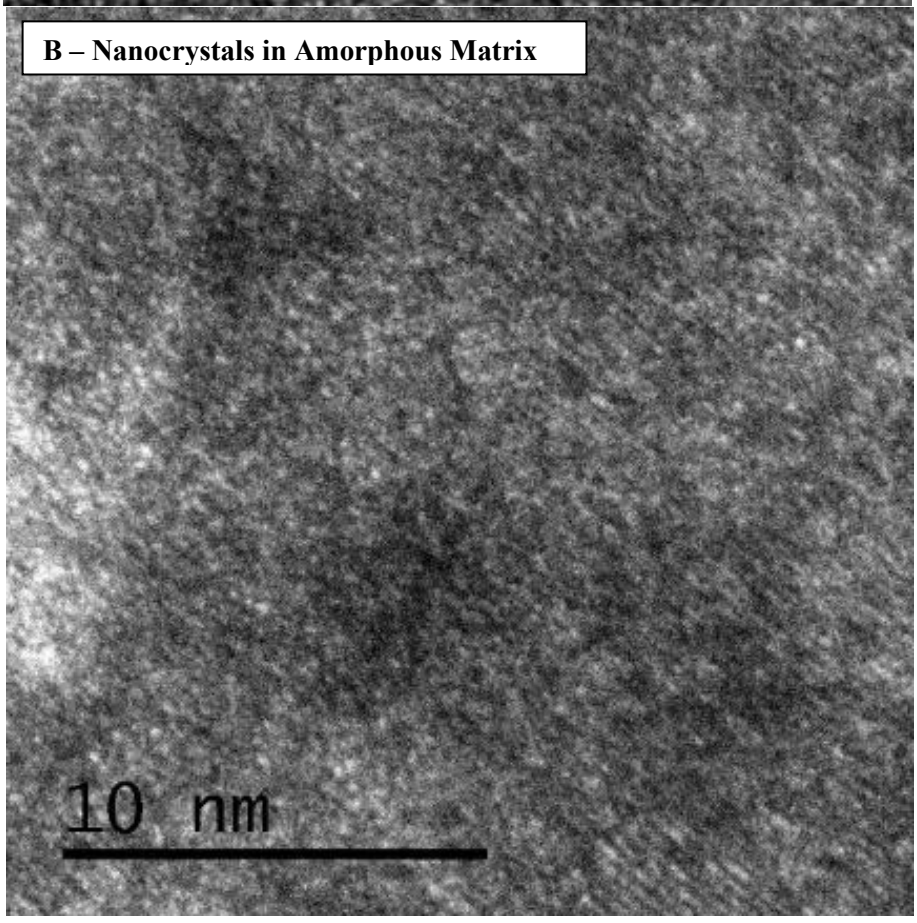
B – Nanocrystals in Amorphous Matrix
10 nm

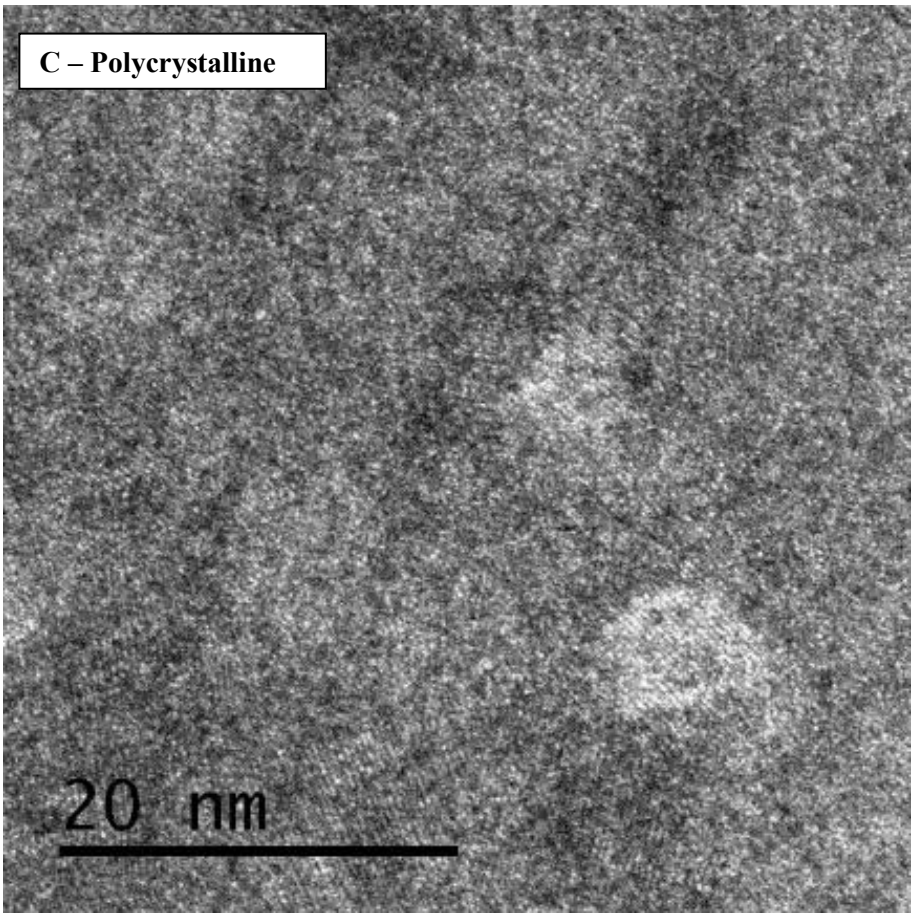

Figure 53: HRTEM analysis in specific points of the ASTAR analysis (A) Amorphous (B) First crystals (C) Polycrystalline

C. Amorphization

On the planar lamella, equivalent measure to the one done with the silicon was done. However, two different layers were apparent. Those layers are not easily discernible. Thus, the results extracted need to be taken with caution.

Those data are still used in the bar chart Figure 54 shows. Three states of the GST are considered:

- The fully amorphized layer (yellow hatched)
- The nanocrystals in an amorphous matrix (yellow)
- the polycrystalline material (blue).

The layer impacted by the ion beam is constituted by both the amorphized layer and the amorphous matrix with nanocrystals.

The lamella is completely amorphized up to 30 nm thick. From there, the first crystals can appear since the intermediate phase begins. Between a thickness of 30 to 45 nm, it forms around 20% of the lamella. With the increase of the thickness, both impacted layers slowly decrease. The first native crystals, not impacted by the beam, appear on 45-60nm lamellas (around 2% of the lamella). This last phase slowly increases with the thickness.

Therefore, for thin lamellas (around 40-60 nm) with a 30 keV thinning, only 2% of the native polycrystalline structure is preserved: the lamella is considered destroyed. For normal lamellas (80-110 nm), they will have between 40 and 55% native crystal.

To conserve 75% of the original network, the lamella requires to be at least 200nm thick. It is too thick to perform an analysis by transmission. Thus, the 30 keV thinning is unsuitable to any kind of analysis.

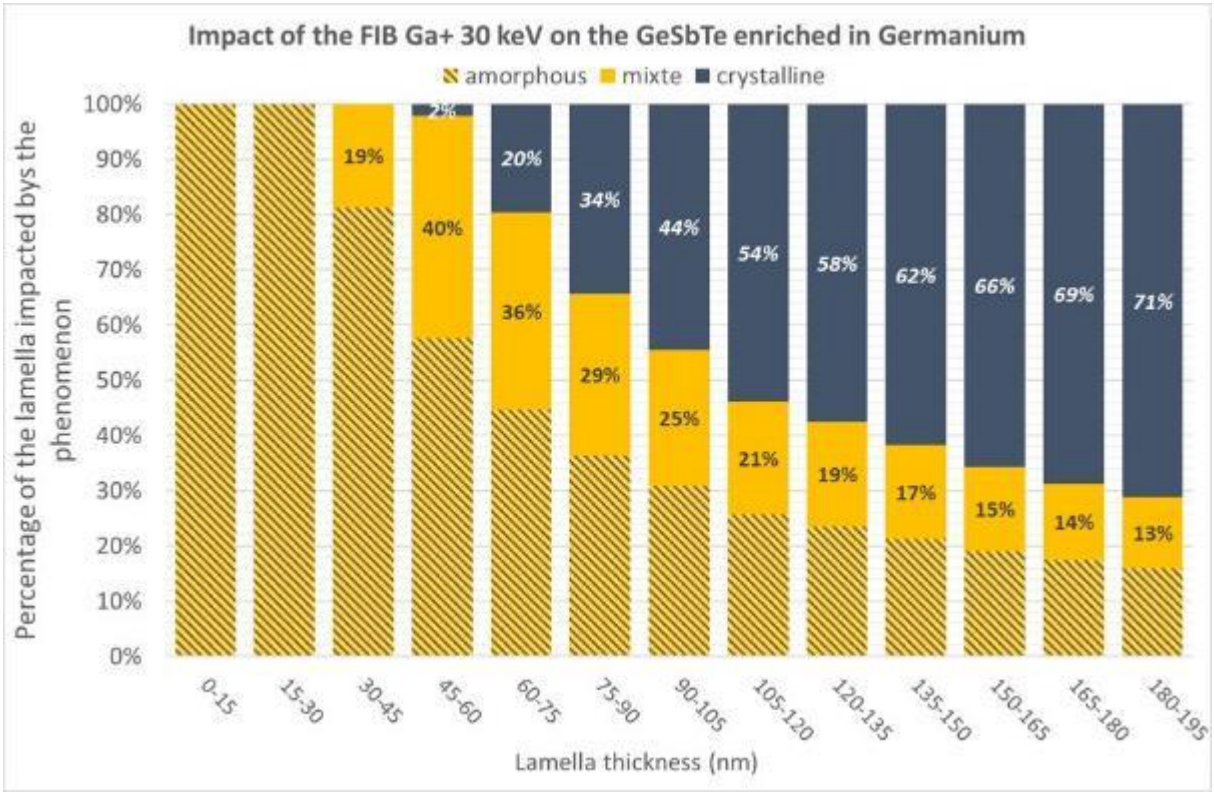

Figure 54: Bar chart of the evolution of the quantity of amorphous, mixed, and polycrystalline material. (mixed + amorphous= impacted material)

Matching these results to the Astar observations, it is possible to assume the quantity of each phase for each observation. The results are shown in the following table.

The first crystal appears for only 2% of polycrystalline materials but also 40% of amorphous matrix and nanocrystals thus the crystals observed may be from either one

The amorphous phase observed by Astar disappears completely (80 nm) when the lamella is at least 44% polycrystalline. In addition to the intermediate layer represents 25% of the lamella.

	Thickness	***%crystalline***	***%Mixte***
1st crystal	55 nm	**2%**	40%
Major amorphous	70 nm	**20%**	36%
Minor amorphous	75 nm	**34%**	29%
Crystalline	85 nm	**44%**	25%

Table 2: Correlation between the bevel-shaped lamella results and the planar lamella results

The 30 keV beam alone is inappropriate for the preparation of lamellas, whether those are thin or thick. Going down to lower energies for better refining is therefore necessary. The 8 keV results with ASTAR bevel results more suited to observation, even on end will quantify the possible improvement.

D. Comparison

The interaction between the gallium ion beam and the enriched GST is simulated by SRIM for acceleration energies of 30, 16, 5 and 2 keV for a grazing ion beam (angle -89.9 degrees). Figure 55 summarizes all the results obtained by simulation and compares the experimental results obtained for a 30 keV thinning.

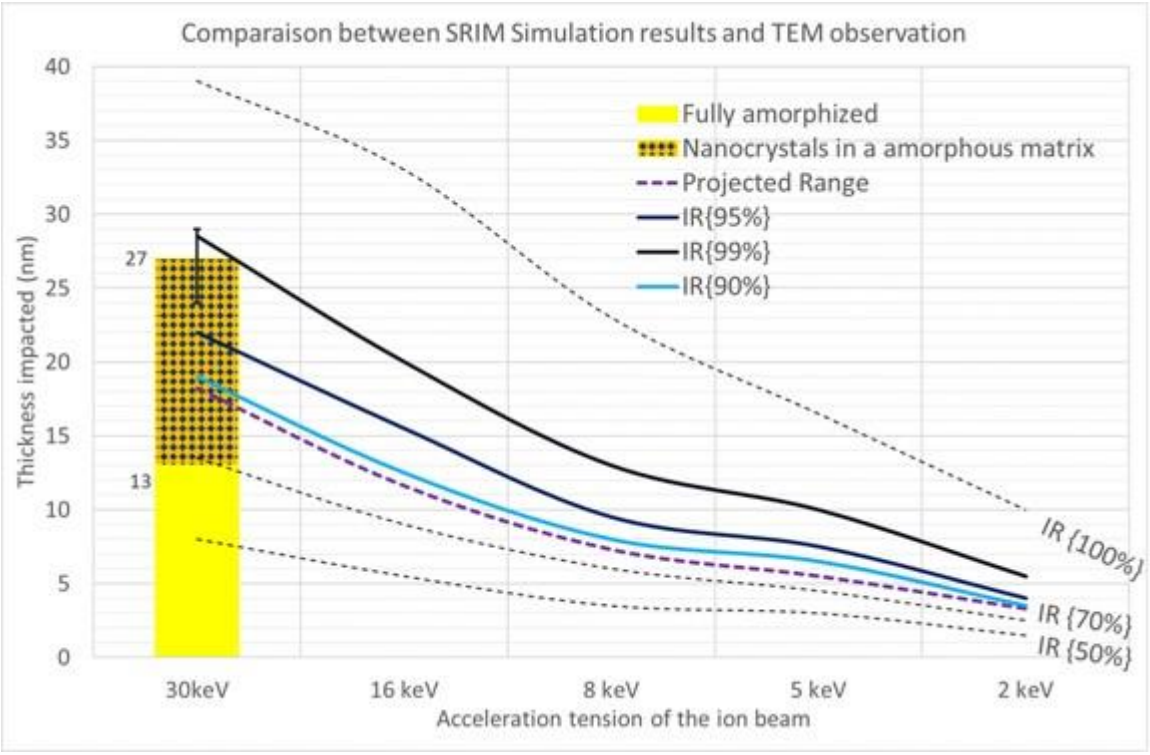

Figure 55: Comparison between SRIM simulation and experimental results

The experimental results are expressed by the bar chart, the fully amorphized layer in yellow and the layer composed by nanocrystals in an amorphous matrix blue/yellow. The simulation results are presented by the curves.

The IR {99%} value provides a good approximation of the thickness of materials really impacted by the 30 keV beam. The complete amorphization is on a reduced thickness (approximate by IR {70%}). However, as the intermediate phase has a significant impact on the quality of the lamella (as seen thanks to the correlation done in Table 2), the approximation of the layer really impacted by the ion beam is important.

In addition, the penetration of gallium measured by EDX matches the result obtained via SRIM (27nm). It will be interesting compares those results for lower energy beams. It would permit to test whether the values of IR {99%} and IR {95%} can be used to estimate the thickness of GST impacted.

Contrary to the case of silicon, the IR {90%}, still like the projected range value, does not allows a good approximation. Thus, it seems that the GST is more sensible to the gallium ion beam than the silicon: between 1% and 5% of the total ion beam can destroy the network (it was around 5-10% for the silicon).

E. Conclusion

Contrary to our former hypothesis, the impact of the gallium ion beam on the GST differs from what was observed with the monocrystalline silicon. Indeed, the amorphous/crystalline transition is indirect, there is an intermediate layer where the GST is partially amorphized. Nanocrystals in an amorphous matrix are detected both on the has a layer on the planar lamella but also looking through the lamella (bevel).

The GST is completely amorphized on 14 nm but the partially amorphized layer can reach 27 nm thick. This impacted layer matches the gallium penetration measured by EDX. The proportion of native polycrystals in a 100 nm lamella, does not exceed 50%. It is therefore impossible to use this kind of preparation for lamella analysis.

A thinning with lower-energy beams is therefore necessary. It will erode both the pure amorphous and the deeper partially amorphized area. Both need to be milled since the intermediate layer has an important impact on the bias observed while looking through the lamella.

Only the 30 keV thinning was analysed, however, it can be considered as the most critical sample preparation. There should be no different artifact like phase transition or bubbles with lower energy beams. However, if the no preferential milling is observed at 30 keV, lower ion beam could be more specific. With less damaging ion beam, the orientation or the composition may have an impact.

Thus, it is necessary to do these analyses according to the protocol, adding the Astar characterisation, to determine the impact of the thinning at lower energy. It would allow the comparison between the simulation and the experiments at lower acceleration and to know how far to go down to optimize the preparation.

VI. General conclusion

Since the 60', the race to miniaturization permits the creation of electronic devices smaller and more performant. Nowadays we do not speak anymore of just electronics but also of microelectronics. It is thanks to those new devices that the new "connected area" emerged.

However, this size reduction led to the emergence of many new needs for the manufacturing of the device but also its characterisation, especially in the support field. Among the many requirements, there is the need to observe smaller and smaller component which require to have a much higher resolution to detect defects. For nano- and microscale components, a full characterisation (structural, morphological, compositional) is eased by transmission electron microscopy.

Though, the TEM requires lamella transparent to the electron beam, thus very thin samples. A few preparation methods exist but the one used at STMicroelectronics is the lift-out technics. A Dual-Beam digs the materials, extract a lamella, and then thins it thanks to an ion beam (gallium). This beam tends to leave artifacts on the lamella, or, in other words, defects attributable only to the preparation. In the case of crystalline materials, there is an important risk of amorphization. The gallium ions mill the sample, but some also enter in the lamella. This ion can destroy the crystalline network. For some analysis, the crystalline network is the decisive criterion to determine the quality of the device.

This is especially true for silicon and the $Ge_2Sb_2Te_5$ used in PCM cells. Both can be crystalline and amorphous, but their intrinsic properties vary in function of their state. For the silicon, both forms will have different uses, as for example the monocrystalline silicon wafer as a substrate. However, for the GST its states will determine the state of the PCM, and thus the tracing of the cell run.

To determine the impact of the ions, beam several experiments were conducted with different acceleration tension for the polishing. Thanks to a bevel-shaped lamella and its extracted planar lamella, it is possible to determine the impact the ion fib and to correlate the results observed to the lamella thickness. EDX analysis allowing the direct measure of the gallium penetration, and conventional TEM and HRTEM the measure of the amorphized layer. This way, it seems possible to characterize the fully impact of the ion beam. These experimental results are coupled to SRIM simulation to see if it is possible to predict the impact and its precision.

The study on monocrystalline silicon wafers was done to check the accuracy of the experimental method. Commonly used in microelectronics, the artifacts of gallium ion beams on the monocrystalline silicon is already known. The results are summarized in Table 3.

Acceleration tension	***30 keV***	***16 keV***	***5 keV***	***2 keV***
Bibliographic	**18-25 nm**	**14-18 nm**	**4-7 nm**	**3-4 nm**
Experimental	**22±1 nm**	**30±1 nm**	**3,5 ±1 nm**	**x**
Simulation	**19-22 nm**	**15,5-20 nm**	**6,5-7,5**	**3,5-4**

Table 3: Comparison of the bibliographic, experimental, and simulated thickness of the amorphous layer for 30keV, 16keV, 5keV and 2 keV polishing

Thus, the results are coherent to the bibliography, and the only aberration (16 keV) is easily explained and allowing an amelioration the protocol. Since the second preparation is critical, the addition of a protective carbon layer is necessary before the platinum deposition. Also, the EDX analysis showed that the experimental gallium penetration was equivalent to the size of the amorphous layer. The amorphization seems thus only due to the penetrating ions and not to any secondary ions. In conclusion, the gallium penetration, both experimental and simulated, equalled the amorphized layer.

Thanks to these observations and improvements, the analysis on enriched $Ge_2Sb_2Te_5$, was conducted. Only the effect of the 30 keV beam polishing was conducted. This beam is the most energetic used for the polishing, so this preparation can be considered critical. All preparations made with less energetic beams should present similar artifacts, at lower thicknesses, since the beams used will have lower energies. The gallium ion entered the lamella around 27 nm which perfectly matches the simulation results. Thanks to TEM and HRTEM an impacted layer could be estimated around 27 nm, there also a similar result to the EDX. However contrary to silicon, if the GST is completely amorphized on 14 nm, there is also a second layer with nanocrystals in an amorphous matrix around 13 nm thick.

However, the lack of contrast between crystals and made it extremely difficult to measure. Thus, some doubts have kept the validity of those results. To improve the protocol and the measure Astar analysis where conducted to obtain a phase mapping. The measured obtained seemed to collaborate the former results, since the bevel-shaped lamella presented also nanocrystals in an amorphous matrix see Figure 56. The remaining crystals do not have any preferential orientations nor compositions (Ge or GST). The non-specificity of the FIB may not be true for lower energy polishing.

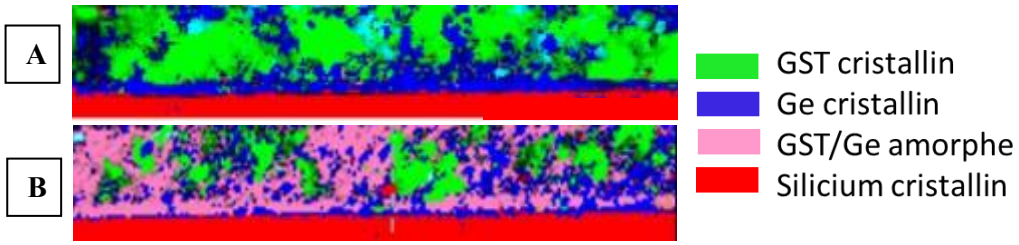

Figure 56: Impact of the 30 keV ion beam on a phase mapping. (A) Non impacted GST lamella (B) Impacted GST lamella

With all analysis, it is evident that the 30 keV polishing is too damaging for the lamella. Especially since the proportion of native polycrystals in a 100 nm lamella, does not exceed 50%. It is therefore impossible to use this kind of preparation for lamella analysis.

A thinning with lower-energy beams is, therefore, necessary to erode both the pure amorphous and the deeper partially amorphized area. Both need to be milled since the intermediate layer is an important bias while looking through the lamella. Thus, it is necessary to conduct a new analysis with a less energetic ion beam, like 16keV or 8 keV. Those new analyses will need Astar characterisation since the HRTEM analysis is insufficient to have a decent structural analysis.

VII. **Bibliography**

[1] KUNIAVSKY, Mike. Smart things: ubiquitous computing user experience design. Elsevier, 2010.

[2] KARL RUPP. 40 Years of Microprocessor Trend Data. Our World in Data. 1971 – 2017

[3] COLLIEX, Christian. La microscopie électronique. Que sais-je? 1998.

[4] AUSTRALIAN MYCROSCOPY, My Scope. TEM FIB. 2013.

[5] MAYER, Joachim, GIANNUZZI, Lucille A., KAMINO, Takeo, et al. TEM sample preparation and FIB-induced damage. MRS bulletin, 2007, vol. 32, no 5, p. 400-407.

[6] HUH, Yoon, HONG, Ki Jung, et SHIN, Kwang Soo. Amorphization induced by focused ion beam milling in metallic and electronic materials. Microscopy and Microanalysis, 2013, vol. 19, no S5, p.33-37.

[7] VOLKERT, Cynthia A. et MINOR, Andrew M. Focused ion beam microscopy and micromachining. MRS bulletin, 2007, vol. 32, no 5, p. 389-399.

[8] PASTEWKA, Lars, SALZER, Roland, GRAFF, Andreas, et al. Surface amorphization, sputter rate, and intrinsic stresses of silicon during low energy Ga+ focused-ion beam milling. Nuclear Instruments and Methods in Physics Research Section B: Beam Interactions with Materials and Atoms, 2009, vol. 267, no 18, p. 3072-3075.

[9] O'MARA, William, HERRING, Robert B., et HUNT, Lee P. Handbook of semiconductor silicon technology. Crest Publishing House, 2007.

[10] MCEVOY, Augustin, MARKVART, Tom, CASTAÑER, Luis, et al. (ed.). Practical handbook of photovoltaics: fundamentals and applications. Chapter IB-1 - Crystalline Silicon: Manufacture and Properties. Elsevier, 2003, p.79-97.

[11] STIHARU, I. MEMS, General Properties. 2001

[12] LIU, X. Q., LI, X. B., ZHANG, L., et al. New structural picture of the Ge2Sb2Te5 phase-change alloy. Physical review letters, 2011, vol. 106, no 2, p. 025501.

[13] GUO, Pengfei, SARANGAN, Andrew M., et AGHA, Imad. A Review of Germanium-Antimony-Telluride Phase Change Materials for Non-Volatile Memories and Optical Modulators. Applied Sciences, 2019, vol. 9, no 3, p. 530.

[14] NONAKA, Toshihisa, OHBAYASHI, Gentaro, TORIUMI, Yoshiharu, et al. Crystal structure of GeTe and Ge2Sb2Te5 metastable phase. Thin Solid Films, 2000, vol. 370, no 1-2, p. 258-261.

[15] SHAYDUK, R. et BRAUN, W. Epitaxial films for Ge–Sb–Te phase change memory. Journal of crystal growth, 2009, vol. 311, no 7, p. 2215-2219.

[16] MORALES-SANCHEZ, Eduardo, PROKHOROV, E. F., MENDOZA-GALVÁN, A., et al. Determination of the glass transition and nucleation temperatures in Ge2Sb2Te5 sputtered films. Journal of applied physics, 2002, vol. 91, no2, p.697-702.

[17] HEGEDÜS, J. et ELLIOTT, S. R. Microscopic origin of the fast crystallization ability of Ge–Sb–Te phase-change memory materials. Nature materials, 2008, vol. 7, no 5, p. 399-405.

[18] BONIARDI, Mattia, IELMINI, Daniele, TORTORELLI, Innocenzo, et al. Impact of Ge–Sb–Te compound engineering on the set operation performance in phase-change memories. Solid-state electronics, 2011, vol. 58, no 1, p. 11-16.

[19] JIANQIANG HU, Jing Zhou, MING_LI, Qiang Gao, et CHORNG_NIOU, Kary WT Chien. Study on the Effect of FIB Electron Beam Assisted Platinum Deposition on TEM Sample Analysis. In : ISTFA 2006: Proceedings of the 32nd International Symposium for Testing and Failure Analysis. ASM International, 2006. p. 71

[20] RAUCH, E. F. et VÉRON, M. J. M. C. Automated crystal orientation and phase mapping in TEM. Materials Characterization, 2014, vol. 98, p. 1-9.

Annexe 1: Riassunto in italiano

Nel 1965, osservando l'evoluzione nei 5 anni precedenti, Gordon Moore predisse l'evoluzione del circuito integrato. Definì allora quella che oggi è conosciuta come Legge di Moore: "il numero di transistor che possono essere posti su un circuito integrato raddoppia ogni due anni" [1]. Da allora, i progressi effettivi hanno seguito quella stima [2].

Questa evoluzione può anche essere vista come se ogni 2 anni la dimensione dei transistor fosse divisa per 2. Questa è la via della miniaturizzazione. Consentendo la possibilità di inserire sempre più transistor su un chip con dimensioni identiche, la capacità di elaborazione è aumentata in modo esponenziale. Pertanto, ha permesso l'ascesa delle nuove tecnologie al giorno d'oggi grazie al miglioramento dei microprocessori, come quelli utilizzati in laptop o smartphone. Questo sarebbe stato impossibile con i circuiti precedenti. [1].

La miniaturizzazione ha portato anche nuovi processi e esigenze analitiche. Dalla litografia all'osservazione del campione, tutti gli aspetti dovevano essere adattati alle dimensioni dei dispositivi, soprattutto quando si trattava di osservare chip microelettronici. Il transistor al giorno d'oggi può arrivare a una dimensione di 7 nm. Per analizzarli è quindi necessaria una risoluzione estremamente elevata. Ecco perché la microscopia elettronica a trasmissione (TEM), con la sua risoluzione di 0,1 nm, è ampiamente utilizzata nell'industria dei semiconduttori. Come, ad esempio, in STMicroelectronics dove ho svolto la mia tesi [3].

Introduzione

Come visto, l'analisi con la tecnica MET è una necessità. Tuttavia, questa tecnica non è priva di inconvenienti. Il parametro più importante è la preparazione del campione. Per consentire la trasmissione elettronica, deve essere trasparente all'elettrone: la lamella deve essere estremamente sottile. Lo spessore inoltre può variare in funzione dell'analisi voluta. Di solito varia da 100 nm a 40 nm. Per ottenere quella sottigliezza, esistono diverse tecniche di preparazione del campione. Tra questi, un approccio consiste nella lucidatura meccanica e con argon di provini in sezione o planari. Tuttavia, questo metodo non consente una selezione precisa dell'area. Questo è il motivo per cui il normale processo viene eseguito utilizzando un doppio raggio, composto da un fascio ionico focalizzato (FIB) e da un fascio elettronico). Il doppio raggio, contrariamente ad altri metodi, permette di selezionare una sezione trasversale su un'area specifica e di estrarla precisamente [3] [4].

I laboratori di caratterizzazione della STMicroelectronics utilizzano un'ampia gamma tecniche a doppio raggio per produrre i campioni per il TEM. La preparazione viene eseguita con un fascio ionico di gallio (Ga +) che taglia il campione in una parte selezionata per estrarre una lamella. Tuttavia, il fascio di ioni Ga + induce una moltitudine di shock balistici, effetti termodinamici nel materiale e quindi provoca amorfizzazione a livello della superficie del campione [5] [6] [7] [8]. Porta anche a una modifica della composizione a causa dell'ingresso di Ga + nel campione.

La conoscenza degli effetti della preparazione e la loro minimizzazione è un importante criterio di qualità per l'osservazione al TEM. Pertanto, ha un impatto importante sulla qualità delle osservazioni e dei risultati.

In effetti, alcuni esperimenti eseguiti su uno strumento MET, come l'imaging ad alta risoluzione o la spettroscopia delle perdite di energia degli elettroni, richiedono campioni più sottili del solito. La sfida è preparare, utilizzando la tecnica FIB, lamelle MET più sottili di 50 nm preservandone l'ordine strutturale e di conseguenza evitando qualsiasi amorfizzazione con il fascio fascio ionico.

Il fascio ionico ad alta energia ha il vantaggio di assotigliare velocementee e di avere una migliore precisione di taglio. Tuttavia, gli ioni che hanno un'energia cinetica più elevata, vanno più in profondità

nel campione. Trasmettono anche più energia agli atomi del reticolo. L'effetto del fascio ionico dipende da molti parametri come la composizione o la struttura atomica [5] [6]. Possono verificarsi altri fenomeni più indiretti come il riscaldamento del campione, particolarmente visibile durante lo studio dei polimeri. Nel nostro studio potrebbe essere necessario rilevare ogni possibile cambiamento di fase (fusione, cambio di fase,…).

Per definire il reale impatto dell'energia del fascio ionico sui materiali, verrà utilizzato un protocollo diverso per l'assottigliamento modificando le fasi di lucidatura. Le impostazioni dei doppi raggi ci consentono di utilizzare un raggio di gallio per accelerare con una tensione di 30keV, 16keV, 8keV, 5keV e 2keV. Le lamelle sono realizzate troncando da un fascio ad alta energia (30keV) e riducendolo al gradino di tensione inferiore.

Su queste lamelle la priorità è determinare la quantità amorfo / cristallino, lo spessore sia della lamella che dello strato amorfo, grazie all'analisi MET convenzionale e ad alta risoluzione. In parallelo, la spettroscopia a dispersione di energia a raggi X (X EDS / EDX) viene utilizzata per determinare la penetrazione del gallio nella lamella.

In una prima parte, questo progetto si concentrerà sul materiale di silicio, una componente importante nel campo della microelettronica i cui risultati sono già noti per verificare la validità del metodo. Successivamente studieremo l'impatto sul composto $Ge_2Sb_2Te_5$, un materiale che fornisce interessanti applicazioni nel campo microelettronico soprattutto per memorie a cambiamento di fase (PCM).

Strumenti utilizzati

Il dual-beam

Il Dual-Beam, mostrato schematicamente nella Figura 1, è la combinazione di un fascio ionico focalizzato (FIB) e un microscopio elettronico a scansione (SEM). La colonna FIB consente di lavorare il materiale su scala micro e nanometrica. Con un fascio di ioni sufficiemente energico, l'impatto degli ioni sul campione espelle gli atomi dalla superficie del campione e consente quindi di svuotare il materiale. L'interazione fascio ionico / materia così prodotta consente l'emissione di particelle: sia ioni che elettroni. Questi aiuteranno nell'imaging del campione.

La colonna SEM (elettroni) consente l'osservazione con meno danni al campione e una buona risoluzione. Separati da un angolo di 52 ° e determinati dalla geometria del Dual-Beam, i due fasci consentono così l'osservazione del campione in preparazione da 2 diverse angolazioni.

Parallelamente, i sistemi di iniezione del gas consentono di effettuare depositi (Si, Cr, Pt) assistiti da un fascio ionico, utilizzato in particolare per la deposizione dello strato protettivo di platino durante la fabbricazione delle lamella MET.

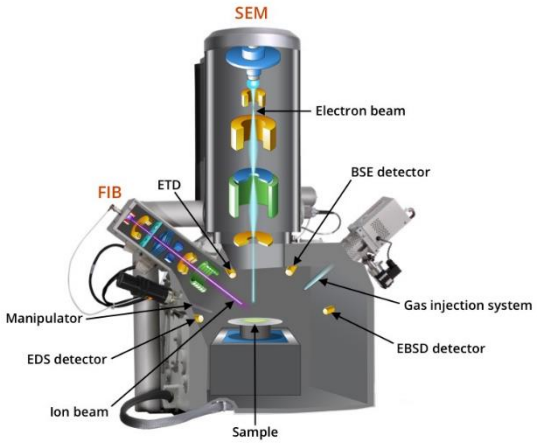

Figura 1: Schema del Dual-beam (source: My Scope Training, Microscopy Australia) CC BY-SA 4.0

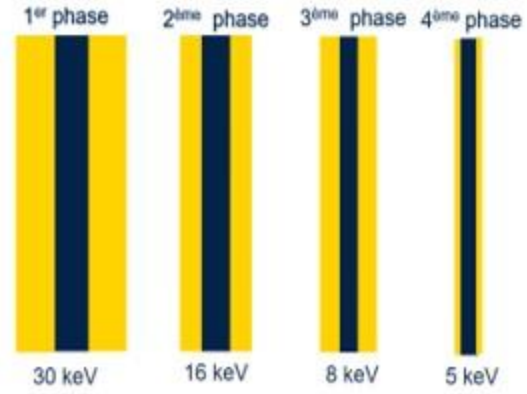

Figura 2 : Fasi di assottigliamento di una lamella TEM, in giallo sono rappresentati gli strati amorfi (in blu la parte cristallina rimanente)

L'energia del raggio di gallio necessaria per affinare la lamella avrà un effetto dannoso su di essa. Oltre a scavare il materiale, entreranno nel campione anche gli ioni di gallio. Ciò indurrà una disorganizzazione del reticolo cristallino e di conseguenza provocherà un'amorfizzazione a livello della superficie del vetrino. Infatti, l'amorfizzazione del materiale dipende dall'energia di accelerazione del raggio. Il raggio di energia da 30 keV avrà un impatto doppio rispetto a un raggio di energia da 8 keV e 5 volte tanto quanto un raggio da 2 keV.

Più energico è il raggio utilizzato, maggiore è la velocità di sputtering e amorfizzazione sulla superficie della lamella come mostra la Figura 2. Il processo di assottigliamento consiste quindi nel ridurre l'energia del fascio di gallio con il progredire della preparazione, consentendo così di ridurre l'amorfo presente ai bordi della lamella.

Il Microscopio Electronico in Trasmissione

L'analisi MET con il progresso della tecnologia elettronica come la nanotecnologia è diventata un punto chiave della caratterizzazione odierna. Infatti, il microscopio ottico con una risoluzione di 0.2µm è diventato rapidamente insufficiente per la risoluzione richiesta. Questo è il motivo per cui l'uso della microscopia elettronica è preferito soprattutto il MET che consente una risoluzione fino a 0,1 nm. Il funzionamento di base di tutti i MET segue la stessa logica: un fascio di elettroni, sotto vuoto spinto, attraversa un sottile campione e grazie ad un set di lenti elettromagnetiche l'immagine proiettata viene ingrandita alla dimensione voluta.

Permette di fare diversi tipi di analisi :

- Dei analisi morphologiche :
    - Immagine conventionale : permette di ossevare il campione
- Dei analisi strutturale :
    - HRTEM o alta risoluzione : permette di osservare il retticolo cristallino
    - ASTAR/Acom-TEM : tecnica recente che permette una mappatura delle fasi presenti nel campione
- Dei analisi compositionale :
    - EDX: permette di determinare la compositione del campione.

Simulazione SRIM/TRIM

SRIM (TRIM), Stopping and Range of Ions in Matter, è un software che simula l'interazione ione-materia. Il suo sistema di calcolo è basato sul metodo Binary Collision Approximation, a sua volta basato sul metodo Monte Carlo. Il materiale è semplificato come un amorfo. Il percorso degli ioni nel materiale

tra ogni impatto è considerato rettilineo. Lo ione perde quindi la sua energia entrando in collisione con i nuclei atomici che compongono il materiale.

Come nella finestra di configurazione, il software viene utilizzato in modalità Sputtering per avvicinarsi alle condizioni di doppio raggio. Il raggio utilizzato è definito dalla sua energia di accelerazione, angolo di incidenza e composizione. Il materiale target viene quindi definito descrivendo la sua composizione / stechiometria e densità. Una volta terminata la simulazione, si ottengonoinformazioni diverse:

- Ion Range IR {95% Ga} o limite di profondità (x) attraversato da meno del 5% di ioni di gallio.
- Ion Range IR {99% Ga} o limite di profondità (x) attraversato da meno dell'1% di ioni di gallio.
- Projected Range corrisponde al percorso medio degli ioni nel materiale proiettato su x (profondità) ey (superficie).

Il Protocollo

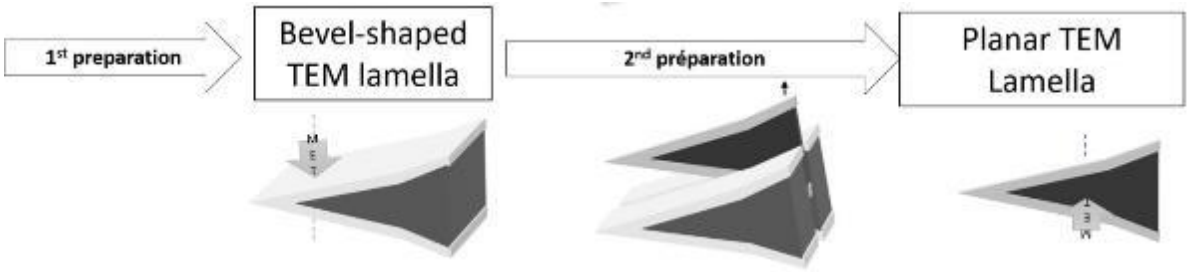

Figura 57: Preparazione della lamella per la caracterizzazione del'impatto di un FIB.

Per studiare l'impatto sperimentale dell'assottigliamento del fascio ionico viene applicato un protocollo specifico. All'inizio, viene realizzata una lamella a forma di smusso (Figura 3A). La sua estrazione è simile alla tecnica Lift-out.

Tuttavia, durante la lucidatura la lamella viene assottigliata con uno smusso e vengono utilizzate diverse energie di assottigliamento, da 30 keV fino all'energia di accelerazione desiderata (16, 8, 5 keV ecc.). I fasci di energia inferiore riducono gli strati amorfi indotti dai fasci precedenti. La preparazione della lamella bisellata permette la conservazione del reticolo cristallino in funzione dello spessore della lamella.

Dopo un prime analisi, il campione viene ricoperto da uno strato protettivo. Faciliterà la seconda preparazione, ma proteggerà anche lo strato danneggiato dalla prima preparazione. In questo modo la seconda preparazione non avrà alcun impatto sulle misure.

Una volta protetta, una lamella planare viene estrattacome mostrato nella Figura 3B. Consente di ottenere una sezione "trasversale" (Figura 3C) dell'ex lamella e quindi di misurare direttamente le fasi amorfa e cristallina.

La lamella planare viene analizzata mediante EDX (analisi composizionale per determinare la penetrazione del gallio) e, successivamente, viene analizzata mediante TEM convenzionale (analisi morfologica) e HRMET (analisi strutturale) per lo studio dello strato amorfizzato.

Il caso del silicio

In un primo momento viene effettuato uno studio sul silicio monocristallino per determinare lo spessore di amorfo generato dal fascio Ga +. Il metodo spiegato prima viene utilizzato su tutte le lamelle per determinarne l'efficienza. Parallelamente, vengono eseguite simulazioni SRIM per conoscere l'impatto della trave sul materiale. Questi determinano il possibile legame tra la penetrazione ionica simulata e lo

spessore dello strato amorfo creato. Tutti questi risultati vengono confrontati con i valori usuali utilizzati sul campo.

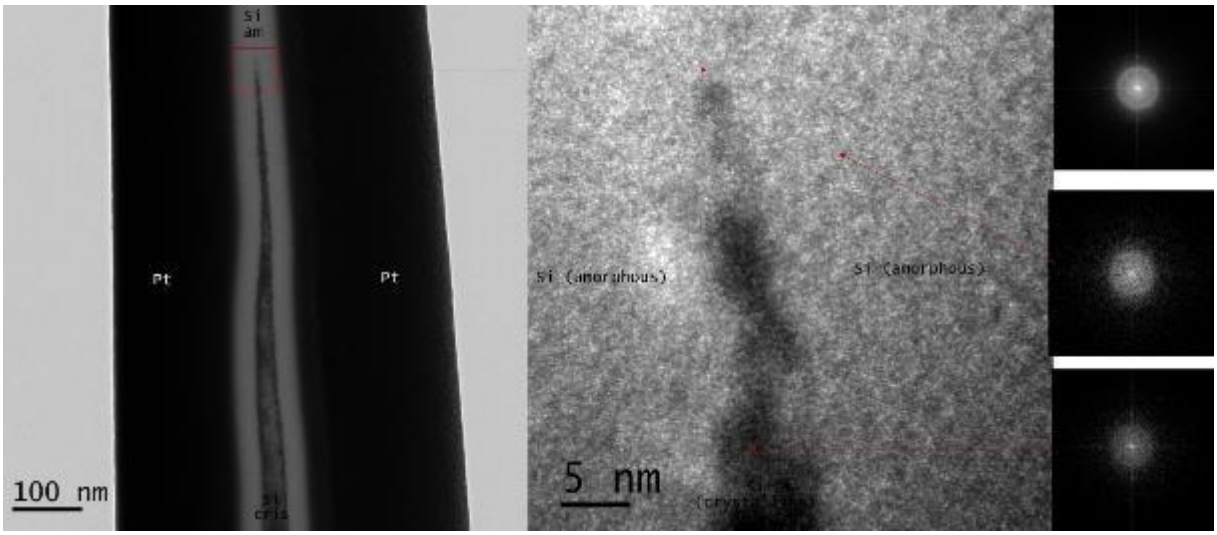

Figura 4: Esempio di amorphizazione da un faccio di ione visibile su la sua lamella planaria

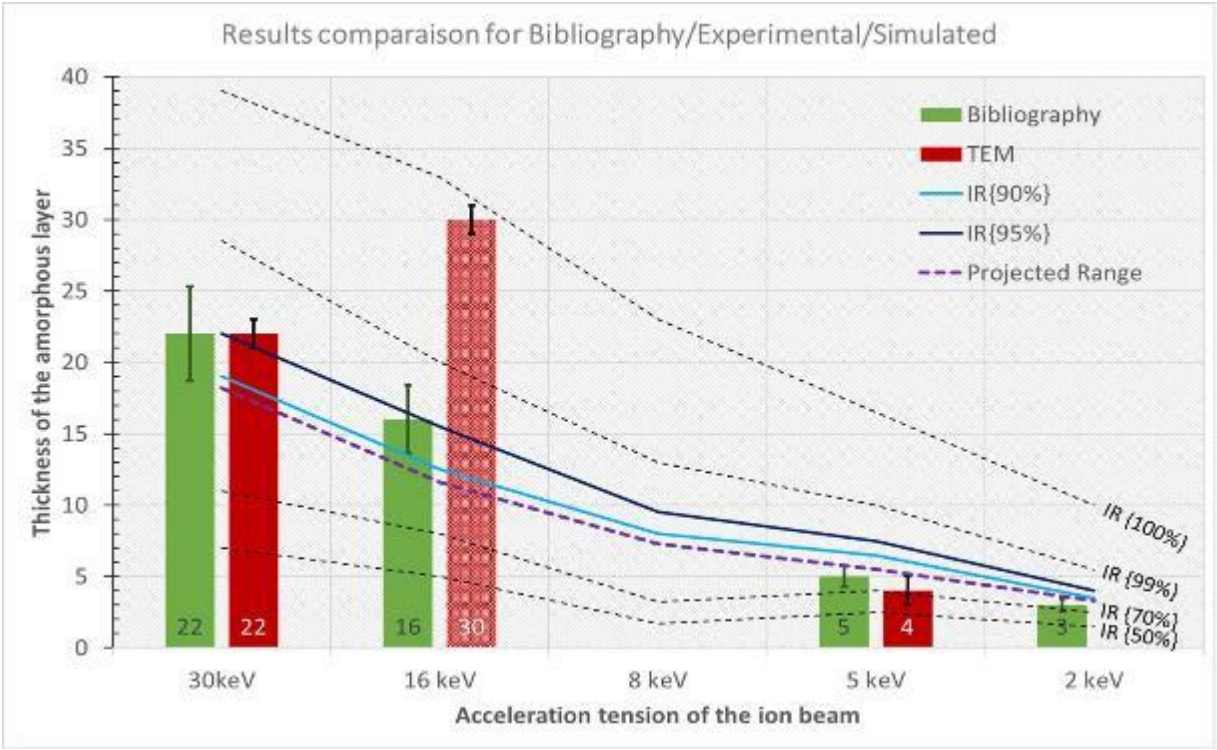

Figura 5: Riassumento dell'amorphizazzione del silicio

Lo strato amorfo creato dalla prima preparazione sul silicio monocristallino è apparso chiaramente grazie all'analisi TEM sia convenzionale che ad alta risoluzione, Figura 4. Lo strato era completamente amorfo e il suo spessore dipendeva direttamente dalla tensione di accelerazione utilizzata come ultima fase di preparazione. Questo strato è anche equivalente alla penetrazione del gallio misurata grazie all' EDX.

Questi risultati sono in accordo con la letteratura e corrispondono all'IR {90%} e IR {95%} (uguale al range previsto) risultanti dalle simulazioni SRIM. Pertanto, per il materiale di silicio, è necessario eseguire varie fasi riducendo l'energia del fascio ionico per preservare il sistema cristallino come lo mostrato in Figura 5.

Il GeSbTe (GST)

Per ragioni di tempo è stata studiata solo la preparazione da 30 keV. Poiché per la preparazione della lamella è stata utlizzata la tensione di accelerazione più alta utilizzata, può essere considerata una preparazione "critica" e dovrebbe dare una buona idea dell'impatto a un'energia inferiore. La lamella a forma di smusso ha uno spessore uniforme di 100 nm di GST.. La lamella planare viene quindi estratta da questa parte e può contenere silicio (il substrato) o TiN (l'elettrodo superiore) poiché questi due strati sono a contatto con il GST. Il GST policristallino è protetto sia da uno strato di platino esterno che da uno strato di carbone interno.

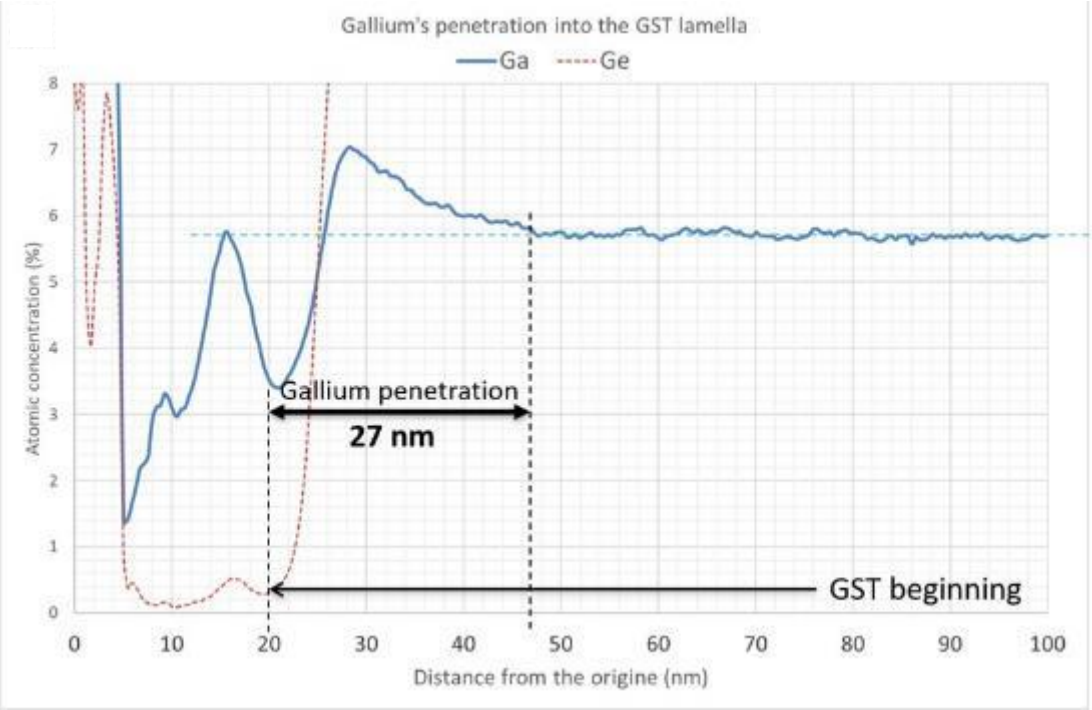

Figura 6: Profilo di composizione in Ge e Ga della lamella di GST

Il grafico nella Figura 6 mostra la concentrazione di Ge e Ga (EDX). La curva del Ge tratteggiata in rosso definisce l'inizio dello smusso GST (da 20 nm). La curva del gallio, in blu, ci interessa solo nella parte GST, quindi da 20nm. Subisce un forte aumento fino a un valore massimo intorno a 28 nm, 8 nm di profondità nella GST, per poi diminuire più gradualmente fino a raggiungere un valore di plateau a 47 nm (27 nm nella GST). Questo plateau è, come per la lamella di silicio, il risultato della seconda preparazione dove gli ioni Ga penetrano in modo uniforme anche la superficie della lamella.

La penetrazione del gallio con 30 keV nel GST durante la prima preparazione è quindi di 27 nm. Tuttavia, esiste un'importante concentrazione di gallio a 7 nm dalle superfici. Inoltre, uno strato amorfo, di uno spessore omogeneo di 27 nm, è visibile su ciascun lato della lamella, come nel caso del silicio.

È stata condotta un'analisi TEM convenzionale, come nel caso del silicio. Tuttavia, la mancanza di contrasto tra le parte cristalline e quelle amorfe rende l'observazione difficile e poco precisa.

Quindi per analizzare meglio la diapositiva sarebbe necessario aumentare il contrasto tra le fasi o fare direttamente una mappatura di fase.

ASTAR o Acom-MET è una tecnica recente di caratterizzazione, implementata dal CNRS e commercializzata da Nanomegas, consente di effettuare la mappatura di fase. Registra per ogni punto un'immagine di diffrazione. Quest'ultimo viene confrontato con un database cristallografico predefinito al fine di identificare quale fase è più probabile. Ciò consente di dedurre l'orientamento dei cristalli.

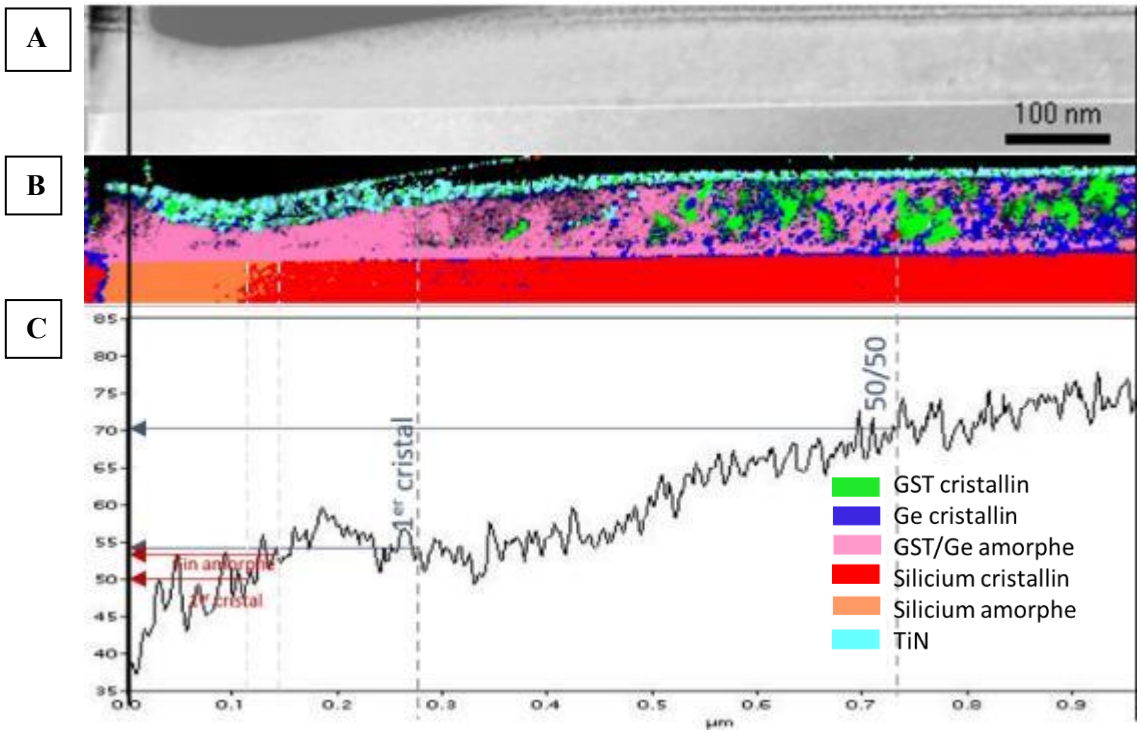

*Figure 8: Immagine TEM, mappa di fase equivalente e profilo associato della lamella a forma di smusso GST 30keV, risoluzione 500 punti * 70 punti, passaggio 2 nm*

Da questa analisi si deduce che, contrariamente alla nostra precedente ipotesi, l'impatto del fascio di ioni di gallio sul GST è diverso da quello osservato con il silicio monocristallino: è presente uno strato intermedio dove il GST è parzialmente amorfizzato (Figura 8B). I nanocristalli in verde (cristalli di GST) e in blu (cristalli di Ge) sono in una matrice di GST/Ge amorfa (roso).

È stato analizzato solo l'assottigliamento di 30 keV, tuttavia si può considerare che la preparazione del campione più critica. Non dovrebbero esserci artefatti diversi come transizione di fase o bolle con fasci di energia inferiore.

Pertanto, è consigliato eseguire queste analisi secondo il protocollo, aggiungendo la caratterizzazione Astar, per determinare l'impatto del dannegiamento a energia inferiore.

Conclusione

Il TEM richiede lamelle trasparenti al fascio di elettroni, quindi campioni molto sottili. Per farle e possibile di usare un Dual-Beam. Scava i materiali, estrae una lamella e poi la assottiglia grazie ad un fascio di ioni (gallio). Questo raggio tende a lasciare artefatti sulla lamella, ovvero difetto imputabile solo alla preparazione. Nel caso di materiali cristallini, c'è un rischio importante di amorfizzazione. Alcuni ioni gallio entrano anche nella lamella e possono amorfizzare il materiale.

Lo studio su wafer di silicio monocristallino è stato condotto per verificare l'accuratezza del metodo sperimentale. Comunemente utilizzati nella microelettronica, gli artefatti dei fasci di ioni di gallio sul silicio monocristallino sono già noti. I risultati ottenuti sono coerenti con la bibliografia, e l'unica differenza (a 16 keV) è facilmente spiegabile e consente un miglioramento del protocollo. Inoltre, l'analisi EDX ha mostrato che la penetrazione sperimentale del gallio era equivalente alla dimensione dello strato amorfo.

Grazie a queste osservazioni e miglioramenti, è stata condotta l'analisi su $Ge_2Sb_2Te_5$. È stato studiato solo l'effetto del fascio da 30 keV. Questo raggio è il più energetico utilizzato per la preparazione delle lamelle, quindi questa preparazione può essere considerata critica. Tutte le preparazioni realizzate con

fascio meno energetico, dovrebbero presentare manufatti simili, a spessori inferiori, poiché i fasci utilizzati avranno energie inferiori.

Tuttavia, la mancanza di contrasto tra i cristalli e ha reso estremamente difficile la misurazione. Per migliorare il protocollo e la misura, è stata condotta l'analisi Astar per ottenere una mappatura delle fasi. La misurazione ottenuta sembrava confermare i primi risultati, poiché la lamella a forma di smusso presentava anche nanocristalli in una matrice amorfa. I cristalli rimanenti non hanno orientamenti o composizioni preferenziali (Ge o GST).

Bibliographia

[1] KUNIAVSKY, Mike. Smart things: ubiquitous computing user experience design. Elsevier, 2010.

[2] KARL RUPP. 40 Years of Microprocessor Trend Data. Our World in Data. 1971 – 2017

[3] COLLIEX, Christian. La microscopie électronique. Que sais-je? 1998.

[4] AUSTRALIAN MYCROSCOPY, My Scope. TEM FIB. 2013.

[5] MAYER, Joachim, GIANNUZZI, Lucille A., KAMINO, Takeo, et al. TEM sample preparation and FIB-induced damage. MRS bulletin, 2007, vol. 32, no 5, p. 400-407.

[6] HUH, Yoon, HONG, Ki Jung, et SHIN, Kwang Soo. Amorphization induced by focused ion beam milling in metallic and electronic materials. Microscopy and Microanalysis, 2013, vol. 19, no S5, p.33-37.

[7] VOLKERT, Cynthia A. et MINOR, Andrew M. Focused ion beam microscopy and micromachining. MRS bulletin, 2007, vol. 32, no 5, p. 389-399.

[8] PASTEWKA, Lars, SALZER, Roland, GRAFF, Andreas, et al. Surface amorphization, sputter rate, and intrinsic stresses of silicon during low energy Ga+ focused-ion beam milling. Nuclear Instruments and Methods in Physics Research Section B: Beam Interactions with Materials and Atoms, 2009, vol. 267, no 18, p. 3072-3075.

Annexe 2: Thickness lamella determination and bias

The determination of the thickness of a bevelled lamella. Thanks to the EELS captor the signal is filtered on a specific electron energy. A non-filtered image is also taken. The software process both signals and give us the thickness map.

However, the calculation method uses a constant directly dependent on the mean free path of the electrons in the material. That constant is thus dependent on the material. In the software the equation used is

$$Thickness = \mathbf{140} \times log\left(\frac{unfiltred\ signal}{filtred\ signal}\right)$$

The constant used is 140, it is the one adapted to the monocrystalline silicon. The thickness measures on the GST may be biased because of this: the mean free path between those two elements is different.

To check if that biased is important, a measure of the thickness of a lamella in on containing both GST (blue rectangle) and silicon (red rectangle) in contact, is necessary, see Figure 1. Since both phases are in contact, they should have been equally thinned. Thus, their thickness profile should be equivalent.

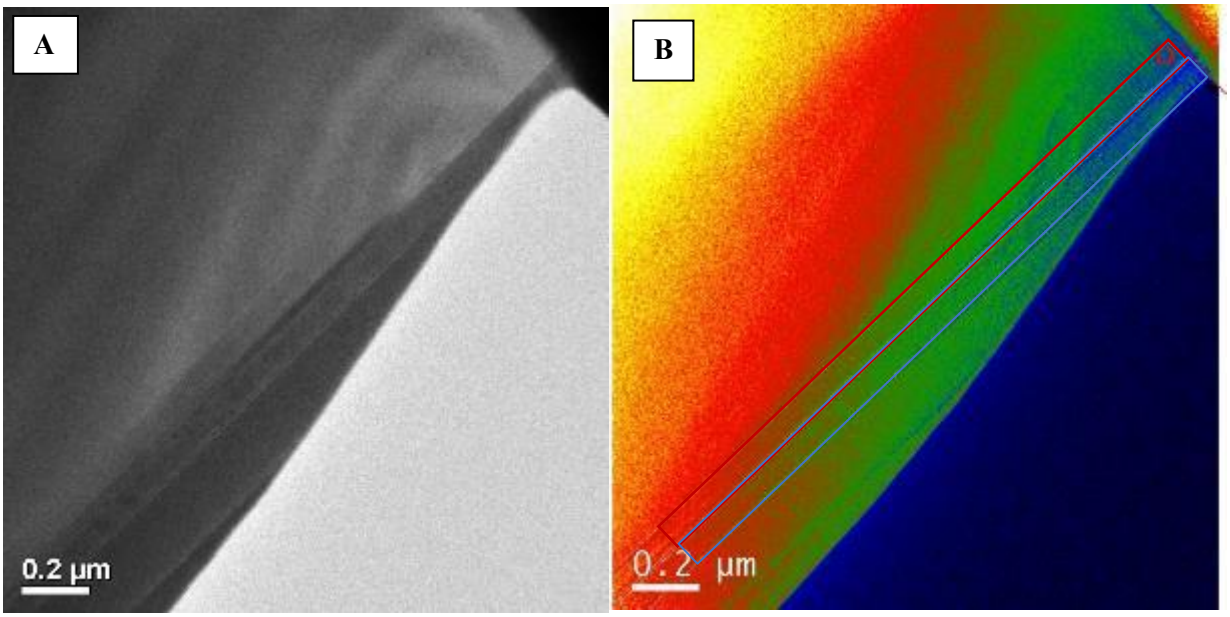

Figure 1: Thickness map of the bevel-shaped GST lamella thinned at 30 keV (TEM image and thickness map associated)

The two profiles extracted from the t-map, Figure 2, are similar. The thickness variation between the two is around 5 nm. This variation in minim. It can be due to the difference of mean free path in the material but also to a real variation of the thickness lamella. Thus, the results given by the software to measure the thickness of a GST lamella are correct.

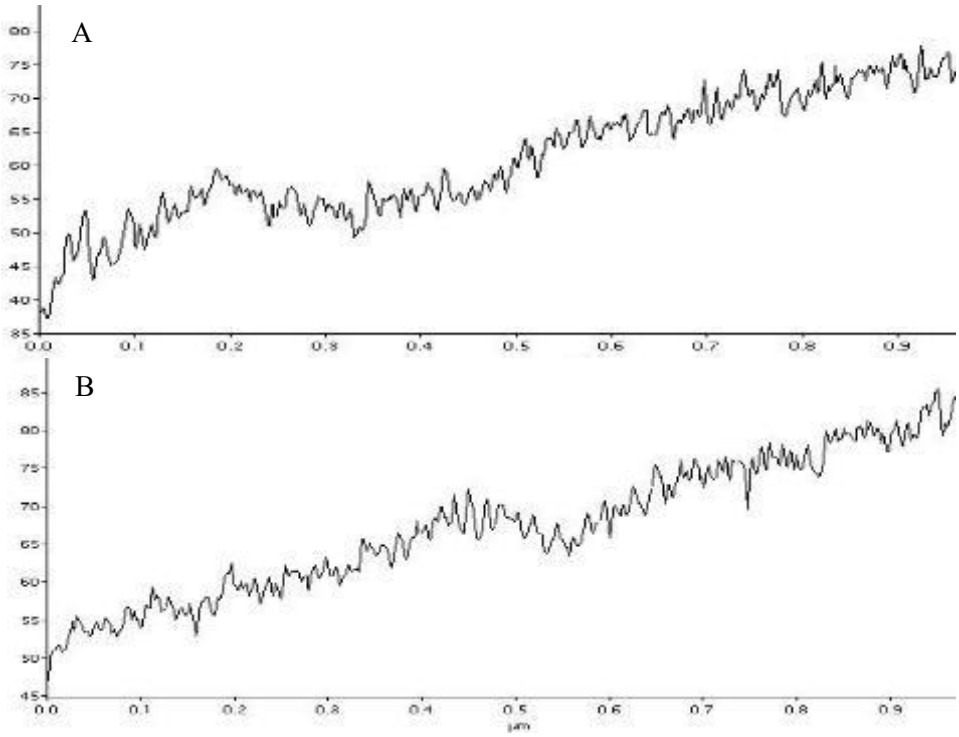

Figure 2: Thickness profile for two adjacent layers of (A) Silicon and (B) GST

Annexe 3: Calculation of IR {x% Ga}

The ion range IR{x%} or the depth limit crossed by less than (1-x) % of Gallium ions. It allows a good approximation of the gallium penetration and amorphization since a sufficient quantity of penetrating ions is necessary to completely destroy the network on a homogeneous layer.

After a simulation thanks to the TRIM software with the wanted parameter, the ion range data are extracted from SRIM thanks to the file RANGE.TXT (in the part Ion / Recoil Distributions).

The file presents the table of the number of penetrating atoms per volume unite (atoms/cm) in function of the depth on the material (see the first 2 columns of the table presented). Thus, it is not the true number of ion in the material but it is possible to process those results to obtain the probability of an ion to exceed a specific depth, it is first necessary to create the cumulative function of Ga.

$$Ga_{cumulative}(x) = \sum_{i=0}^{x} Ions(x)$$

The probably comes from the cumulative percentage.

$$\%_{Ga}(x) = \frac{\sum_{i=0}^{x} Ions(x)}{\sum_{i=0}^{+\infty} Ions}$$

The following table presents the results for a grazing Ga ion beam (30 keV) in monocrystalline silicon. An example of data processing is shown in Table 1. The two first column can be extracted from the files; the two last are the calculation done to obtain the wanted results

Depth (A)	*Ga*	Cumulative Ga	Cumulative percentage
10,01	*89009,00*	89009,00	5,39%
20,01	*106010,00*	195019,00	11,80%
30,01	*124010,00*	319029,00	19,31%
40,01	*129010,00*	448039,00	27,12%
50,01	*126010,00*	574049,00	34,75%
60,01	*144010,00*	718059,00	43,46%
70,01	*121010,00*	839069,00	50,79%
80,01	*139010,00*	978079,00	59,20%
90,01	*94009,00*	1072088,00	64,89%
100,01	*92009,00*	1164097,00	70,46%
110,01	*79008,00*	1243105,00	75,24%
120,01	*64006,00*	1307111,00	79,12%
130,01	*62006,00*	1369117,00	82,87%
140,01	*44004,00*	1413121,00	85,53%
150,01	*42004,00*	1455125,00	88,07%
160,01	*39004,00*	1494129,00	**90,44%**
170,01	*36004,00*	1530133,00	92,61%
180,01	*35003,00*	1565136,00	**94,73%**
190,01	*17002,00*	1582138,00	95,76%
…	…	…	….

Table 1: Results of the Simulation and data processing

Those results can also be presented as in as a graph like in Figure 1. It represents the cumulative percentage in function of the depth or the probability of penetration of the ion in the material.

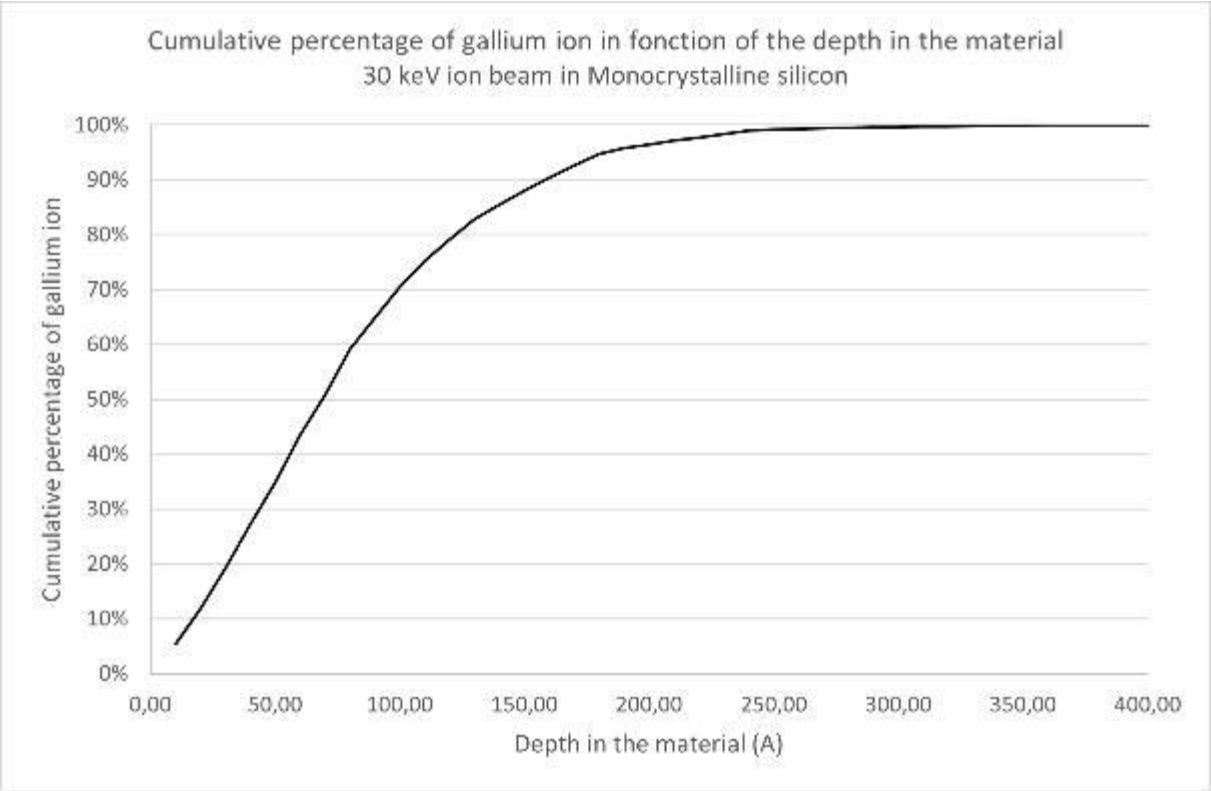

Figure 1: Plot of Cumulative percentage of gallium penetration for a 30 keV grazing ion beam

The IR {x} values are extracted from the tables, as the first depth where the cumulative percentage is superior to x. Thus, when less than (100-x) % atoms have passed this limit.

Annexe 4: Analysis ASTAR on Monocrystalline Silicon

The Astar analysis was done for the GST, however since it is on a silicon substrate, see Figure A it is also possible to observe the results for the monocrystalline silicon. The lamella thickness profile is determined one the silicon area, thanks to the t-map already used for GST.

Done on the silicon, the phase map presented in Figure B, present two distinct and separate phases: in orange the amorphous silicon and in red the crystalline silicon. There is thus a direct transition between the amorphous and the crystalline phase observed. This transition is for a lamella thickness between 55-60 nm.

However, the former analyses on the silicon planar lamella (3.Thickness impact) have shown that at this thickness, there is already 10 nm of monocrystalline silicon in the lamella (around 20%).

Therefore, there seems to be limit to the crystalline phase diffraction. It seems that under 10 nm, the crystal diffraction is not important enough to be detected.

To check if there was a similar phenomenon with the HRTEM imaging, the detected between amorphous/crystalline is observed with it, see Figure . It seems that there is a direct transition between the amorphous material (up) and the crystalline material (down)

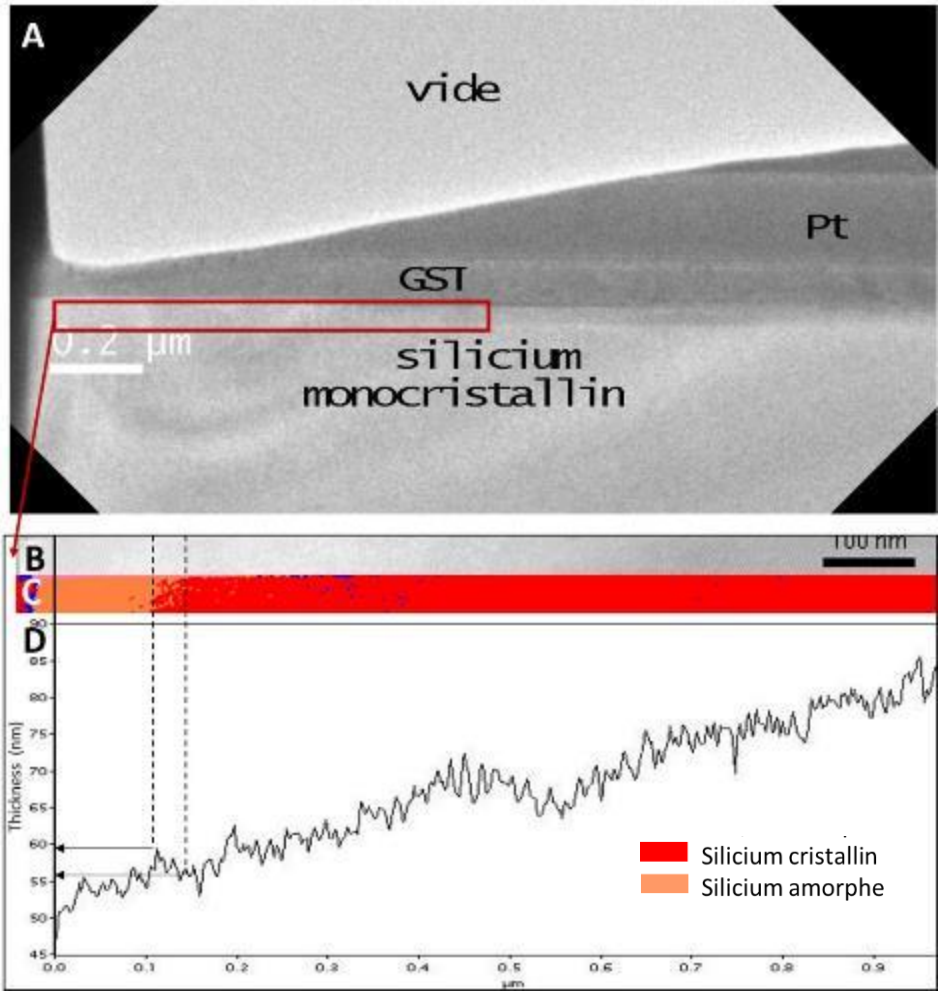

*Figure 1 : TEM image, equivalent phase map and associated profile of the 30keV silicon part of a bevel-shaped lamella, resolution 500 pts * 70 pts, step 2 nm*

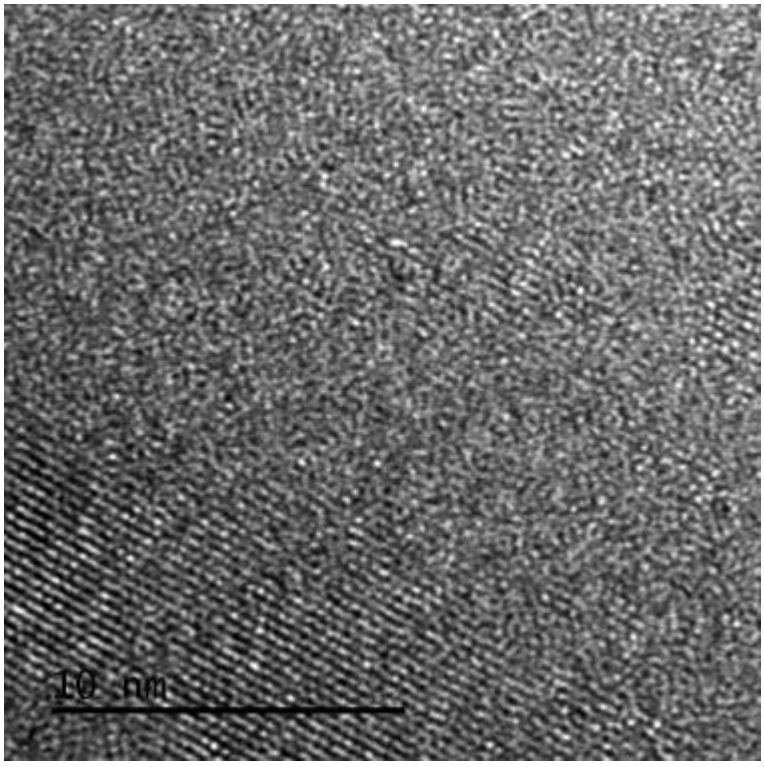

Figure 2: HRTEM imaging of the transition between amorphous and monocrystalline silicon (55-60 nm thickness)

In comparison, with the same lamella, at a thickness of 100nm, a perfectly organized monocrystal is observed in Figure . At this lamella thickness, the electron beam passes through 55-60 nm of crystals (55-60% crystalline) and 40-50nm of amorphous silicon.

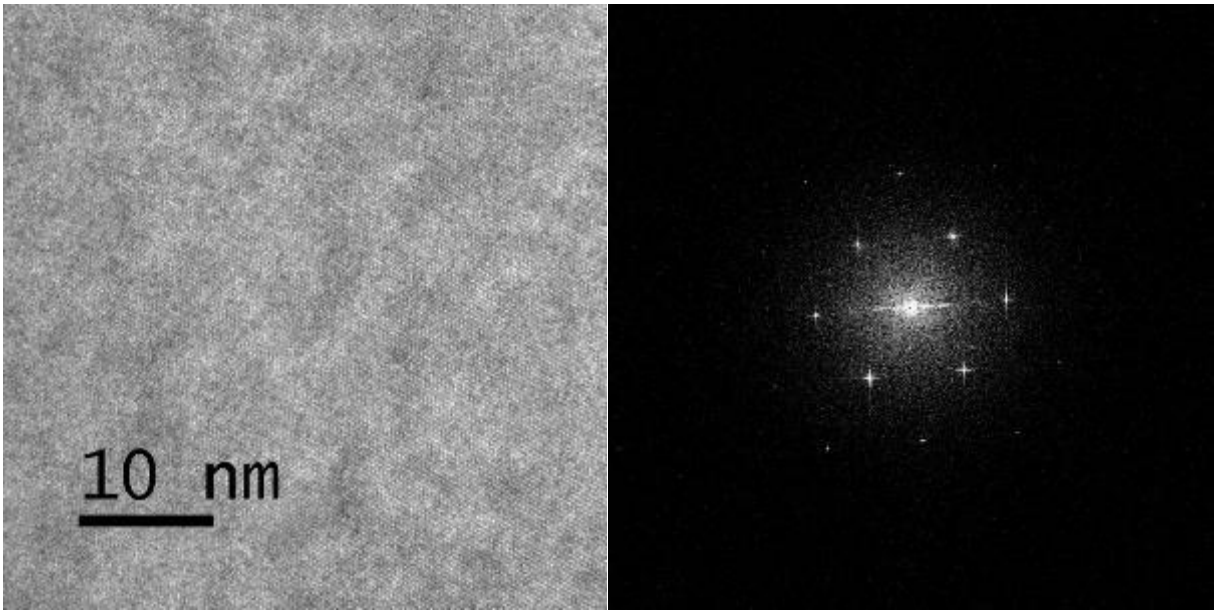

Figure 3: HRTEM imaging of the transition between amorphous and monocrystalline silicon (around 100 nm thick) with the corresponding FFT pattern